63-3-4

AEDC-TDR-63-92

ALBEDO AND PLANET RADIATION INTERCEPTED BY AN EARTH SATELLITE

By

C. D. Fitz, S. J. Lukasik, E. A. Mayer, and D. R. Simon
Vitro Laboratories
Division of Vitro Corporation of America
West Orange, N. J.

TECHNICAL DOCUMENTARY REPORT NO. AEDC-TDR-63-92

May 1963

AFSC Program Area 850E, Project 7778, Task 777801

(Prepared under Contract No. AF 40(600)-951 by Vitro Laboratories, Vitro Corporation of America, West Orange, N.J.)

ARNOLD ENGINEERING DEVELOPMENT CENTER
AIR FORCE SYSTEMS COMMAND
UNITED STATES AIR FORCE

NOTICES

ALBEDO AND PLANET RADIATION INTERCEPTED BY AN EARTH SATELLITE

By

C. D. Fitz, S. J. Lukasik,
E. A. Mayer, and D. R. Simon
Vitro Laboratories
Division of Vitro Corporation of America
West Orange, N.J.

(The reproducibles used in the reproduction of this report were supplied by the authors.)

May 1963

FOREWORD

This Technical Documentary Report summarizes the results of an investigation of the characteristics of secondary radiation in the vicinity of the earth. The secondary radiation considered includes the reflected radiation (albedo) and re-radiated energy (planet radiation). Feasible tolerances to be placed on the simulation of these characteristics are also examined.

To round out this report, Arnold Engineering Development Center personnel have prepared two supplementary notes to this study. These supplements summarize typical secondary radiation data obtained by instrumentation on the TIROS II and III meteorological satellites.

The research was conducted by Vitro Laboratories, Division of Vitro Corporation of America, West Orange, New Jersey, under Contract No. AF40(600)-951.

Vitro Laboratories' personnel who participated in the research and in the preparation of this report were C. D. Fitz, Head, Physics and Space Science Dept., S. J. Lukasik, E. A. Mayer, and D. R. Simon. Arnold Engineering Development Center personnel were Captain W. J. Kerzon, USAF, and Flight Lieutenant G. MacFarlane, RCAF.

The basic report has been assigned Vitro Laboratories Report No. VL-2244-11-0.

ABSTRACT

The characteristics of the secondary radiation environment of an earth satellite were analyzed and compared with the characteristics of solar radiation. Of the total incident radiation, 27% is reflected from earth and clouds and 9% is scattered, bringing the total albedo contribution to 36%. The remaining 64% of the incident energy is absorbed by the earth and re-radiated as planet radiation. Of this energy, 17% is radiated as thermal radiation from the earth, and 47% as thermal radiation from the stratosphere.

The spectral distribution of the reflected solar radiation corresponds to that of a blackbody at 6000°K while the energy, which is reradiated, corresponds to a blackbody at approximately 250°K. In the wavelength region below 4 microns, albedo radiation has the higher spectral intensity, peaking at about 10^{-1} watts/cm^2 μ; above 4μ peak spectral intensity is approximately 10^{-3} watts/cm$^2\mu$.

An analysis was made of the angular distribution of the solar, albedo, and planet radiation received by an earth satellite. Solar radiation has only a 32-minute spread or collimation angle from the sun-earth direction. The intensity of the albedo on area differentials on the satellite surface were calculated as a function of altitude, orbital position with respect to the earth-sun axis, and orientation of the differential area on the satellite surface, using the model suggested by Dennison. The albedo has a maximum intensity on the lower side of the satellite at an orbital position directly between the sun and the earth. This intensity decreases with altitude and with the angle between the actual position and the sun-earth axis falling to zero on the shadowed side of the earth. This analysis of albedo angular distribution was compared with the analysis by Feigelson et al (a group of Russian investigators) which is based on experimental data but is not as complete in the number of parameters considered. The results of the two analyses compare closely, however. The third type of radiation planet radiation was found to be independent of the orbital angular position. Intensity and angular distribution of this radiation are dependent only on the altitude and the amount of cloud cover.

Tolerances on simulating the radiation characteristics were analyzed based on possible thermal and material effects upon a space vehicle. It was concluded that the spectral distribution should be matched with a reasonable tolerance in the ultraviolet for material effects, and in the region of maximum spectral irradiance for thermal effects. The angular energy distribution should

be matched within 8% to insure a temperature deviation no greater than 2%. The degree of accuracy or tolerance on simulation techniques should be based on economical as well as technical considerations.

PUBLICATION REVIEW

This report has been reviewed and publication is approved.

G. M. Arnold
Chief, Engineering Division
Space Systems Office

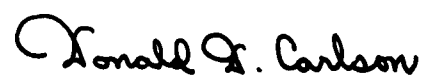

Donald D. Carlson
Lt Col, USAF
Chief, Space Systems Office

George MacFarlane
Flt Lt, RCAF
Engineering Division
Space Systems Office

TABLE OF CONTENTS

LIST OF ILLUSTRATIONS

LIST OF ILLUSTRATIONS (Continued)

LIST OF TABLES

I. INTRODUCTION

A satellite orbiting the earth is exposed to radiant energy from a number of fields. The principal source of this energy is the sun which provides: (1) direct or solar radiation, (2) radiant energy reflected from the earth and clouds or albedo radiation, and (3) radiant energy absorbed by the earth and atmosphere and reradiated at longer wavelengths as thermal or planet radiation.

Primary and secondary radiation fields incident upon an earth satellite are illustrated in Figure 1. Above the sunlit hemisphere, the satellite intercepts solar radiation unattenuated by the earth's atmosphere. As it moves from the sunlit into the shadowed region, the satellite briefly encounters a zone where atmospheric attenuation is a factor. Beyond this zone, the satellite enters the shadow of the earth where no direct solar radiation is intercepted.

While in the sunlit hemisphere, the satellite is also irradiated by the sunlight reflected and scattered by the earth and its atmosphere (albedo). This reflected radiation also vanishes as the satellite enters the earth's shadow.

The unreflected portion of the incident solar radiation is absorbed by the atmosphere and the earth and is re-emitted as planet radiation. For thermal equilibrium to be maintained, the absorbed energy must be reradiated at a rate equal to the energy absorption rate. This reradiation process is continuous at all times and in all directions without regard to the position of the sun.

The several radiation fields have thermal and material effects upon the satellite. Unfortunately theoretical techniques are not sufficiently accurate to predict the magnitude of these effects. In the case of thermal effects for example, temperature conditions cannot be determined to better than 50°K. It is highly desired that this thermal error be reduced by at least an order of magnitude. Through testing under simulated radiation conditions a more accurate determination of effects may be accomplished.

Although exact simulation of radiation characteristics is certainly preferred the technical difficulty and expense make it necessary to provide tolerances

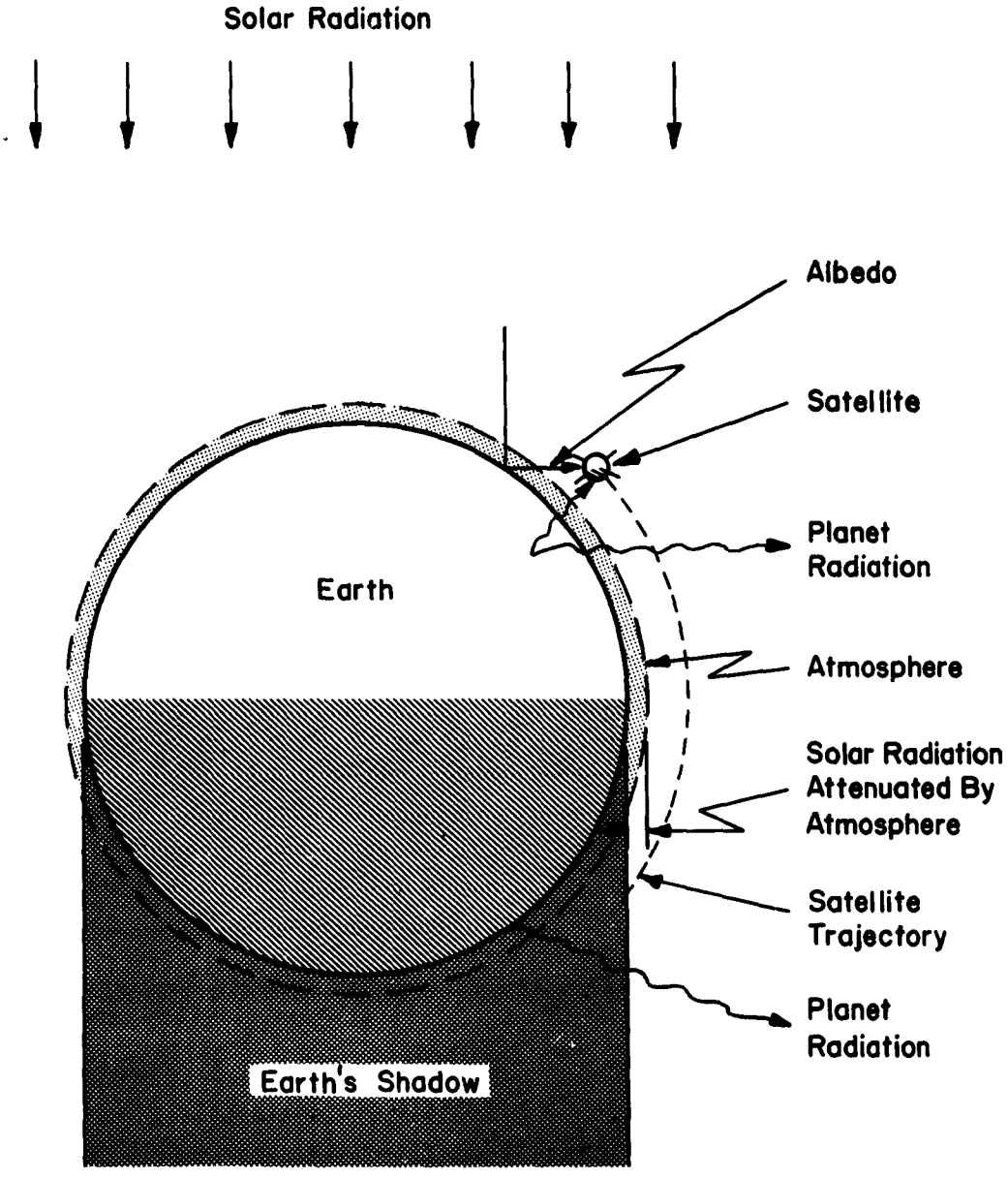

Fig. 1 Radiation Fields Affecting Earth Satellite

on the simulated characteristics. The magnitude of the tolerance depends in turn upon the radiation effects.

The properties of direct or solar radiation have been determined and tolerances established. The characteristics of secondary radiation (albedo and planet radiation) have not been examined to a comparable extent and exact values of the several properties under various conditons are not known.

In this report an attempt has been made to review the available information on the characteristics of albedo and planet radiation, particularly as this radiation would be received by an earth satellite, and to recommend a preliminary set of tolerances and specifications for simulation of these characteristics.

II CHARACTERISTICS OF PRIMARY SOLAR RADIATION

An understanding of albedo and planet radiation requires first of all a knowledge of the properties of solar radiation, the primary source of energy for the several radiation fields. Table I lists the principal characteristics of solar radiation at the earth's distance from the sun.

The first characteristic, the spectral distribution, is a function principally of the energy exchange between the sun's photosphere, chromosphere, and corona. Although the ultraviolet and x-ray portion of the solar spectrum has several strong lines, such as the Lyman alpha line at 1216 A and the lines at 584A and 304A from neutral and ionized helium[1*], studies performed at National Research Corporation[2] indicate that the solar spectrum below 2000A has only minor effects on space vehicles. Above 2000A, the spectrum is a continuum corresponding roughly to blackbody radiation from a 6000°K radiant source. The spectral distribution in this and the higher wavelength region is known as the Johnson curve, after F. S. Johnson, who compiled extensive solar data and extrapolated these data to zero air mass conditions[3].

While the relative spectral distribution is independent of the distance from the sun to the earth, the absolute intensity decreases with increasing distance. At the earth's distance from the sun, the total radiant flux below the Johnson curve or the "Solar Constant" is 0.1396 ± 0.0028 watts/cm^2. This intensity varies by $\pm 3.4\%$ over the year due to the ellipticity of the earth's orbit and the changing earth-sun distance. Although sun spot activity indicates some variation in intensity over the sun's surface, this variation can be ignored for simulation purposes. At the earth's distance the sun subtends an angle of 32 minutes. Therefore the solar rays from opposite edges of the sun's periphery vary from the parallel by a 32-minute angle, the angle of collimation. Outside of this 32' disc, a satellite or receiving body will see only cold black space and will radiate to this outer region.

The influence of the positions of the sun and earth on the radiation characteristics should also be considered. Fortunately, from a simulation point of view, the sun can be considered fixed in its position in space. During the portion of the satellite's orbit in which the satellite is behind the earth, the earth blocks out the solar radiation. Further, the enormous distance between the sun and the earth as compared to the satellite altitude reduces any variation of solar characteristics with altitude to a negligible value. In view of the comparatively small dimensions of the satellite, complete uniformity of radiation exists across the vehicle.

* References are collected in Chapter VI, p. 68.

TABLE I

CHARACTERISTICS OF SOLAR RADIATION

Spectral Distribution	Corresponds to blackbody radiating at temperature of 6000°K
Total Intensity	0.1396 ± 0.0028 (watts/cm^2) ± 3.4% over year.
Collimation Angle	32'
Position of Radiating Source	Constant
Duration of Radiation	While in sunlit hemisphere
Altitude Effect	Not appreciable
Uniformity	Constant

III ALBEDO AND PLANET RADIATION CHARACTERISTICS

The secondary radiation incident upon an earth satellite is produced by the interaction of the primary solar radiation with the earth. For a vehicle in a solar orbit or for an earth satellite in an orbit far from the earth, this radiation will of course be absent. The same processes responsible for secondary radiation from the earth will operate in a qualitatively similar, but quantitatively different, way to determine the secondary radiation from the moon, Mars, Venus, etc.

The description of secondary radiation can be best presented in three separate aspects. The first concerns the reflection and backscattering of the primary solar radiation by the earth, clouds, and atmosphere. For this component, the spectral distribution is directly related to the spectral distribution of the incident primary radiation. The second aspect concerns the thermal radiation from the earth and the atmosphere that is the result of the absorption of the incident solar radiation. The spectral distribution of this component of secondary radiation is related to the temperature of the radiating material and is in the far-infrared region of the spectrum. The third aspect of the secondary radiation concerns the characteristics of the energy in the ultraviolet region of the spectrum. Analysis of this less-understood spectral region has required special treatment. These three aspects are discussed in greater detail in the following.

A. REFLECTION AND BACKSCATTERING

One contribution to the secondary radiation is that of primary radiation that has been reflected from the earth and clouds. This radiation is in the ultraviolet, visible and near infrared region of the spectrum and has a spectral distribution characteristic of the 6000°K solar blackbody spectrum. However, the primary spectrum is modified by the spectral dependence of the reflectivity and by the existence of atmospheric absorption in bands throughout the visible and infrared portion of the spectrum and particularly in the ultraviolet region. Clearly, the polarization and collimation of the primary radiation is changed. One conventionally describes this and all other components of secondary radiation as having a cos Θ (Lambert Law) angular dependence characteristic of a diffuse surface.

A second contribution to the secondary radiation consists of primary radiation that has been backscattered by the atmosphere. Several types of scattering processes occur depending on the wavelength of the incident radiation and on

the type and size of the scattering particle. For wavelengths that are large compared to the size of the scattering particle, the incident electromagnetic wave induces an oscillating dipole polarization in the individual scattering molecules which then reradiate the energy (Rayleigh scattering). For wavelengths that are of the same order of magnitude as the size of the scattering particles, we have an electromagnetic boundary value problem. The case of spheres has been treated exactly (Mie scattering). For wavelengths small compared to the size of the scattering particle, the problem is one of geometrical optics.

The various types of scattering particles that are present in the atmosphere are atoms and molecules ($\simeq 10^{-3}\mu$), water particles or aerosols (1 - 10μ), and solid particles (dust, carbon, salt, living organisms). Further complication arises from the finite optical depth of the atmosphere. This means that multiple rather than single scattering must be considered, thereby requiring the application of the theory of radiative transfer[4].

Under clear sky conditions primary radiation is reflected from the earth's surface with a reflectivity of about 6%; under these conditions, atmospheric backscattering amounts to about 9% or a total contribution of 15% to the albedo. For a completely overcast sky, the total contribution of reflection and backscattering to the albedo is 55%. Weighting the clear-sky and overcast-sky values by 48% and 52% respectively, on the basis of world-wide meteorological observations, gives an average albedo of 36%. The average reflected contribution to this total albedo is 27%.

These reflected radiant energy values were determined from astronomical and meteorological studies performed by Danjon[5], Simpson[6], Baur and Phillips[7,8], Fritz[9], and Houghton[10]. In his recent review of this subject, Camack[12] indicated that measurements on satellite temperatures, meteorological satellites, and satellite-borne experiments on the earth's heat budget have verified previous predictions but have not made substantial improvements over the older studies.

Among the interesting techniques used prior to balloon, rocket, and satellite experiments, was the measurement of the illumination of the dark area of the moon by light reflected from the earth. Measurements[11] taken in France indicated a greater illumination of the moon in the evening hours than in the early morning hours. This variation was interpreted as due to a greater reflection from the ocean areas during the French evening than from the land areas of Asia, Europe, and Africa occuring during the French pre-sunrise hours.

This last result indicates the spatial and temporal variations which may be expected in the reflected radiation. A precise description of the characteristics of reflecting regions would require a detailed knowledge of the reflectance of desert areas, grasslands, forest cover, snow and ice, oceans, and clouds as well as the relation between the amount of cloud cover and the type of terrain. For example, more cloud cover is present over water areas than over land. The southern hemisphere with its much greater water area has therefore more cloud coverage and reflectance than the northern land hemisphere.

In spite of this obvious discrepancy, the reflecting energy determined for the northern hemisphere has been assumed to apply over the entire earth. Other variations in the reflected energy such as seasonal variations and short time variations due to changing terrain and cloud cover are undoubtedly important but are not well known. These variations are, therefore, treated as second-order deviations and one assumes that they average out in satellite applications. For instance, the rotation of the earth as well as the orbital motion of the satellite cause a satellite to be influenced by the seasonal extremes at a given time of the year in either hemispherical section of its orbit. Camack[12] integrated the seasonal variations given by Baur and Phillips to determine the average reflection for various times of the year. These calculations indicated that a negligible error is introduced when the annual average is used for both hemispheres. A latitude-by-latitude comparison of the averages of the two seasons with the annual mean indicated only a small error except in the polar regions.

Figure 2 summarizes the preceeding discussion in graphical form. This figure shows:

(a) the incident primary radiation over the spectral region 0.3 - 3.2 μ

(b) the average reflected and backscattered contribution to the secondary radiation based on an albedo of 0.36

(c) an upper limit on the reflected and backscattered contribution to the secondary radiation assuming completely overcast skies; under this condition the albedo is 0.55

(d) a lower limit on the reflected and backscattered contribution based on completely clear skies; under this condition the albedo is 0.15.

Note that in all of the above calculations, the albedo has been assumed to be independent of wavelength. Also, the reflection and backscattering has been

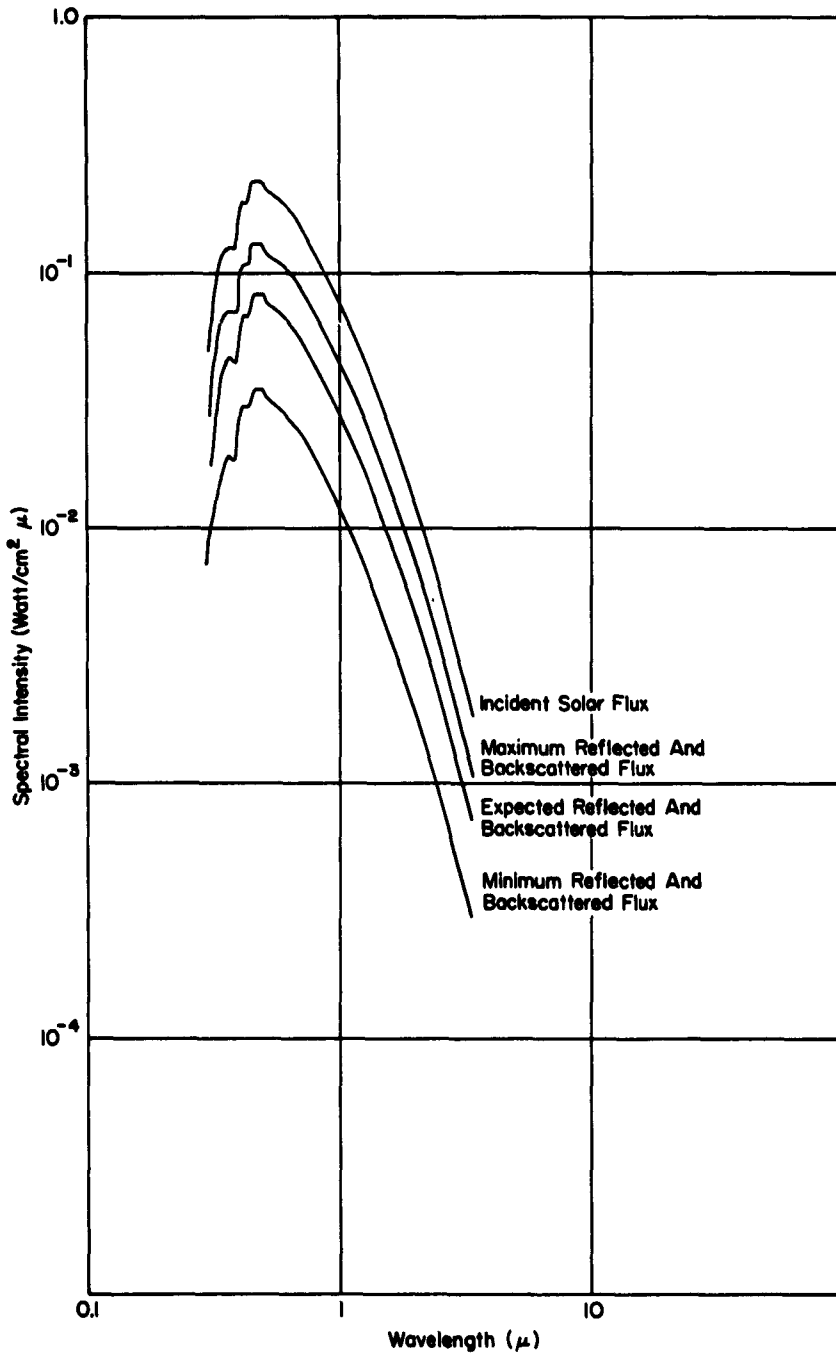

Fig. 2 Reflected and Backscattered Flux Compared to Incident Solar Flux over the 0.3-3.2μ Spectral Region

treated as though it occurred at the top of the atmosphere. Actually, the reflection and backscattering takes place at the upper surfaces of clouds or deep within the atmosphere or at the earth's surface. Hence, there is an opportunity for energy absorption due to transitions between the various possible molecular energy levels of the atmospheric constituents to operate on both the incoming and on the outgoing radiation. Therefore, the estimates in Figure 2 are incorrect to the extent that the neglect of these two effects is unjustified.

The values in Figure 2 can be considered as representative of the energy flux at an average height (h = 10 km) intermediate between that of the earth's surface (h = 0) and the top of the stratosphere (h = 20 km). Taking the radius of the earth to be the average of the equational and polar radii, 6367 km, then the effective radiating radius is R_o = 6377 km. In view of the earth's oblateness of 21 km, the exact value of the effective radiating radius is uncertain by at least 10 km anyway. To correct the values in Figure 2 to some altitude h, one adjusts the fluxes so that the total energy is unchanged. Thus the intensity I(h) at an altitude h is given by

$$I(h) = I_o\left(\frac{R_o}{R_o + h}\right)^2$$

where I_o refers to the plotted energy fluxes and R_o is the effective average atmospheric radius of 6377 km. Thus at a satellite altitude of h = 100 mi = 161 km, the values in Figure 2 should be reduced by the factor $(1.025)^{-2}$ or about 5%.

B. PLANET RADIATION

It has been shown in the preceeding section that, on the average, about 36% of the incident primary solar radiation is reflected or backscattered. The remaining 64% of the incident primary solar radiation is absorbed by the atmosphere and earth. In order to maintain the thermal equilibrium of the atmosphere and earth, this energy must be reradiated. The energy radiation is fixed by the energy absorption rate; this, in turn, fixes the temperature and hence the spectral distribution of this radiation. The radiation is variously called "thermal," "terrestrial," or "planet" radiation. It is completely in the infrared region of the spectrum and has an energy distribution characteristic of a blackbody at about 250°K.

The effective temperature of this radiation can be stated more precisely if the transmission properties of the earth's atmosphere are considered. Since the energy of infrared photons corresponds to molecular energy level spacings, the details of the atmospheric transmission coefficient will depend on the composition of the atmosphere and on the concentration of its various components. The thermal radiation can be divided, for the sake of discussion, into two parts. The first part consists of those wavelengths for which the atmosphere is transparent. The relative intensity of these wavelengths is characteristic of the earth's temperature, about 288°K. This represents an upper limit on the thermal radiation spectrum. About 17% of the incident solar radiation is reradiated in this way[13].

The second part of the thermal radiation consists of those wavelengths for which the atmosphere is partially or completely opaque. In these spectral regions the earth radiation is absorbed in the atmosphere and is reradiated from the upper levels of the atmosphere. The spectrum of this radiation is characterized by a blackbody temperature given by the average temperature of the isothermal stratosphere, about 218°K. About 47% of the incident solar radiation is removed in this way[13].

These two contributions are shown in Figure 3 taken from Camack[12]. The solid line is the actual spectral emission of the thermal component of the planet radiation. It is bounded at the top by the 288°K blackbody curve. This curve, and those portions of the actual spectral emission bounded by it, represents emission through a totally transparent atmosphere. One notes that the strongest thermal radiation occurs at 9 and 11μ under conditions of a transparent atmosphere. The actual spectral emission is bounded at the bottom by a 218°K blackbody curve representative of the stratosphere. Radiation that follows this curve represents thermal emission of the second type corresponding to an opaque atmosphere. Although the spectral emission for the atmospheric radiation is smaller than that for the earth radiation, when the respective energy fluxes are integrated over all wavelengths, nearly three times as much energy is found in the atmospheric thermal component.

This information is replotted in Figure 4 along with the limits over which the thermal radiation can be expected to vary. There is, of course, no unique way to specify these limits although the most precise response would be to state values that would be exceeded for a specified fraction of the time; e.g., the radiation will be less than 0.5 of the tabulated values no more than 5% of the time. Lacking the kind of statistical information on which such a precise statement must be based, we resort to a more intuitive approach.

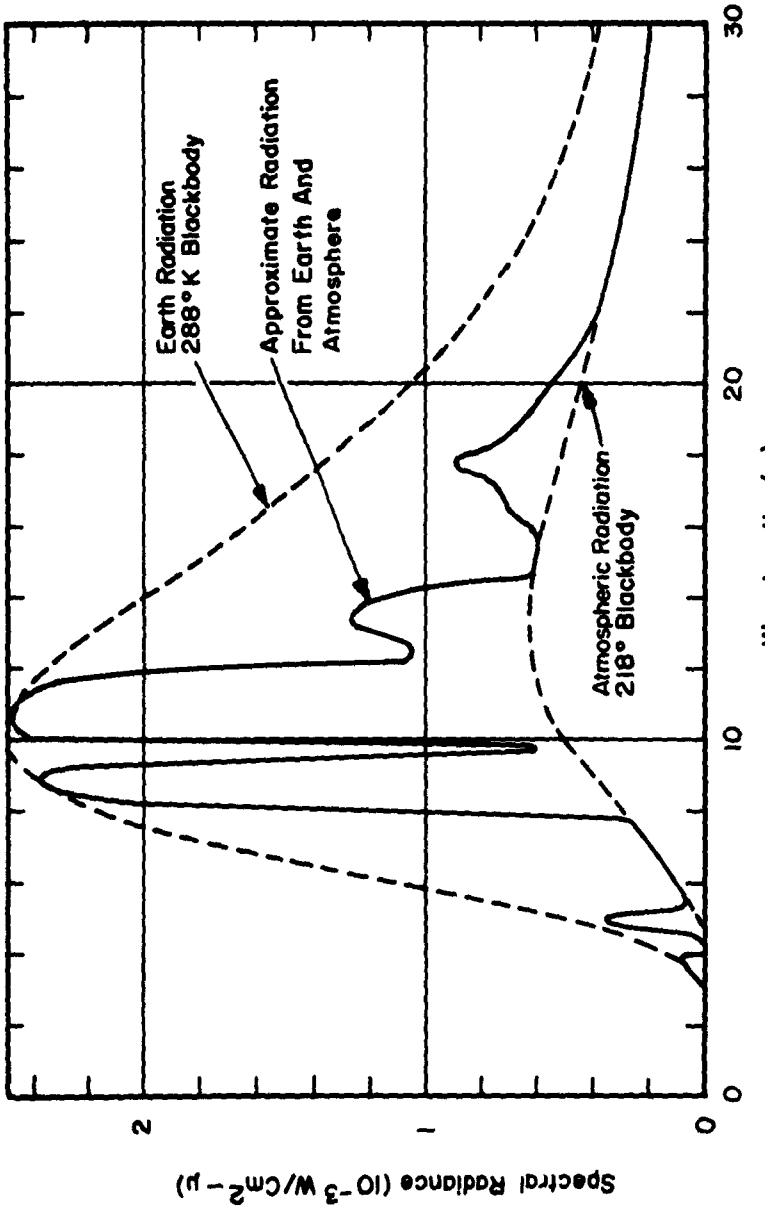

Fig. 3 Spectral Distribution of Planet Radiation Reference 12

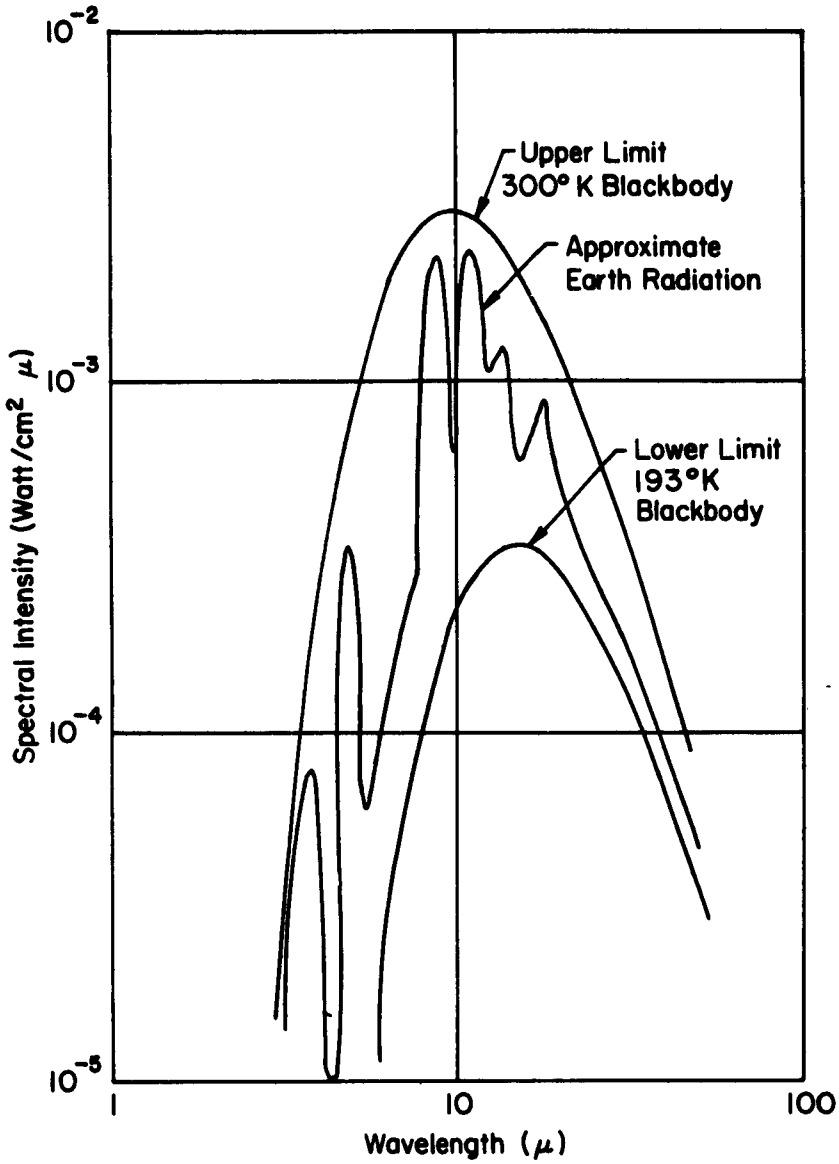

Fig. 4 Limits on the Spectral Distribution of Planet Radiation

Reference 12

For a lower limit, we assume that the thermal radiation will never be less than that for a blackbody temperature of 193°K. This corresponds to observed mean stratospheric temperature soundings at low latitudes of -80°C. It also assumes complete opacity of the atmosphere of all wavelengths.

For an upper limit, we assume that the thermal radiation will never exceed that for a blackbody temperature of 300°K. This is simply a choice of a reasonably high earth temperature and further assumes complete atmospheric transmission.

C. ULTRAVIOLET RADIATION

Previous sections of this chapter considered the various components of secondary radiation down to wavelengths of 3000A°. Thus, the part of the ultraviolet region lying between 3000A and 4000A has already been treated quantitively. The ultraviolet portion of secondary radiation between 2000A and 3000A is considerably more complicated however.

Examination of the solar spectrum at the surface of the earth reveals a sharp cut-off at about 3000 A. This cut-off is due to the absorption of all shorter wavelength radiation by the earth's atmosphere. In the region between 2000 and 3000A, the atmospheric constituent that is responsible for this absorption is ozone. Figure 5 shows the absorption coefficient as a function of wavelength for ozone at NTP[14]. The maximum value of the absorption coefficient of ozone is about 120 cm^{-1} at a wavelength of 2550A. Since the equivalent thickness of the ozone in the atmosphere at NTP is about 0.3 cm, the ultraviolet radiation at this wavelength is attenuated by a factor of about e^{-36} in traversing the atmosphere. Clearly atmospheric ozone is a significant absorber of ultraviolet radiation. Even at 3000 A, the absorption coefficient is about 5 cm^{-1} so that there is an attenuation of about $\bar{e}^{1.5}$ in traversing the atmosphere.

Figure 6 shows typical measured vertical distributions of ozone in the upper atmosphere[14] There one observes that the ozone is to be found at altitudes between 15 and 35 km. Since most of the atmosphere and clouds lie below 15 km, most of the molecular scattering, particulate scattering and cloud reflection occurs below this altitude. Hence, the calculation of the ultraviolet component of the planet radiation below 3000A can be divided into three parts:

(a) A fraction of the incident radiation will be backscattered before reaching the top of the ozone layer at 35-km altitude.

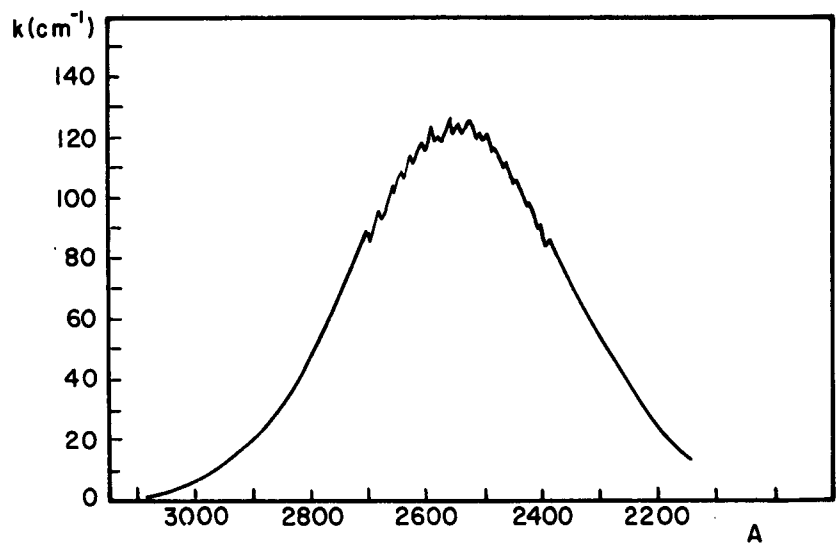

Fig. 5 Continuous Absorption Per Centimeter NTP of Ozone

Reference 14

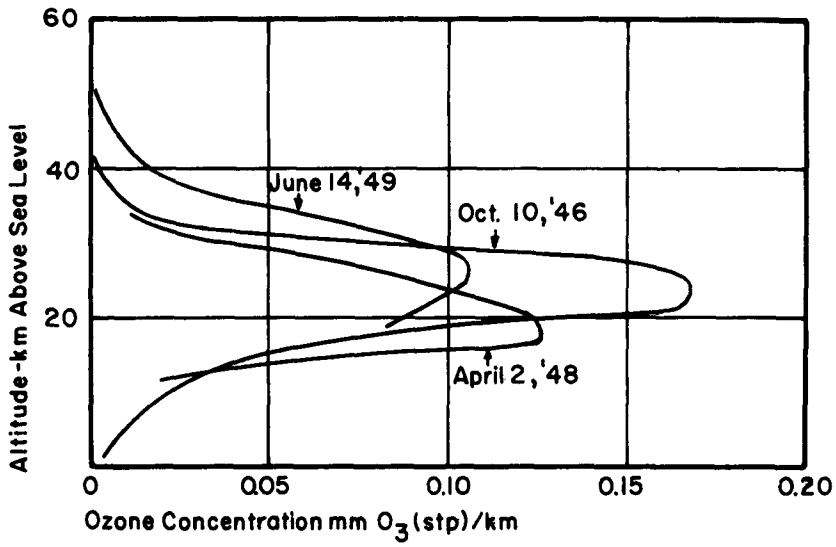

Fig. 6 Vertical Distribution of Ozone

Reference 14

(b) Some of the incident radiation will be backscattered or reflected within the ozone layer between 15 and 35 km altitude.

(c) A portion of the incident ultraviolet radiation will penetrate the ozone layer completely. This will then be reflected or scattered in essentially the same way as discussed previously and will retransit the ozone layer in the upward direction.

One expects that process (a) above will provide the maximum ultraviolet flux of planet radiation below 3000 A. If this is the case, then the problem becomes one of determining the fraction f of the incident radiation that is involved.

Process (b) starts with a fraction 1 - f of the incident radiation. As the radiation proceeds into the ozone layer, it is exponentially absorbed but also backscattering and reflection take place continually. The reflected and back scattered radiation are further absorbed exponentially on their outward journey.

The contribution of process (c) can be calculated by applying to the backscatter calculations discussed above, a factor representing two traversals of an ozone layer 0.3 cm thick. The absorption coefficient shown in Figure 5 would be used.

Figure 7 illustrates this discussion by showing the altitude at which various wavelengths in the ultraviolet and soft x-ray region of the spectrum are reduced to half-intensity[14]. There it can be seen that above 3100 A the atmosphere is completely transparent (except for absorption bands due to molecular absorption in the visible and infrared). But for a wavelength of 3000 A, the incident radiation intensity is reduced by one-half at an altitude of about 20 km.

Numerical estimates of the contribution of the various processes to the total upward ultraviolet flux have been made for various wavelengths. In order to estimate the ultraviolet flux due to process (a), the approximation has been made that the fraction of the total reflection and backscattering taking place above 35 km altitude is given by the fraction of the gaseous atmosphere above 35 km. This fraction is 6.04×10^{-3} on the basis of the ICAO model atmosphere[15]. The (c) process is also relatively simple to calculate since the reflection-plus-backscattering flux presented in Figure 2 should be reduced by the factor e^{-2kL} where k is the wavelength-dependent attenuation coefficient shown in Figure 5 and L = 0.3 cm.

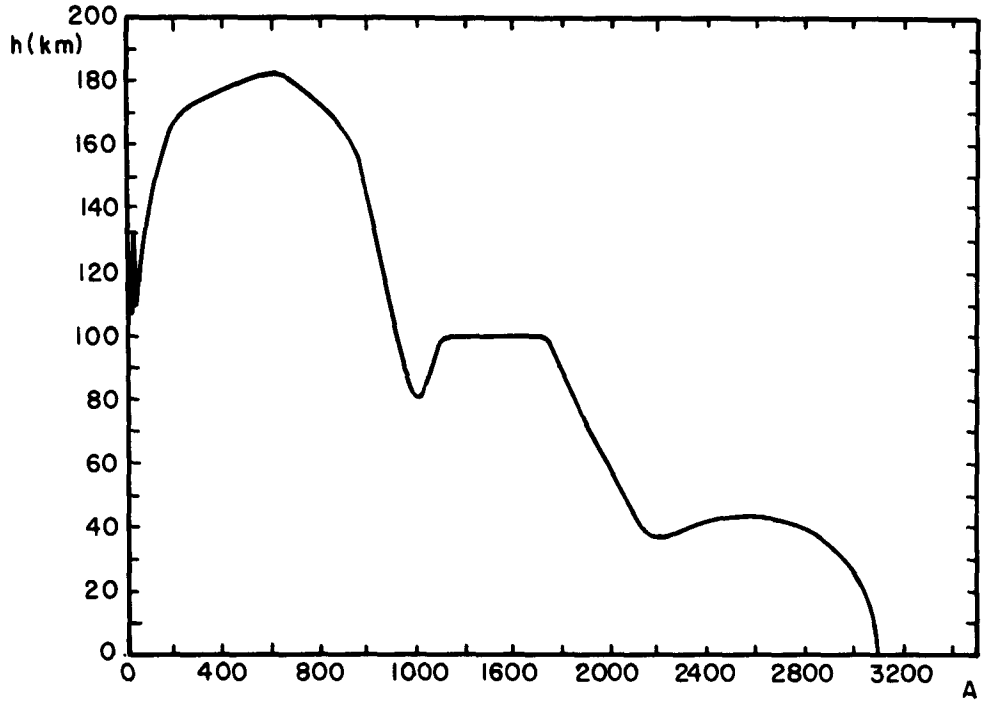

Fig. 7 Altitudes at Which Atmosphere is 50 Percent Transparent as a Function of Wavelength

Reference 14

However, the (b) process is quite difficult to calculate exactly. The following simple model has been constructed in order to obtain exploratory order-of-magnitude estimates. On the basis of Figure 6, a representative uniform ozone layer is constructed. This ozone layer has been divided into a number of altitude intervals. Separate rays have been allowed to traverse the ozone layer; each incoming ray is attenuated by its appropriate exponential attenuation factor and for each interval there is a backscattering probability dependent on the local particle number density at the center of the interval. The outgoing ray is then further attenuated.

The results of these calculations show that the contribution of the various processes depends strongly on the value of the attenuation coefficient and hence on the wavelength. Table II shows the results for two typical values of the attenuation coefficient. There we see that for 2000 A, for which the attenuation coefficient k has the relatively small value of 2 cm^{-1}, most of the radiation traverses the ozone layer unattenuated. Process (c), reflection and backscattering in the lower atmosphere, is the most important. Furthermore, the detailed calculation of the (b) process shows that, since attenuation is unimportant, the largest contribution to the backscattering comes from the lower, denser part of the ozone layer. However, the situation is considerably different at 2200 A where the attenuation coefficient is about ten times greater. Now the (c) process is totally insignificant and the (a) process is the most important. Reflection and backscattering from within the ozone layer is small and the detailed calculations show that it is reflection from the upper part of the ozone layer that is the greatest since the contributions of the lower layers are too severely attenuated.

It is clear from the above that, when the attenuation in the ozone layer is large, only backscattering from above the ozone layer can be significant. Radiation entering the ozone layer is totally lost except for an insignificant portion returned from a thin surface region at the top of the absorbing layer.

Table III summarizes the results of calculations to date for the expected ultraviolet albedo flux for the wavelength region between 2000 and 3000 A. In all cases, the values refer to the (a) process of backscattering from above 35 km, except for 2000, 2100 and 3000 A when the (c) process is most important. In all cases the (b) process has been neglected.

TABLE II

ULTRAVIOLET FLUX CHARACTERISTICS FOR 2000 A AND 2200 A WAVELENGTHS

Wavelength (A)	Attenuation Coefficient (cm^{-1})	Process (a) Expected UV Flux Due to Scattering Above 35 km ($watt/cm^2\mu$)	Process (b) Expected UV Flux Due to Scattering Within Ozone Layer ($watt/cm^2\mu$)	Process (c) Expected UV Flux Due to Return From Below Ozone Layer ($watt/cm^2\mu$)
2000	2	3.6×10^{-5}	34.9×10^{-5}	139×10^{-5}
2200	23	10.2×10^{-5}	2.2×10^{-5}	0.001×10^{-5}

TABLE III

EXPECTED ULTRAVIOLET ALBEDO FLUX

Wavelength (A)	Attenuation Coefficient (cm^{-1})	Expected UV Albedo Flux ($watt/cm^2\mu$)
2000	2	1.4×10^{-3}
2100	7	1.2×10^{-4}
2200	23	6.7×10^{-5}
2300	54	8.6×10^{-5}
2400	90	1.1×10^{-4}
2500	121	1.3×10^{-4}
2600	118	1.6×10^{-4}
2700	88	1.8×10^{-4}
2800	47	2.1×10^{-4}
2900	17	2.3×10^{-4}
3000	5.6	1.5×10^{-3}

D. COMBINED CHARACTERISTICS

The information on the intensity and spectral distribution of albedo and planet radiation presented in earlier parts of this chapter is summarized in Table IV and Figure 8. The major physical processes and the gross characteristics of the radiation are also presented in Table IV. Figure 8 shows the spectral distribution of the secondary radiation over the wavelength region from 0.2μ to 50μ. As discussed earlier, both maximum and minimum secondary radiation intensities are presented in order to assist in determining simulation tolerances.

From Figure 8, it can be seen that in the wavelength region around 4μ, a cross-over occurs. Below about 4μ, albedo radiation is more important but since this is characteristic of a 6000°K blackbody, the spectral intensity decreases rapidly with increasing wavelength. Above about 4μ, planet radiation is more important and it is characteristic of a blackbody temperature of 250°K.

The relative importance of these two contributions is somewhat distorted by the logarithmic abscissa in Figure 8. Despite the fact that the maximum spectral intensity of the planet radiation is more than an order of magnitude less than that of the albedo radiation, when summed over all wavelengths the planet radiation provides almost twice as great a contribution to the total secondary radiation as the albedo radiation.

The same sort of calculations have been made for the secondary radiation from other planets in the solar system. Very similar results for the radiation from Mars and Venus have been obtained[16].

TABLE IV

COMPONENT PARTS OF SECONDARY RADIATION

Component	Process	Fraction of Incident Radiation	Approximate Black Body Temperature	Remarks
Solar	Reflection from Earth and Clouds	0.27	6000°K	modified by reflection and absorption characteristics of the atmosphere
Solar	Scattering	0.09	6000	scattering probability depends on wavelength
Terrestrial	Thermal Radiation from the earth	0.17	288	occurs at wavelengths where the atmosphere is transparent
Terrestrial	Thermal Radiation from stratosphere	0.47	218	occurs at wavelengths where the atmosphere is absorbing

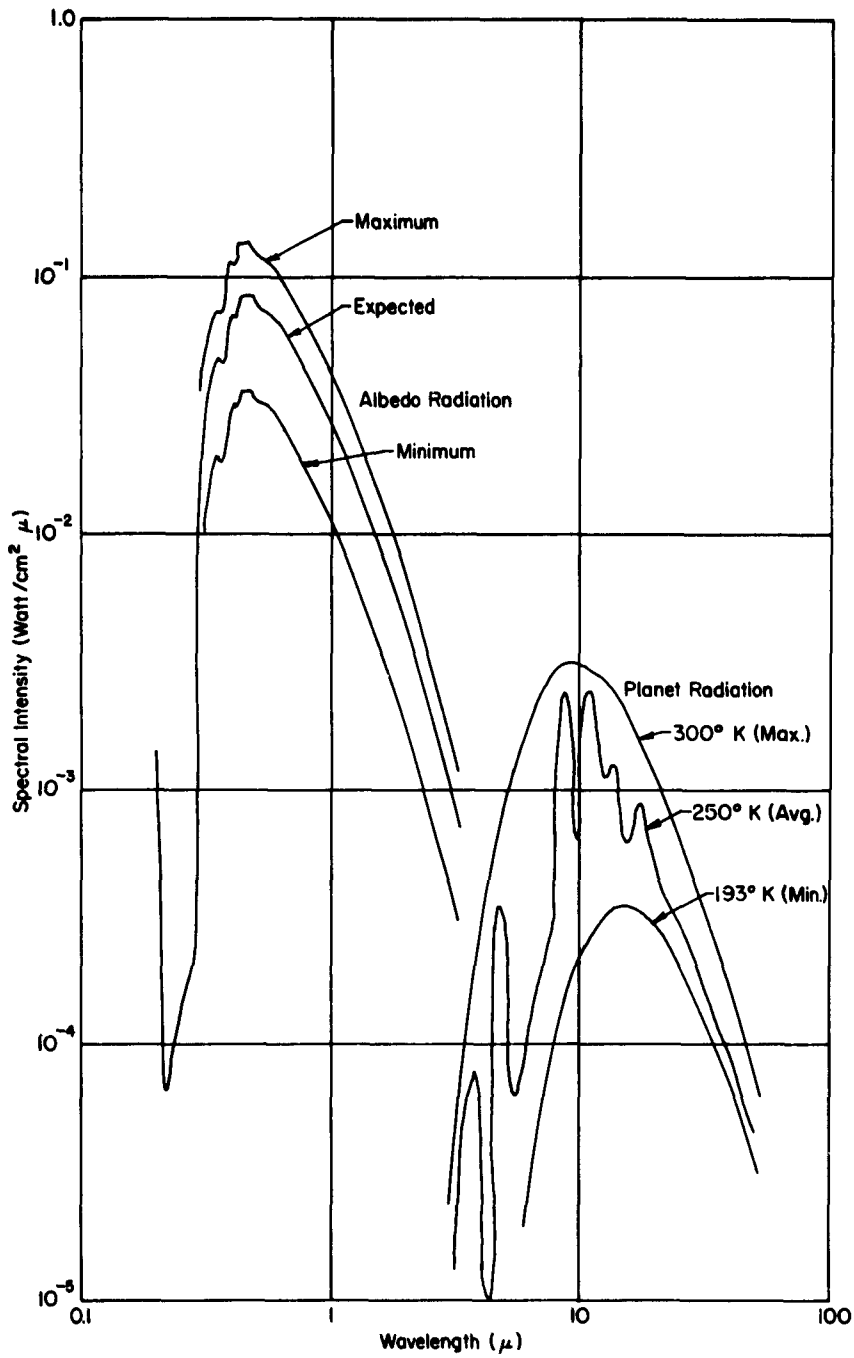

Fig. 8 Spectral Distribution of Secondary Radiation

IV. RADIATION INCIDENT UPON AN EARTH SATELLITE

Looking outward from its surface, an earth satellite sees a continuously changing combination of radiating and reflecting surfaces. Fortunately, from the simulation point of view the largest component, solar radiation, emanates from a source whose intensity, angular size, and position or direction from the satellite remain constant. In addition the intensity and angular size of the source of planet radiation are nearly constant except for altitude effects. On the other hand the direction of planet radiation relative to the direction of solar radiation is continually changing as the satellite orbits the earth.

The radiation characteristics of albedo are even more dynamic. In this case the intensity, source size, and source direction are all changing as the satellite's orbital position changes. At an orbital position directly in line between the sun and earth, the satellite sees the reflecting region as a large bright area directly below the satellite. At a satellite position away from the sun-earth axis, the satellite sees a bright area on the earth slightly offset in the direction of the sun-earth axis. Lines of equal intensity drawn around the central maximum would be elliptical or crescent in shape. At a satellite position angle approaching 90°, the satellite sees both the sunlit and the shadowed hemisphere. This complicated and varying combination of radiation sources would be extremely difficult to simulate.

On the other hand it is not the sources per se which are of interest for test purposes but rather the radiation received by the satellite. Thus the objective of an experimental facility is to simulate the characteristics of radiation fields illuminating a satellite, not the duplication of crescent-shaped radiation source areas. This objective could be met by providing the correct energy intensity and spectral distribution over the entire solid angle surrounding the satellite corresponding to a specific satellite position and time instant. This distribution is of course the sum of the solar, albedo and planet radiation.

The solar component of the angular intensity distribution is not difficult to determine. On surfaces whose normal vector is not parallel to the sun vector, the intensity upon a unit area decreases as the cosine of the angle between the surface normal and the sun vector. Due to the angular width of the sun, the intensity at large surface orientation angles is increased slightly over the amount indicated by the cosine relation. The more complex distributions of secondary radiation are examined in the following sections.

A. ALBEDO ILLUMINATION

A. J. Dennison[17, 18] has described a method for determining the intensity of the albedo incident upon surface sections of an earth satellite as a function of surface orientation angles, satellite position angle, and satellite altitude. In this analysis, it is assumed that the portion of the earth's surface illuminated by the sun is a hemisphere. At any point within this hemisphere, the incident energy E_E is:

$$E_E = E_s \cos \eta \tag{1}$$

where

E_s = Solar radiation intensity

η = Angle between the sun vector and the normal to the surface section

The radiation reflected from these points is assumed to obey Lambert's law for diffuse reflection, i.e., to have an intensity in any direction proportional to the cosine of the angle between that direction and the normal to the surface.

The reflected energy, E, incident upon a unit surface of a space vehicle, is expressed by Dennison as:

$$E = a E_s F \tag{2}$$

in which:

a = Albedo constant, the average intensity of reflected energy expressed as a fraction of the solar constant

E_s = Solar radiation intensity

F = Illumination factor or geometrical factor.

The illuminating factor is a double integral of functions of several parameters defined as:

$$F = \int_{\phi_L}^{\phi_u} \int_{\theta_L}^{\theta_u} \frac{r_E^2}{\Pi} \frac{\sin \phi \cos \sigma_E \cos a_E \cos a}{\rho^2} d\theta d\phi \quad (3)$$

The terms used in the above equation, which are shown schematically in Figure 9,are defined as follows:

ϕ, θ = angles defining the position P of the radiating incremental area

r_E = earth radius

ρ = distance from the reflecting region P to the vehicle segment

σ = angle between earth-satellite vector and earth-sun axis

σ_E = angle between earth-sun axis and the normal to the reflecting region P

a_E = angle between ρ and earth normal at P

a = angle between ρ and the vehicle surface normal at Q

β, γ = angles defining the orientation of the receiving section on the satellite

β, the elevation angles, corresponds to a pitching motion towards the earth-sun axis

γ, the azimuth angle, corresponds to a yawing motion of the receiving section

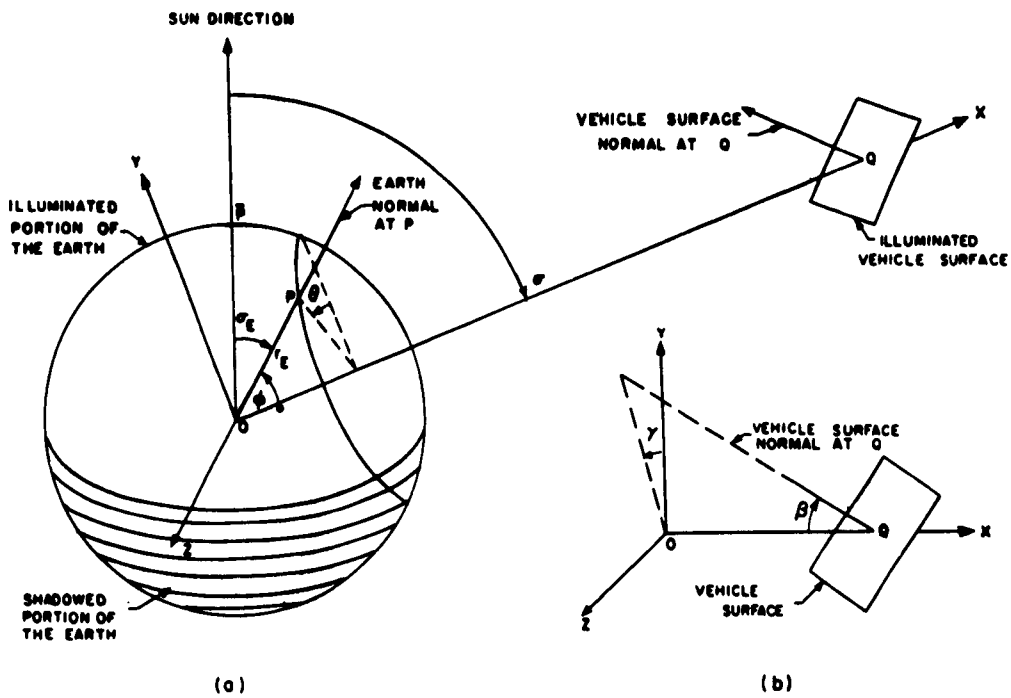

Fig. 9 Earth-Sun-Satellite Geometry

(Reference 17)

The illumination factor, F, has been evaluated for various satellite altitudes and angular positions and for various regions on the satellite's surface.

First the influence of altitude upon the illumination of a differential area oriented at $\beta = 0°$ and $\gamma = 0°$ is plotted in Figure 10. The decrease of F with altitude shown in this figure would be expected since the illumination of a surface is functionally related to the inverse square of the distance from the illumination source.

The effects on F caused by σ, the angular position of the satellite relative to the sun-earth vector, and by β, the pitch orientation of a section of the satellite surface relative to the earth normal are plotted for a number of altitude conditions in Figure 11. In these curves the yawing orientation angle, γ, is assumed equal to zero.

The following properties are illustrated:

1. F decreases with increasing σ dropping to small values at $\sigma = 90°$.

2. F values on the σ curves for 0°, 30°, and 60° decrease with increasing altitude.

3. F values for $\sigma = 90°$ increase with increasing altitude at the lower altitude. F values at the 10,000 mile altitude are however lower than at 1000 miles.

4. $\sigma = 0°$, $\beta = 0°$, $\gamma = 0°$ are necessary conditions for maximum F.

5. The functional relation of F to the pitch orientation angle, β, appears similar to a Gaussian distribution curve. For the orbital position, $\sigma = 0°$, this curve peaks at $\beta = 0°$. At other orbital positions the peak F value is perturbed in the positive β direction.

These characteristics are also physically reasonable. The decrease of the illumination factor F with increasing orbital angle σ would certainly be expected since increasing σ corresponds to the movement of the satellite away from the more highly illuminated areas on the earth.

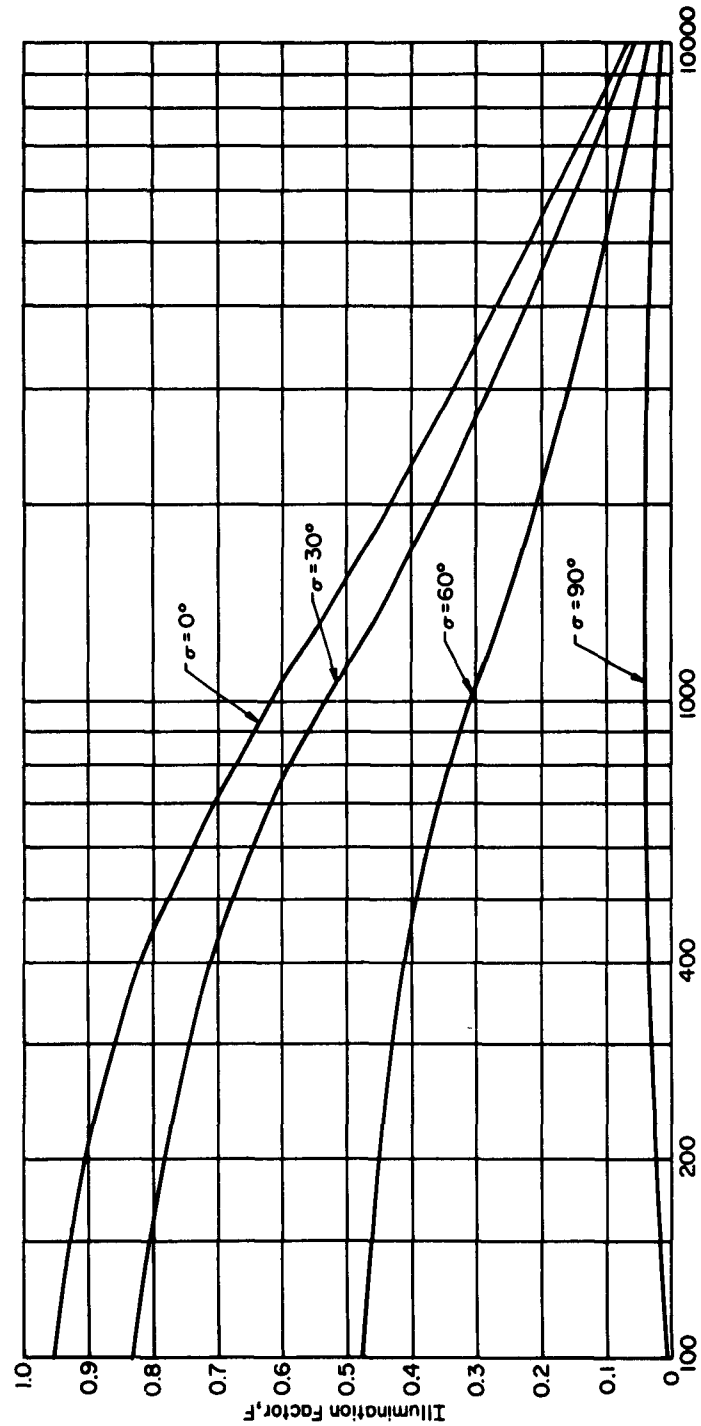

Elevation Angle, $\beta = 0°$
Azimuth Angle, $\gamma = 0°$

Fig. 10 Illumination Factor as a Function of Altitude for Parametric Values of Orbital Position Angle, σ

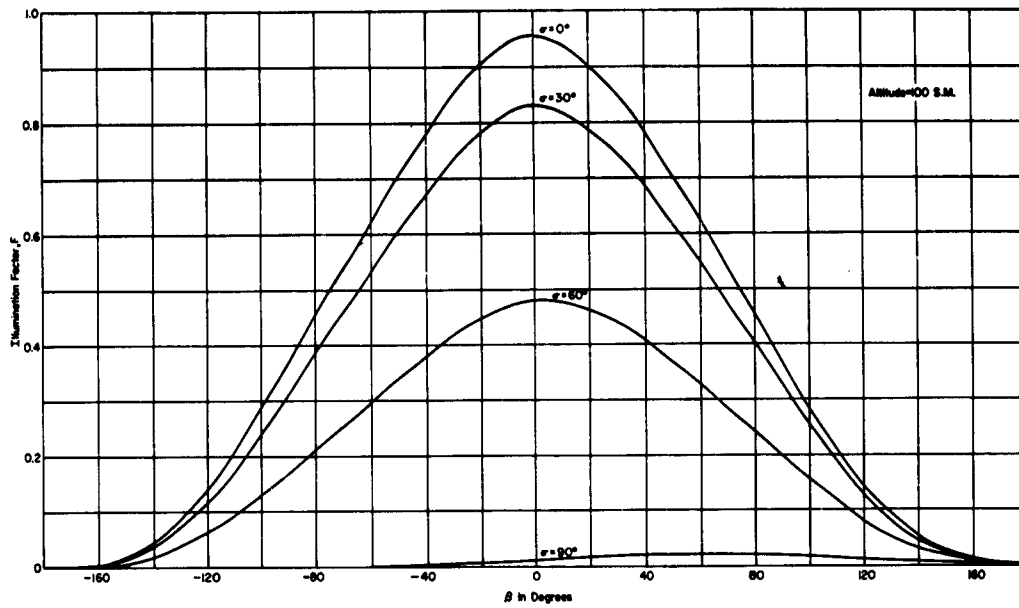

a. At 100 S. M. Altitude

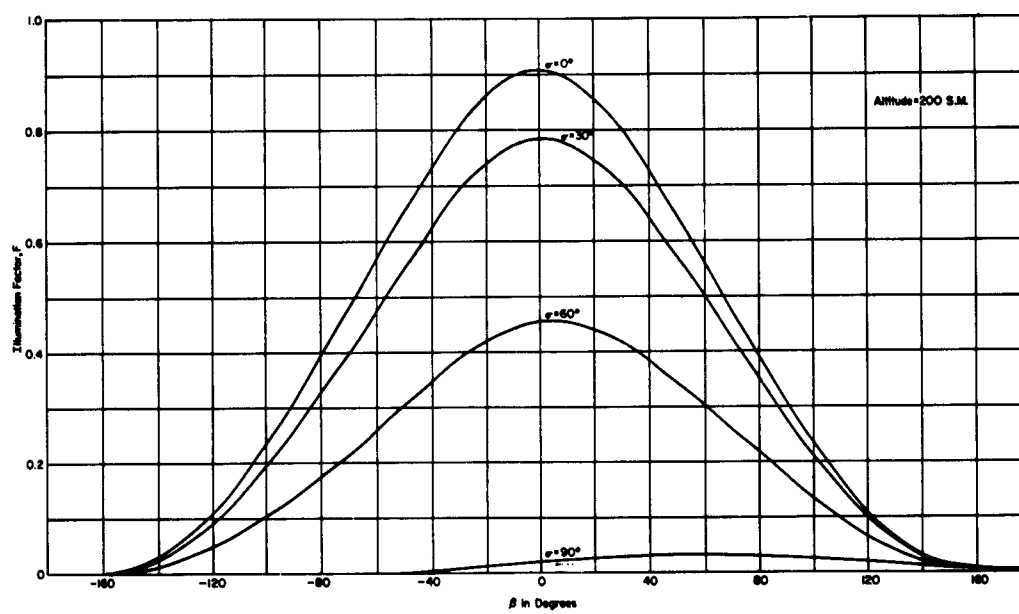

b. At 200 S. M. Altitude

Fig. 11 Illumination Factor as a Function of Elevation Angle, β, for Parametric Values of Orbital Position Angle, σ, at Various Satellite Altitudes

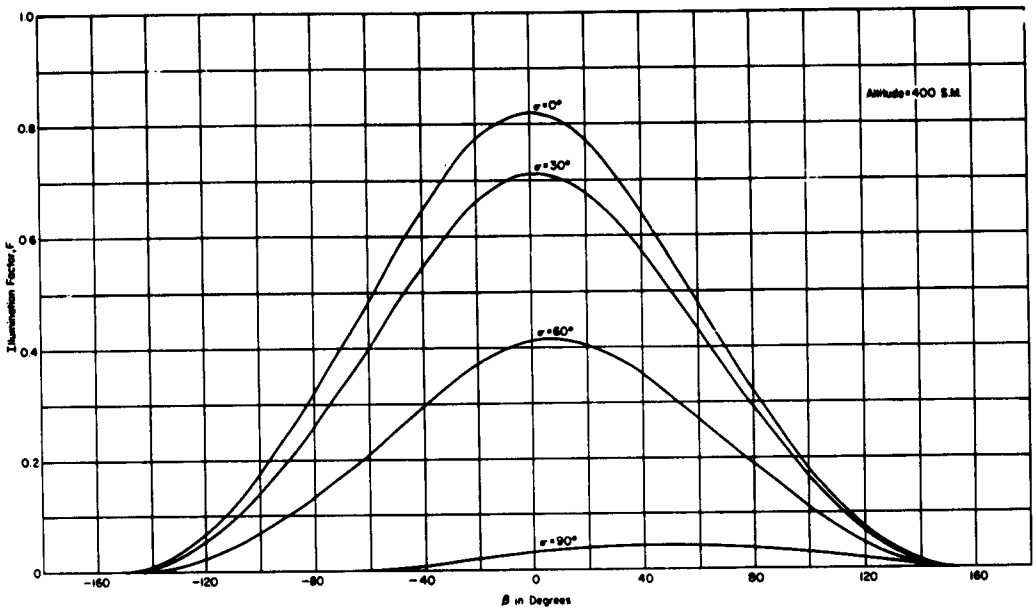

c. At 400 S. M. Altitude

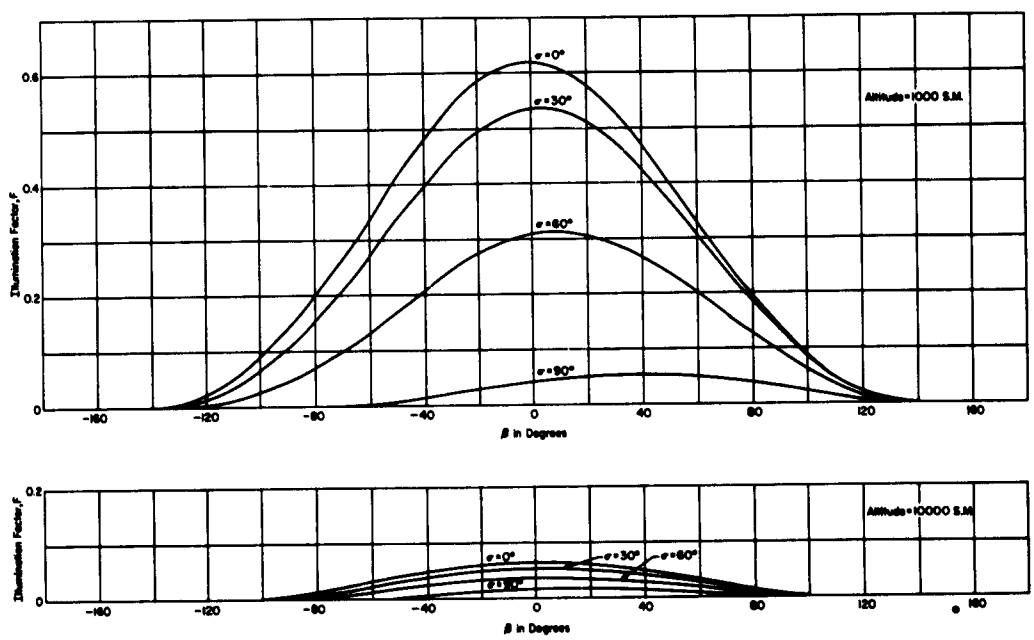

d. At 1000 and 10000 S. M. Altitude

Fig. 11 Concluded

At a low altitude a satellite located at $\sigma = 90°$ receives reflected energy from a very small region. As the altitude is increased at this orbital position, the reflecting region contributing albedo to the satellite is increased and F increases. Beyond an altitude somewhere between 1000 miles and 10,000 miles this increasing region of reflection is counterbalanced by the decreasing effect of the square of the distance.

A satellite located directly between the sun and the earth at $\sigma = 0°$ not only receives the maximum amount of reflected radiation, but also receives this radiation from a symmetrical distribution of reflecting regions. The satellite section whose surface normal points straight down, $\beta = 0°$, $\gamma = 0°$, therefore receives the maximum albedo.

At other orbital positions, $\sigma \neq 0°$, the reflecting regions are no longer symmetrically distributed relative to the satellite. Thus the shift of the peak F value along the β axis corresponds to a change in the viewing direction towards a region of greater illumination. This asymmetry is most pronounced at high σ values.

Variation of the yawing orientation, γ, can be visualized as the rotation of the unit area about the earth normal at Q. Stated in another way, γ can be treated as an azimuth angle about the earth normal at Q. As shown in Figure 12, rotation of the unit area 180° about the earth normal through Q, from a given β angle, say $\beta = +30°$ brings the unit area to $\beta = -30°$. Therefore the illumination at $\gamma = 0°$ corresponds to F at $\beta = +30°$ and the illumination at $\gamma = 180°$ to $\beta = -30°$. Furthermore since the illumination is symmetrical on either side of the plane formed by the sun-earth line and the earth normal through Q, this rotation can be accomplished in either direction.

If F is taken as a function of β and γ alone, the maximum value occurs for $\gamma = 0°$. Figure 13 shows that for β positive, F is a monotonic decreasing function of γ. Since the F variation between these extremes is small, a straight line approximation between extremes can be used.

Dennison's analysis and curves for describing the earth's albedo neglect a significant factor, the scattering of light within the atmosphere. A method which does include the effect of scattered radiation as well as diffuse reflected radiation has been developed in Russia by Feigelson, et al[19]. The Feigelson analysis is also based on limited experimental scattering data.

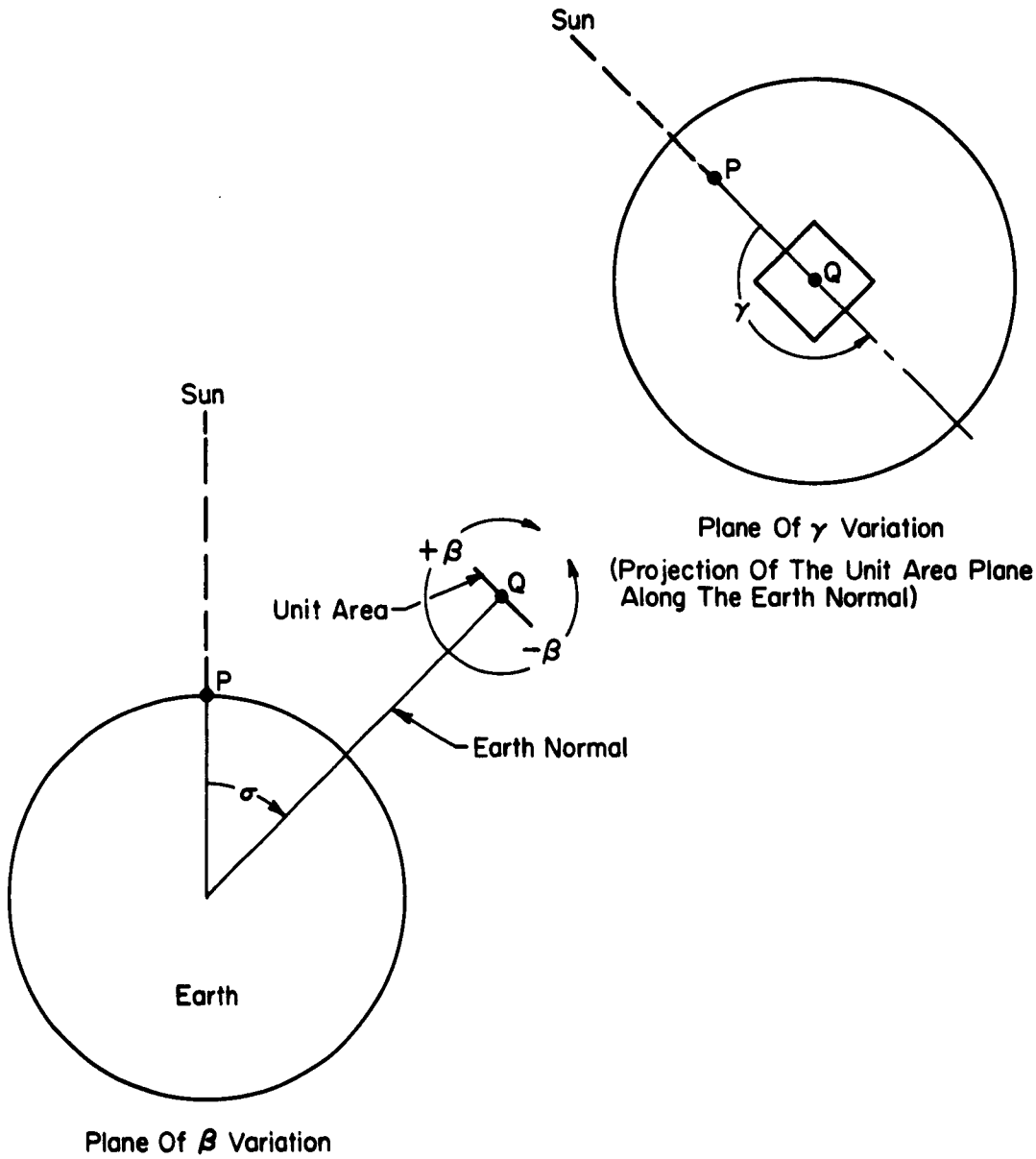

Fig. 12 Geometry of Azimuth Angle, γ

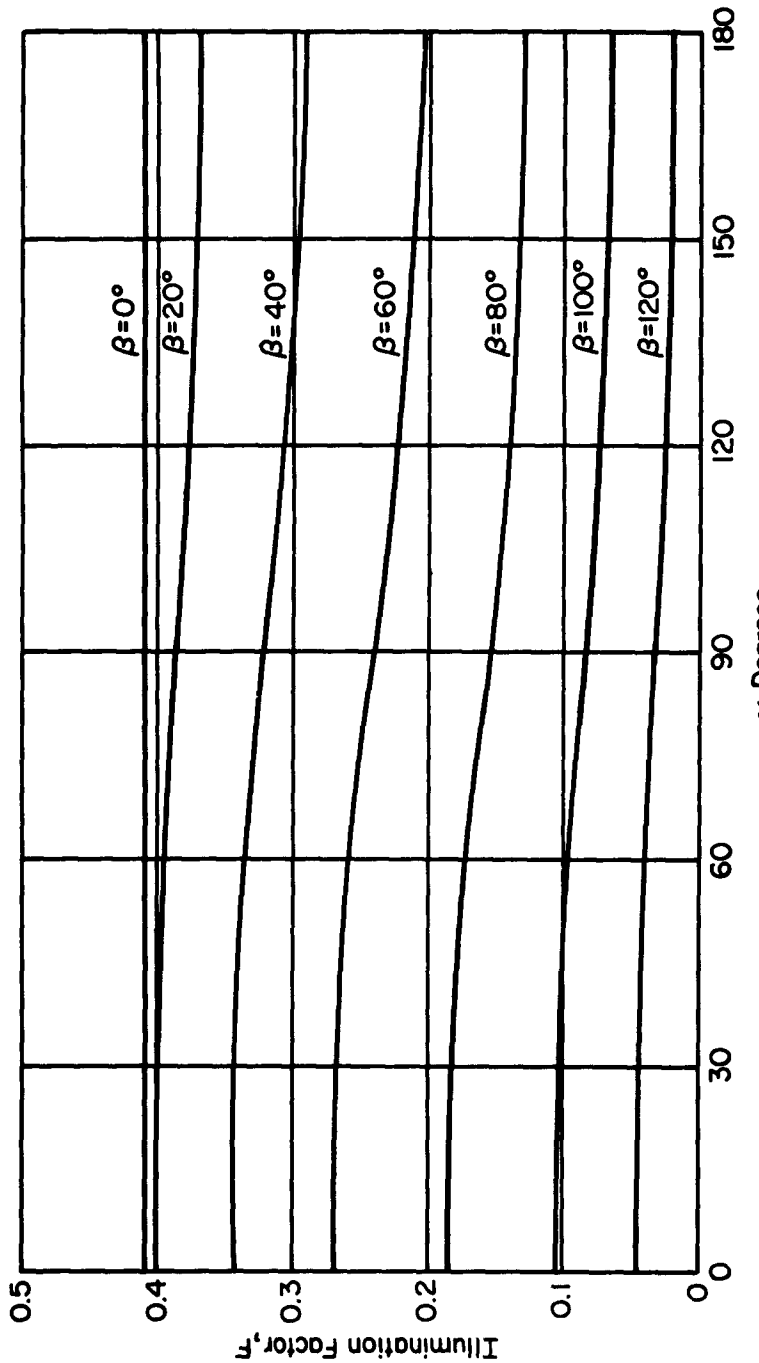

Position Angle, σ = 60°
Altitude = 400 S.M.

Fig. 13 Illumination Factor, F, as a Function of Azimuth Angle, γ for Parametric Values of Elevation Angle, β

While this method considers only the magnitude of the illumination escaping from the top of the atmosphere, the results can be extrapolated for other altitudes. Feigelson's work,which was done primarily to discover to what extent anisotropy of scattering should be taken into account when determining the conditions for propagation of light, may also be used in establishing the characteristics of the angular distribution of albedo.

The experimental scattering data for Feigelson's analysis were determined at three altitude levels. First, at the earth's surface, measurements were made of the brightness of a horizontal searchlight beam at various angles to its axis. Second for altitudes in the lower atmosphere, Feigelson refers to Waldram[20] who carried a nephelometer to a height of about 10 km and determined the dependence of the scattering functions on height for three types of atmosphere; very transparent, cloudy and transparent, and misty. The third method, covering very high altitude scattering characteristics, involved measurement of brightness of the sky in the circumsolar halo.

In order to simplify the mathematics, a number of assumptions were made regarding the relative character of the scattering relations as a function of height. A model of the atmosphere was assumed in which experimentally determined scattering functions were correlated with "atmospheric thicknesses." The optical thickness τ^* is assigned values from zero to unity in which 0.1 - 0.2 correspond to a very transparent atmosphere, 0.2 - 0.4 to a transparent atmosphere, 0.4 - 0.6 to a cloudy atmosphere, and 0.6 - 0.8 to a very cloudy atmosphere.

The earth's reflection, q, was assumed to obey Lambert's law and to vary between 0 and 1; that is, no reflection and total reflection. In addition a model was introduced to examine the illumination (I) at the top of the atmosphere in terms of the geometric parameters shown in Figure 14. The angles noted in this figure can be compared to similar angles in Dennison's work. ζ is equivalent to Dennison's σ; Θ is equivalent to Dennison's β, and ψ is equivalent to Dennison's γ.

The scattering functions and corresponding atmospheric optical thicknesses were substituted into the radiation transfer equations. Solutions to the integrodifferential equations were obtained by the method of successive approximations in terms of relative intensity units. Absolute values, however, may be obtained by multiplying the relative intensity I by (solar constant /2Π).

Figure 15 indicates the relationship between relative intensity and atmospheric

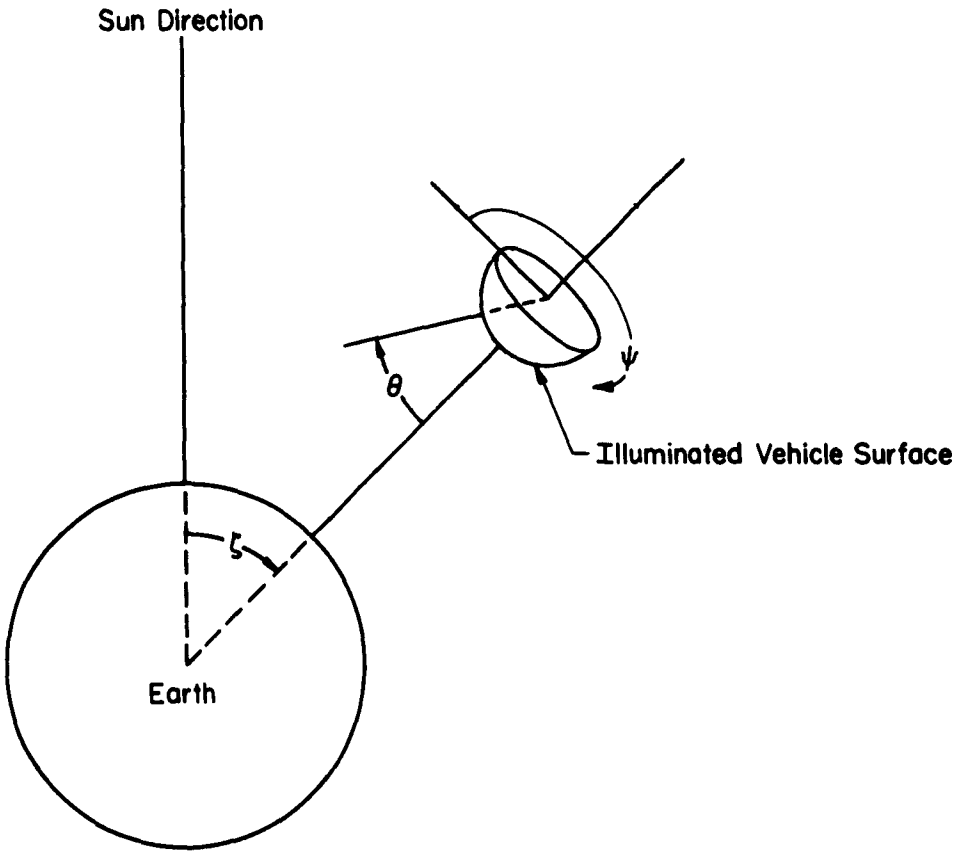

Fig. 14 Earth-Sun-Satellite Geometry for Analysis by Feigelson

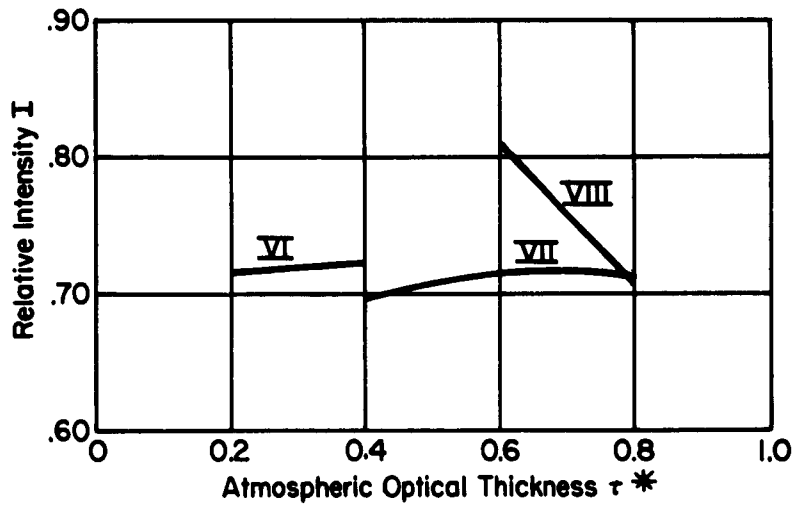

$q = 0.4, \quad \zeta = 30°$
$\Theta = 0°, \quad \psi = 0°$

Fig. 15 Relative Intensity as a Function of Atmospheric Optical Thickness for Three Scattering Functions

optical thickness for three selected scattering functions, VI, VII and VIII, under the stated conditions. This curve indicates that a variation in the scattering function has about a 12% effect on the relative intensity and that an increase in optical thickness tends to balance out the variation in the scattering function.

Variation of relative intensity with ζ is illustrated in Figure 16. The dotted curve represents data from Dennison. The important characteristic to note here is the slope of the two curves. The absolute value of Feigelson's curve is based on representative conditions. Variation of altitude is not considered in Feigelson's work while Dennison's is based on a 100 sm altitude.

Figure 17 indicates the importance of the reflection of the earth. Examination of data in the original text (Reference 19)indicates that, at about $q \approx 0.2$, the effect of the earth reflection becomes stronger than the effect of scattering on the relative intensity of illumination.

Figure 18 illustrates the variation of the relative intensity with azimuth angle ψ. The ψ variation corresponds closely to variations in γ as determined by Dennison except at $\Theta = 75°$ and $\zeta = 75°$ where an unexpected variation is found. The anomaly merits further examination.

The general results of the Feigelson et al analysis are in good agreement with Dennison's work. While Feigelson's analysis is by no means complete, it does show the direction towards improvement of the numerical values of the albedo distribution. Dennison however considered the altitude effect on intensity, not just intensity at the top of the atmosphere. Furthermore he included in his analysis a full variation of the orbital position and the satellite section orientation.

It is recommended therefore that the Dennison model of albedo distribution over the solid angle be used as a working model for initial design purposes. Further, it is recommended that experimental data on albedo intensity, angular distribution and spectral distribution be obtained at the altitudes of interest for satellite operations. Additional theoretical work using this data and following Feigelson's approach should be accomplished to refine the working model.

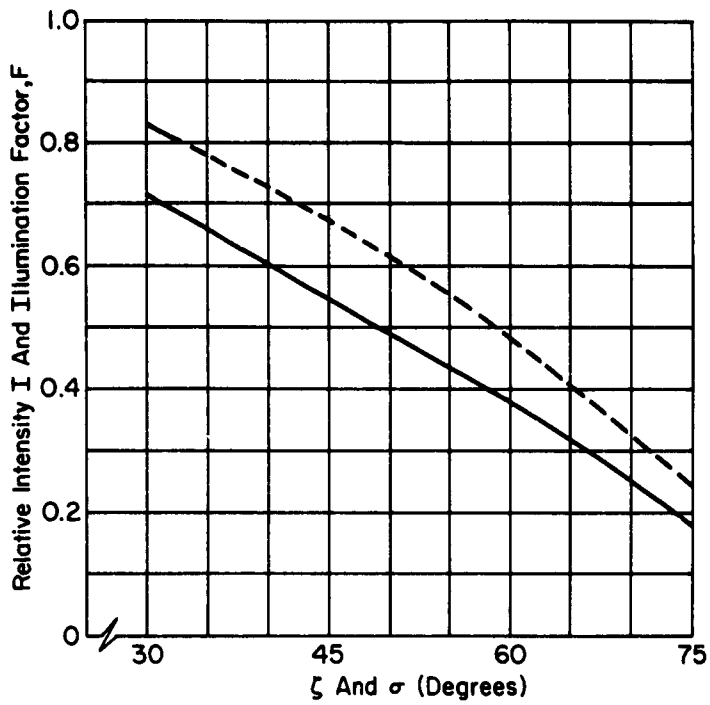

---DENNISON
β = 0°, γ = 0°
ALTITUDE = 100 S.M.

——FEIGELSON
q = 0.4, τ* = 0.6
Θ = 0°, ψ = 0°
Scattering Function: VII

Fig. 16 Comparison of Dennison's Illumination Factor, F, with Feigelson's Relative Intensity, I

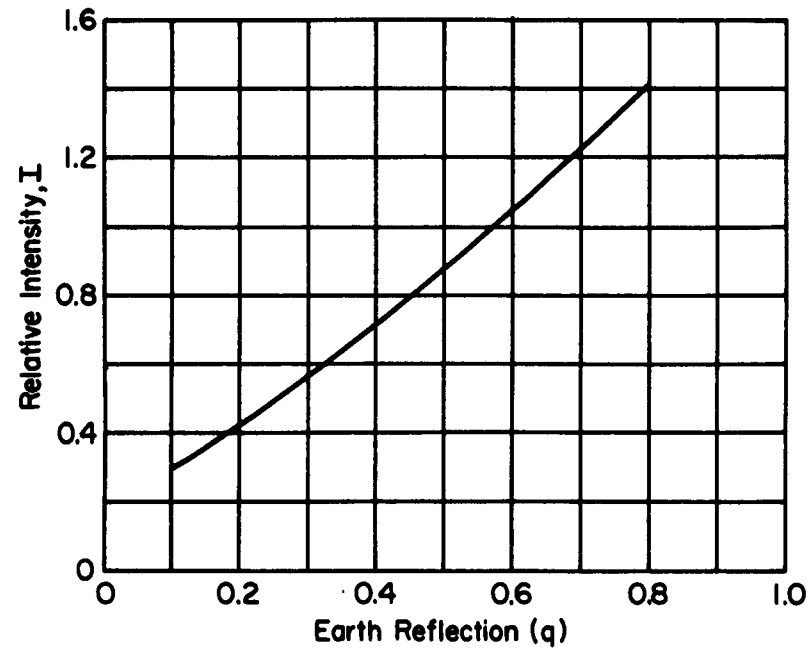

$\zeta = 30°$, $\tau^* = 0.6$
$\Theta = 0°$, $\psi = 0°$

Fig. 17 Relative Intensity as a Function of Earth Reflection

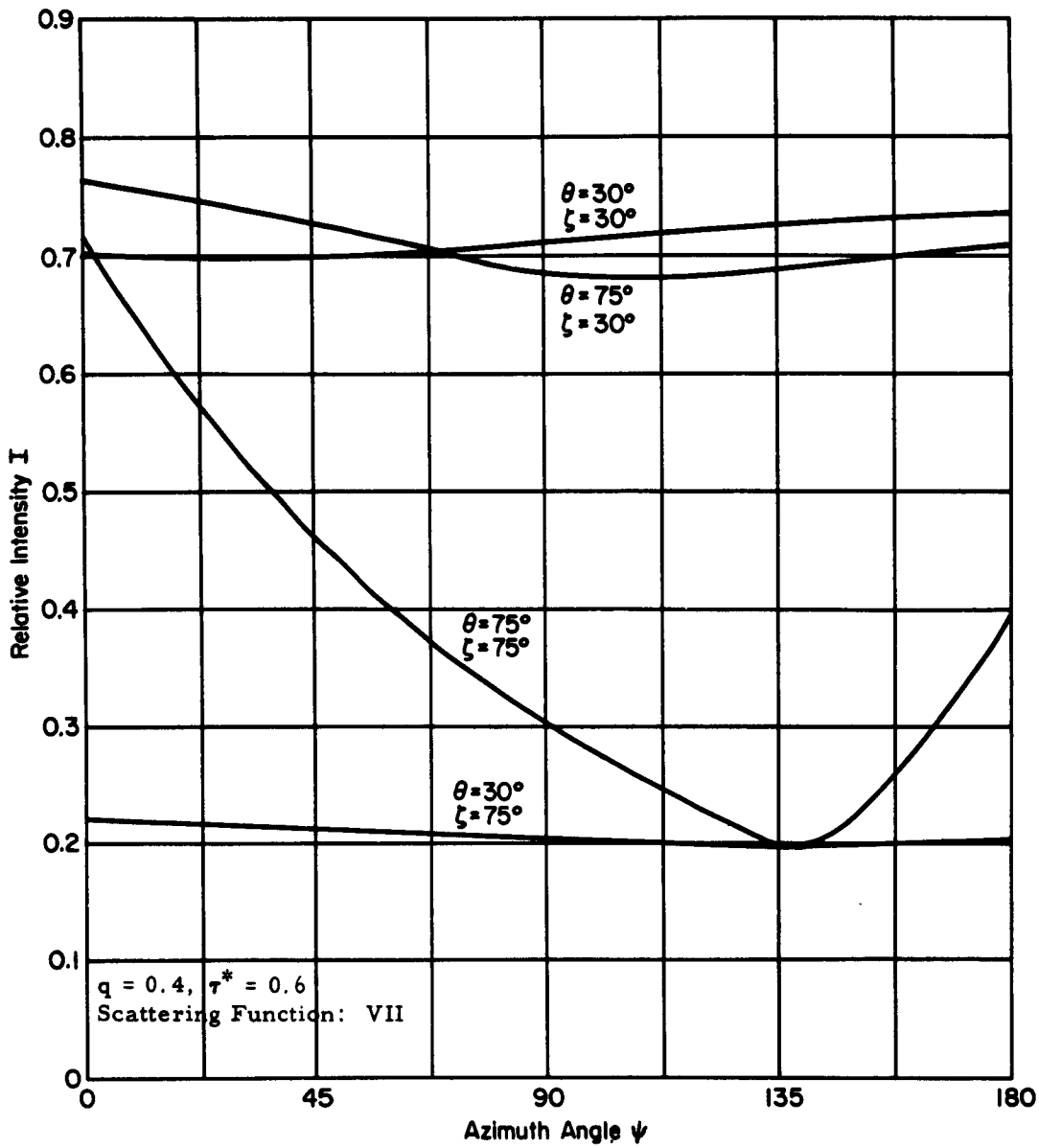

Fig. 18 Relative Intensity, I, as a Function of Azimuth Angle, ψ, for Four Positions

B. PLANET RADIATION

In comparison with albedo, the characteristics of planet radiation are somewhat easier to determine and to simulate. For instance, the earth radiates uniformly in all directions and all the time, a situation much simpler than the complicated position function found in the case of albedo. To a receiving satellite, planet radiation intensity again has an inverse square decrease with altitude and, again, the angle subtended by the earth decreases with altitude.

To an earth-oriented satellite, planet radiation always appears to be arriving from the same direction. To a satellite with this orientation the solar component would appear to be changing its direction of incidence. To a sun-oriented satellite, however, the solar component would appear fixed and the planet radiation would appear to change its incident direction.

The planet radiation, I_e, incident upon a satellite section has been expressed by Goetze and Grosch[21] as:

$$I_e = \frac{\alpha dA\, F_o}{\Pi} f_e \tag{4a}$$

$$f_e = \iint \frac{(\bar{r} \cdot \bar{n})\ (-\bar{r} \cdot \overline{N_1})}{r^4}\, d\Delta \tag{4b}$$

where

dA = Incremental surface element attached to satellite

F_o = Thermal power per unit area radiated into space

$\bar{r}$ = Vector having its initial point at dA and its terminus on the earth

$\bar{n}$ = Unit vector directed normally outward from dA

$\overline{N_1}$ = Unit vector directed normally outward from the earth at the terminus of r

$d\Delta$ = Dummy surface element

α = Average absorbtance of $d\Delta$ for the spectral content of the earth emitted radiation at the temperature prevalent on $d\Delta$.

These quantities are shown geometrically in Figure 19.

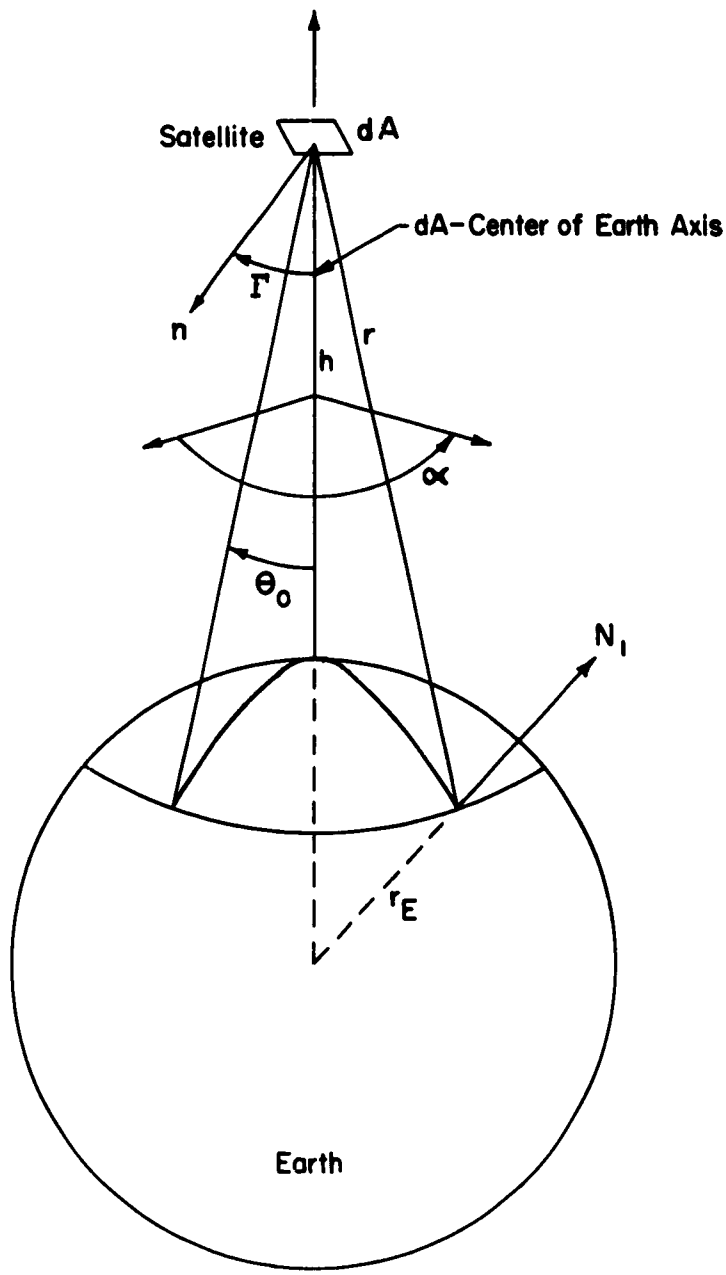

Fig. 19 Earth-Satellite Geometry for Analysis by Goetze and Grosch

Integration is performed over the portion of the earth's surface which is instantaneously visible to the particular surface element under consideration.

The illumination integral f_e may be simplified by application of the divergence theorem of vector analysis. The resulting equation may then be evaluated for the case in which the following relations are simultaneously satisfied.

$$\bar{r} \cdot \bar{n} \geq 0$$

$$\bar{r} \cdot \bar{N}_1 \geq 0$$

The expressions used to evaluate f_e for particular values of the view angle, Γ, and the ratio of altitude, h, to earth radius, r_E, are shown in Table V. Curves of the integral, fe, as a function of altitude and Γ are presented in Figure 20.

Yet another approach to the problem of computing the solar, albedo, and planetary radiation incident on a satellite utilizes a vectorial analysis method[27].

Supplement 1 compares the radiation data from TIROS II with the material in this report. Supplement 2 summarizes preliminary results on TIROS III radiation data.

TABLE V

ILLUMINATION INTEGRAL, f_e, FOR VALUES OF VIEW ANGLE, Γ

View Angle, Γ	Illumination Integral, f_e
0 to $\frac{\pi}{2} - \theta_0$	$\pi \sin^2 \theta \cos \Gamma$
$\frac{\pi}{2} - \theta_0$ to $\frac{\pi}{2} + \theta_0$	$a_0 \cos \Gamma \sin^2 \theta - \sin \Gamma \sin a_0 \sin \theta_0 \cos \theta_0 + \tan^{-1} (- \cos \Gamma \tan a_0)$
$90°$	$- \sin \theta_0 \cos \theta_0 + \theta_0$
$\frac{\pi}{2} + \theta_0$ to π	0

where: $\theta_0 = \sin^{-1} \left[\frac{1}{1 + \frac{h}{r_E}} \right]$

$a_0 = \cos^{-1} (- \cot \Gamma \cot \theta_0)$

$0 \leq a_0 \leq \pi$

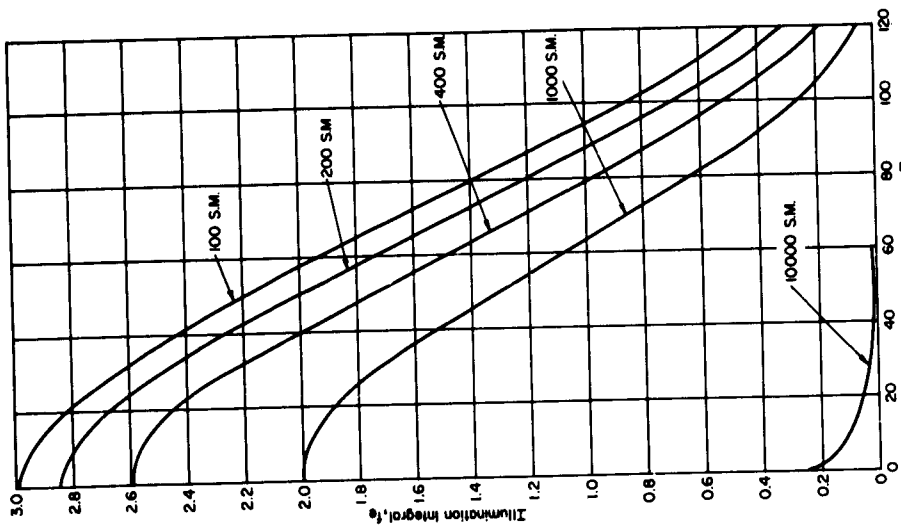

Fig. 20b Illumination Integral, f_e, As a Function of View Angle, Γ For Parametric Values of Satellite Altitude

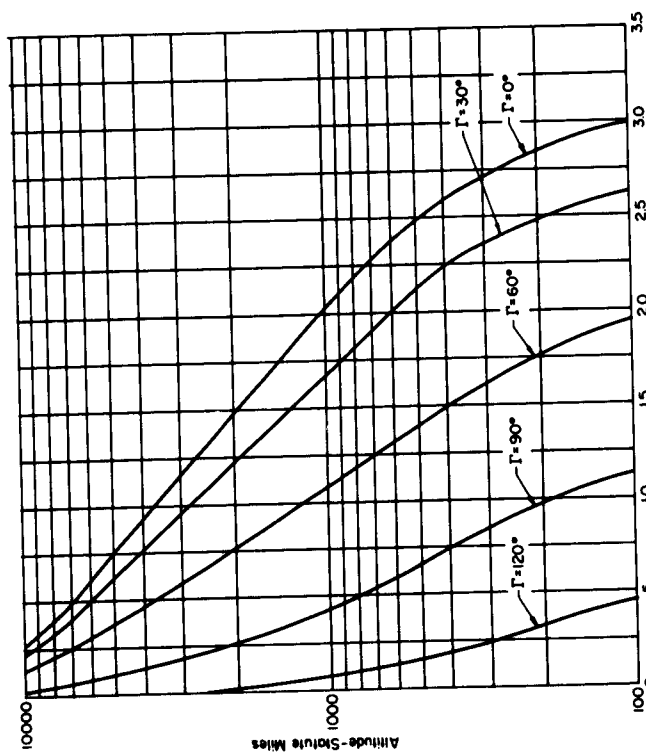

Fig. 20a Altitude of Satellite as a Function of the Illumination Integral, f_e, For Parametric Values of View Angle, Γ

C. TOTAL RADIATION INCIDENT ON A SATELLITE

Figure 21 presents the angular distribution, with respect to the elevation angle β, of the solar, albedo, planet and total radiation for several orbital positions of the satellite. The altitude selected for these curves was 100 statute miles and Dennison's model and notation for albedo distribution were used.

It is significant to note that the magnitude of the total secondary radiation at $\sigma = 0°$, $\beta = 0°$ is almost one-half of the maximum solar radiation (see Figure 21a).

In these curves the solar intensity was assumed to be 1396 watts/m^2. The albedo intensity was determined by multiplying the solar intensity by 0.36, the average reflection, and then multiplying again by the appropriate F factor for the position under consideration. Planet radiation intensity was determined by multiplying the appropriate f_e factor by F_o/π where F_o is taken as 200 watts/m^2 at the surface of the earth.

Unfortunately, the several components of total radiation do not have exactly the same spectral distribution. The spectral distribution of albedo is sufficiently close to the solar spectrum, however to be considered the same for simulation purposes. Planet radiation, corresponding to radiation from a 250° blackbody, must be treated separately.

The ambient radiation in the vicinity of the earth therefore may be considered to be composed of two principal parts. The first is the radiation whose spectral distribution corresponds to a 6000°K blackbody and whose angular distribution is the sum of the solar plus albedo at each angular position. The second part is radiation with a 250° blackbody spectral distribution and the angular distribution previously determined for planet radiation. Figure 22 illustrates these two radiation elements over a range of β values at an orbital position of $\sigma = 30°$.

A last characteristic which must not be ignored is the property of uniformity. The region over which the radiation properties may be considered constant is considerably greater than the physical size of any foreseeable space vehicle. Thus over any test region the radiation properties must be uniform.

The several characteristics of albedo and planet radiation discussed in the last two chapters are summarized and compared with the properties of solar radiation in Table VI.

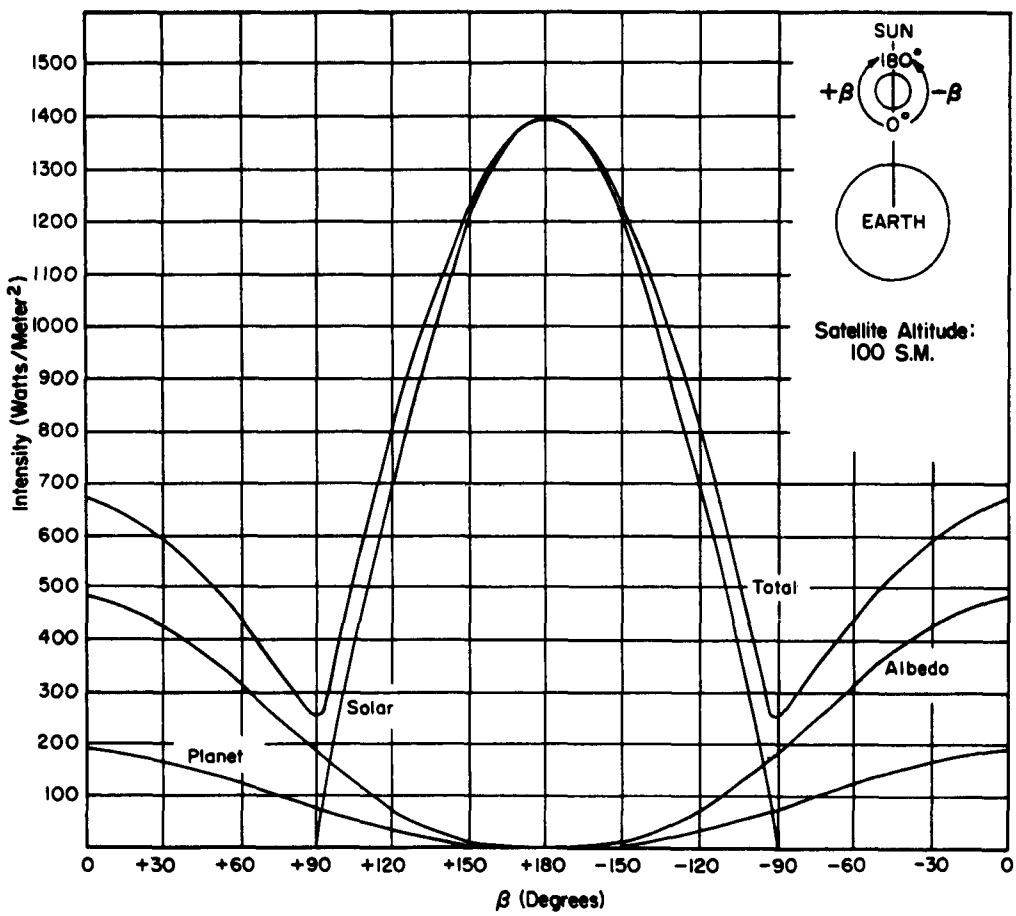

a. Radiation Intensity for $\sigma = 0°$

Fig. 21 Intensity of Solar, Albedo, Planet and Total Radiation as a Function of β for Various Values of σ

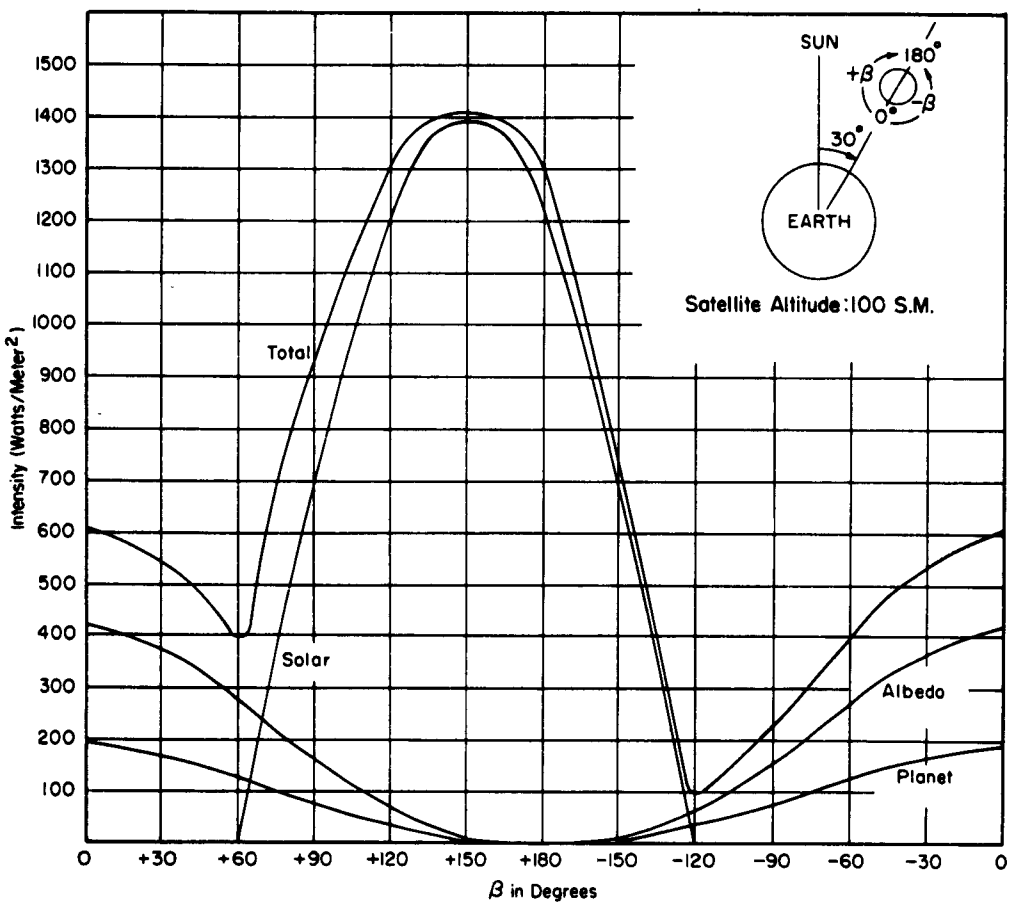

b. Radiation Intensity for $\sigma = 30°$

Fig. 21 Continued

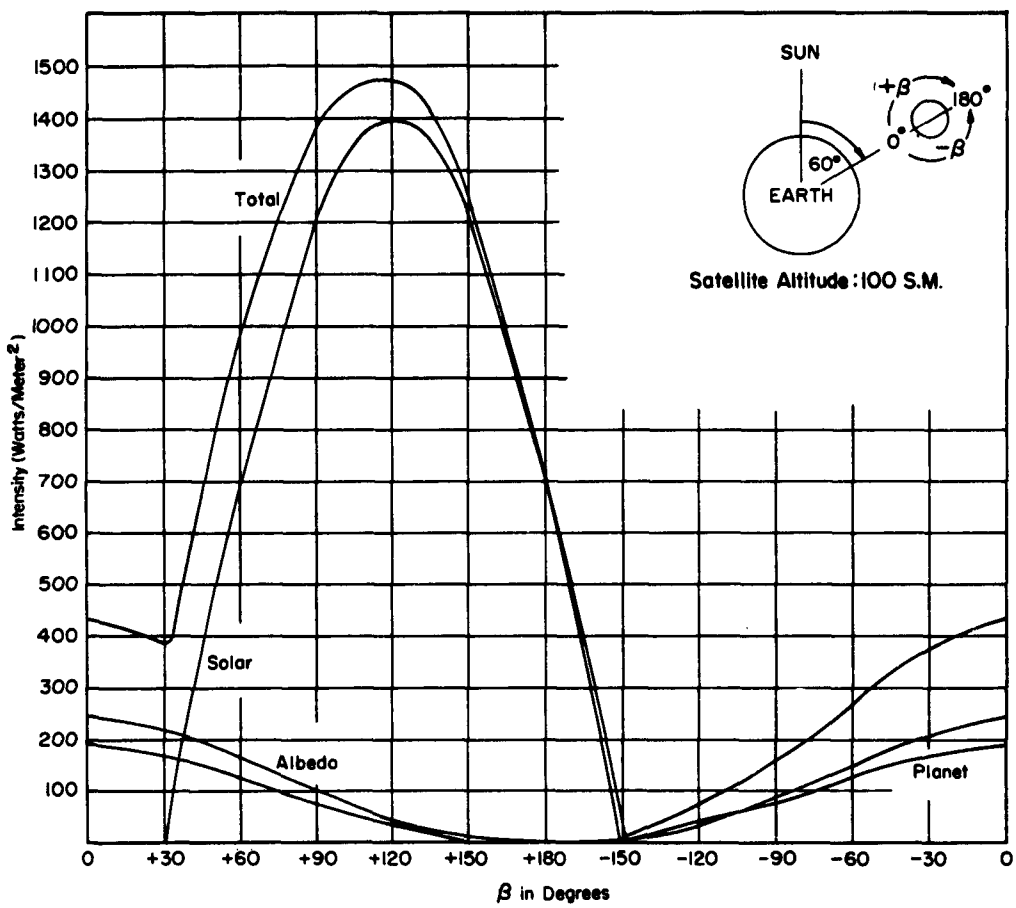

c. Radiation Intensity for $\sigma = 60°$

Fig. 21 Continued

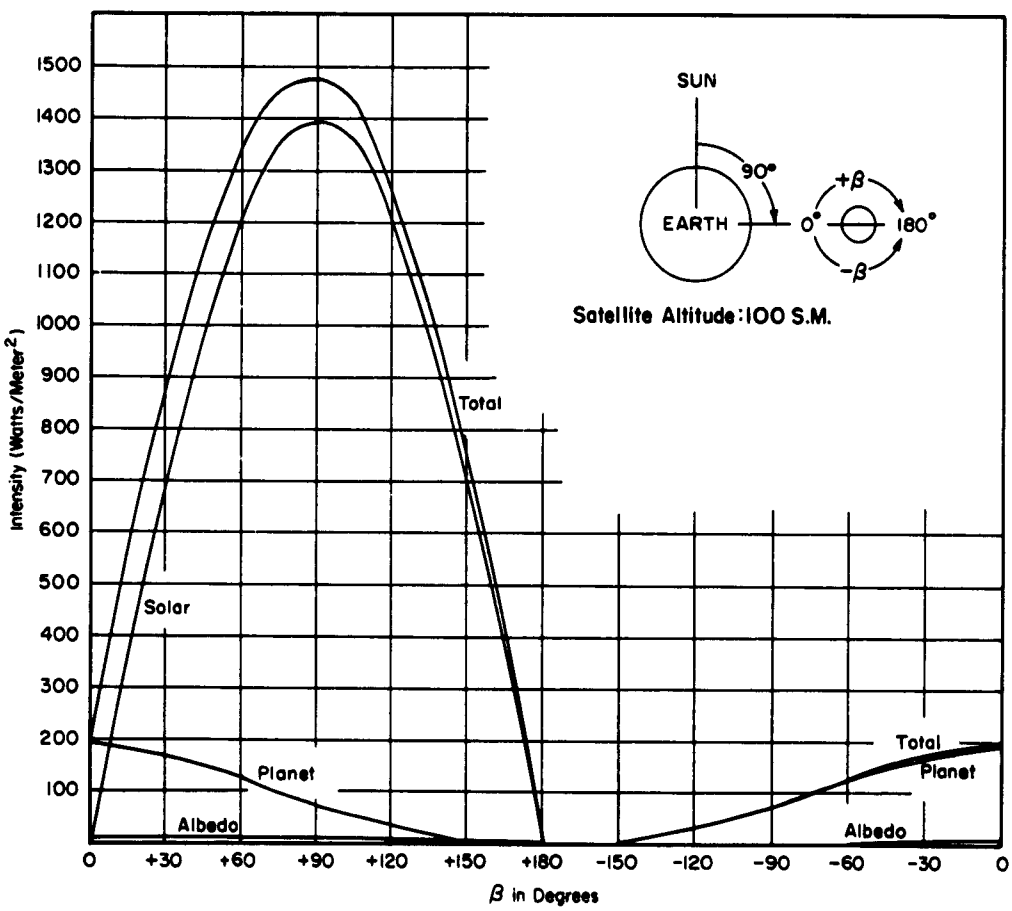

d. Radiation Intensity for $\sigma = 90°$

Fig. 21 Continued

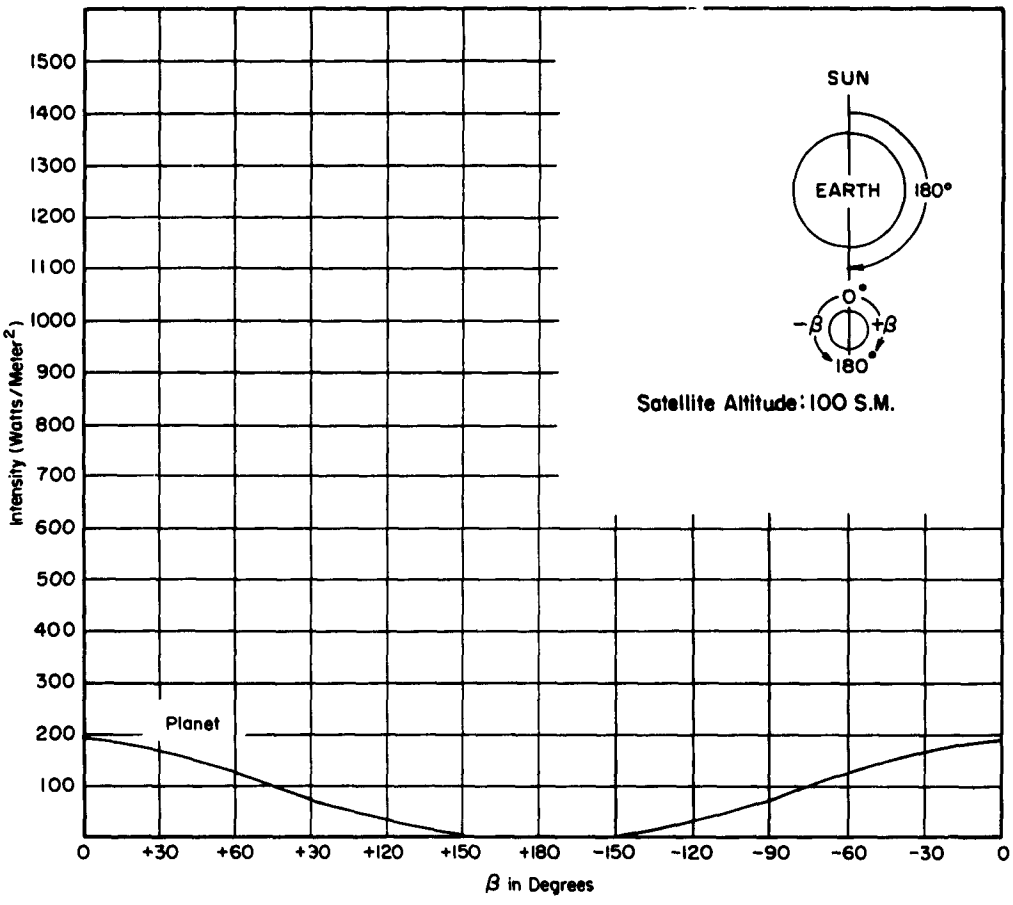

e. Radiation Intensity for $\sigma = 180°$

Fig. 21 Concluded

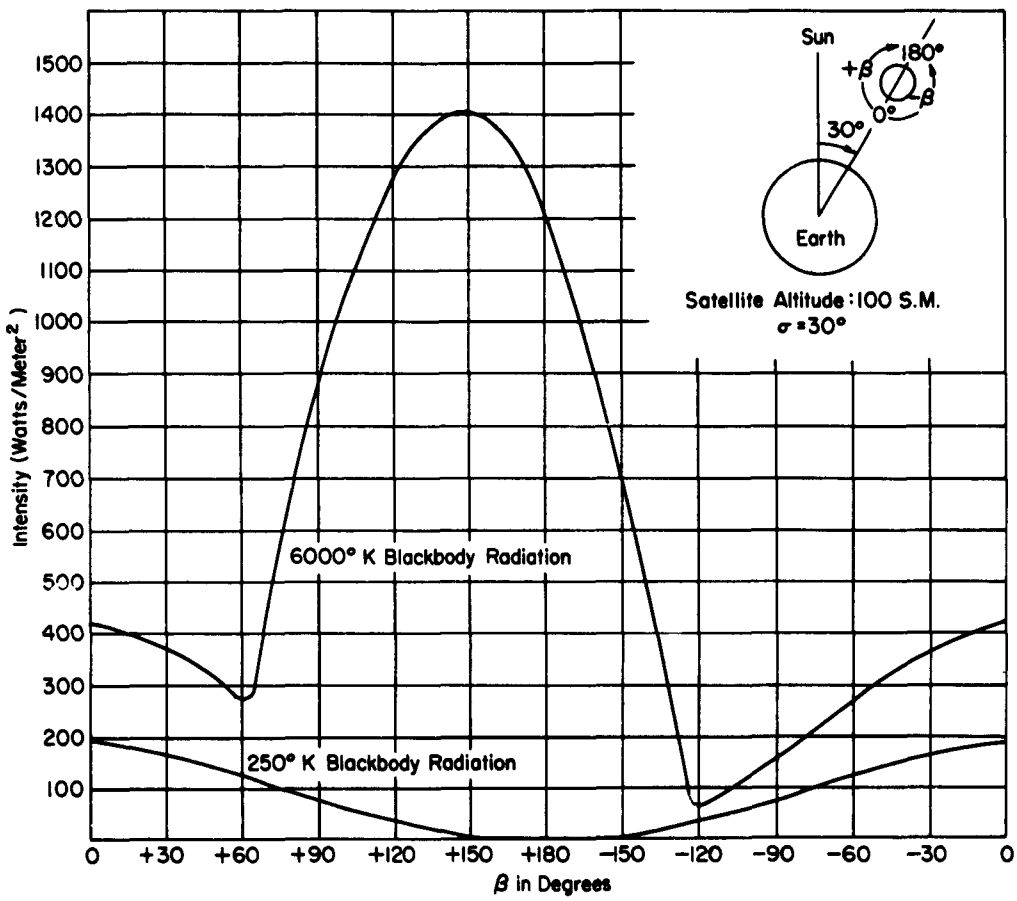

Fig. 22 Radiation Intensity upon an Earth Satellite from a 6000°K Blackbody and a 250°K Blackbody

TABLE VI

CHARACTERISTICS OF SOLAR, ALBEDO, AND PLANET RADIATION

	SOLAR	ALBEDO	PLANET RADIATION
Spectral Distribution corresponds to blackbody radiating at temperature	6000°K	6000°K	250°K
Total Intensity (watts/cm^2)	0.1396 ± 0.0028 ± 3.4% over year	0.0500(maximum) (varies with position)	.0224
Collimation Angle	32'	154° at 100 s.m.	154° at 100 s.m.
Position of Radiating Source	Constant	Moving	Moving
Duration of Radiation	While in sunlit hemisphere	While in sunlit hemisphere	At all times
Altitude Effect	Not appreciable	Inverse square	Inverse square
Uniformity	Constant	Constant	Constant

V. RADIATION EFFECTS AND SIMULATION TOLERANCES

Simulation of the radiation characteristics described in Chapter IV would be a difficult and expensive task. The problems encountered in simulating the properties of solar radiation alone have proved severe. Adding to the solar radiation properties, the changing characteristics of albedo and planet radiation can be expected to increase the complexity and cost by a substantial amount.

On the other hand it should not be necessary to simulate exactly the properties of the several radiation fields. By reducing the accuracy with which each radiation characteristic is simulated, the technical difficulty and the cost of the facility should decrease.

The question then is "How much of an accuracy reduction can be allowed without impairing the value of the tests to be performed in the facility?" This question is best answered in terms of the possible test effects.

A. RADIATION EFFECTS

Radiation effects on space craft can be grouped in two principal classes: thermal effects and material effects. Thermal effects depend upon the temperature and, therefore, the energy balance. Energy absorbed by the satellite will heat the satellite to a temperature at which energy is reradiated at the same rate as it is absorbed. If the equilibrium temperature is not within the design temperature range, the satellite structure, satellite surface, and, most important, the payload may not function correctly. Material effects such as chemical degradation, variations in the surface absorptivity, emissivity, photoconductivity, and photovoltaic effect can take place. Changes in the mechanical and thermal properties of inorganic and organic materials also can be expected.

1. Thermal Effects

Let us consider first the relation between the equilibrium temperature and the energy sources. Assuming the time to establish a uniform temperature throughout a satellite system is short in comparison to the time the satellite takes to pass into the thermal environment, the equation for temperature rate of change of a surface section may be expressed as:

$$\frac{dT}{dt} = \frac{\Sigma e_{\lambda\,sol}\,\alpha_\lambda + \Sigma e_{\lambda\,alb}\,\alpha_\lambda + \Sigma e_{\lambda\,pla}\,\alpha_\lambda + Q - \epsilon\,\sigma_s\,T^4}{mc} \qquad (5)$$

where:

T = Temperature of the satellite section

$e_{\lambda sol}$ = Solar radiation energy rate at wave length λ

$e_{\lambda alb}$ = Albedo energy rate at wave length λ

$e_{\lambda pla}$ = Planet radiation energy rate at wave length λ

α_λ = Absorptivity of surface at wave length λ

$\Sigma e_{\lambda sol} \alpha_\lambda$ = Total solar energy absorbed by surface section

Q = Thermal power generated by payload

ϵ = Emissivity of surface

σ_s = Stefan-Boltzmann Constant

mc = Heat capacity of satellite

This equation is valid only for small sections on a satellite over which the radiation intensity does not change appreciably. It is particularly adaptable to low-thermal-conductivity surface sections of the type which will probably be used in the second generation expanded satellites for space stations, rendezvous missions, etc. Over such structures the surface temperature will vary from point to point depending upon the incident energy on the differential section.

To apply Equation 5 to the entire satellite, the rate of heat transfer by conduction from one part of the shell to another must be much greater than the rate of heat transfer by radiation between the surface of the shell and the surrounding environment.

It should be noted that the temperature of a surface section is dependent upon the absorptivity characteristics of the surface element as well as the incident energy. In turn, absorptivity varies widely with materials and has a strong spectral dependence. As an example, Figure 23 illustrates the wavelength dependence of the absorptivity of aluminum for two surface conditions.

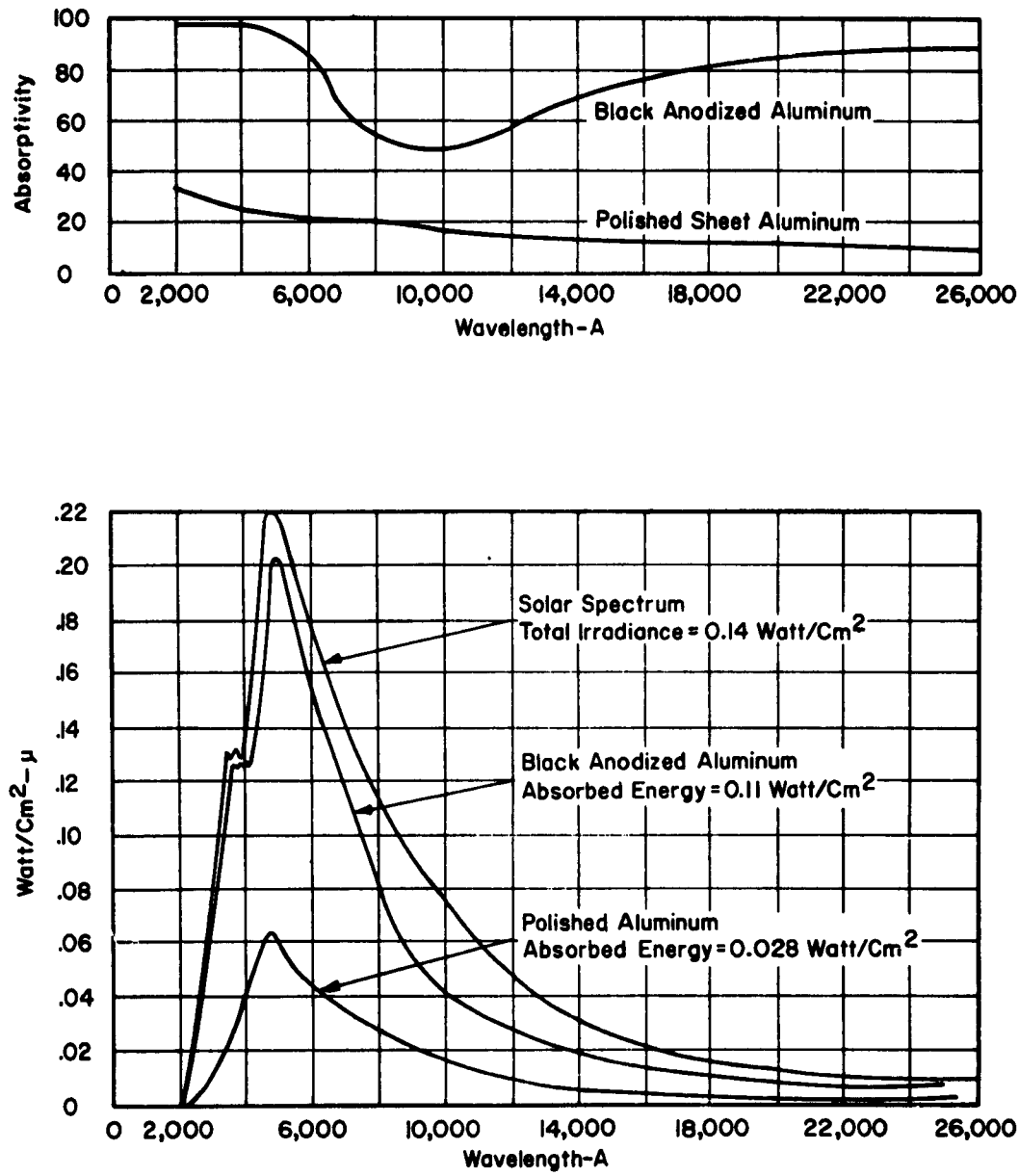

Fig. 23 Solar Energy Absorbed by Two Aluminum Surface Conditions

It also shows solar energy absorbed by these materials as compared to the total solar energy. In this case the energy absorbed by the black anodized aluminum is nearly three times that of the polished aluminum.

Still another problem is the possible change of absorptivity following exposure to radiation fields. Radiation may cause a chemical degradation of the surface material accompanied by a change of absorptivity which would completely change the energy balance and the equilibrium temperature.

2. Material Effects

Most material effects are caused by radiation in the ultraviolet region. Radiation longer than 4000 A is not likely to cause extensive damage to engineering materials. If a material cannot withstand exposure to these wavelengths, commonly encountered at the earth's surface, the material is not likely to be of engineering interest[22].

Incident electromagnetic radiation can affect the properties of a material only if it is absorbed in the material; for major changes to occur, the radiation must be strongly absorbed so that there is a high dose rate per gram of material. This strong absorption means that the radiation will probably penetrate only to a shallow depth. Accordingly, damage induced by electromagnetic radiation is most likely to occur in external surfaces, coating and exposed optical surfaces.

Metals and Alloys: Metals and alloys are unaffected by radiation-induced ionization and excitation. Displacement can be caused only by wavelengths below 10^{-1} A. Such radiation amounts to 10^{9} to 10^{10} photons/cm^2-yr. The solar photons will displace 10^{-16} to 10^{-14} of the atoms within their range. As metals and alloys withstand displacements of 10^{-6} of their atoms or more without detriment to engineering properties, these materials will not be damaged by solar photons.[22]

Semiconductors: The engineering properties of semiconductors will not be permanently changed by solar radiation. Although minority carrier effects in semiconductor devices can be permanently changed by displacement of 10^{-12} to 10^{-10} of the atoms, the 10^{-16} to 10^{-14} displacement fraction produced by solar photons is several orders of magnitude smaller. However, changes will occur in the electrical properties because of electron hole pairs created by ionization and electron excitation.

Inorganic Insulator: The engineering properties of inorganic insulators are affected by atomic displacements only when 10^{-11} or more of the atoms are displaced. Again the 10^{-16} to 10^{-14} fractional displacements per year provided by sunlight would affect only the surface. Changes in dimensions and mechanical properties may take place, but, confined to such thin surface layers, they are likely to be important only in inflatable structures.

The effect of most interest is probably the increased optical absorption. Wavelengths up to 3000 A cause electronic excitation which affect optical behavior. The mechanism is as follows: excitation or ionization releases electrons from their equilibrium positions in the crystal lattice; some electrons do not return to these positions but become trapped elsewhere in the lattice, forming "color centers"; the "holes" remaining may also be trapped. Color centers absorb light in certain spectral regions (usually in the visible or ultraviolet regions) causing a change in the color of the material and producing a general darkening. This darkening is important in transparent optical surfaces and in light-colored pigments used in temperature-control surfaces.

Most glasses will undergo color center development and corresponding loss of optical transmission on exposures to the solar radiation of space. These color centers will be partially bleached by exposure to the longer ultraviolet and visible radiation accompanying the discoloring short wavelengths. "Non-browning" optical glasses, containing cerium, have been developed for high resistance to discoloration by neutrons and gamma rays. Discoloration by ultraviolet radiation is also reduced by cerium and perhaps by lead.

Organic Materials: Organic materials, like inorganic insulators, will receive ionization dosages of 10^{12} to 10^{15} erg/g-yr from sunlight of 100 to 1000 A wavelength in surface layers 10^{-4} to 10^{-7} cm thick. Such doses will cause severe damage to the properties of thin exposed layers of all known polymers. The changes in optical properties, reflectivity, absorptivity and transmission--are most likely to be of importance. However, the success of the organically coated "Transit" satellite series has cast some questions on the actual magnitude of the deterioration. Electronic excitation produced by the solar wavelengths 1000 to 3000 A can also produce significant property changes to considerably greater depths. Even if the 5×10^{11} erg/cm^2-yr contained in sunlight below 3000 A is absorbed over a distance as great as 10 cm (about 10 g/cm^2), the excitation dose would be 5×10^{10} erg/g-yr. Ionization doses of this magnitude damage most organics; excitation doses may cause somewhat less damage but are still likely to be significant.

The changes produced in polymers by ultraviolet light are due to excitation producing free radicals which cause two general types of chemical change in high polymers: first, decomposition of polymer chains into smaller fragments, and second, cross-linking of the chains. The decomposition,which is retarded in vacuum is usually accompanied by loss of mechanical strength and elastic deflection and degradation of electrical properties. The second process, cross-linking, is more important in space. Cross-linking, up to a point, increases mechanical hardness and strength and does not degrade the electrical properties. Cross-linking reduces elastic deflection and is, therefore, usually undesirable in elastomers. If continued, it eventually embrittles other polymers to the point where surface flaking and fractures occur.

Some experiments have been reported on irradiation of polymers with wavelengths of 100 to 3000 A.[22] In the later experiments, films of commercial phenyl silicone, vinyl chloride, and methyl methacrylate polymers underwent appreciable cross-linking on exposure equivalent to a few days in space sunlight at 70°C (160°F); unvulcanized natural rubber underwent appreciable cross-linking in less than a day. At exposures corresponding to a week or two in space, polyethylene, polyethylene terephthalate(mylar),polyvinyl chloride (plasticized) and in some tests polytetrafluoroethylene, were discolored and lost much of their mechanical strength and elongation or flexibility[24]. The absorption coefficient increased moderately and indications are that most of the discoloring would occur in the first few weeks of exposure to sunlight. Regarding the mechanical properties at exposures equivalent to a month to a year in space, a phenyl methyl silicone (at 90°C) suffered severe loss of bend flexibility.

A recent test series reported by M. Simpson[25] relating to the UV exposure of propellant actuated devices showed that after 180 hours of exposure to solar radiation 75% of the test cartridges failed to ignite and after 504 hours, 100% of the test cartridges failed to ignite. The units that did fire indicated an abnormal condition resulting in greater peak pressures.

B. SIMULATION TOLERANCES

The material effects requiring testing can generally be examined in small space simulation chambers. Large chambers such as the Mark I facility at Arnold Engineering Development Center probably would be reserved for tests of complete vehicles. In such tests it is expected that the thermal effects will be the most important.

On this assumption let us attempt to assign numerical values in consistent units to radiation simulation tolerances using Equation 5 as a base. Let us also assume that:

1. The internally generated thermal power, Q, is ignored.

2. The temperature has reached an equilibrium condition, i.e.,

$$\frac{dT}{dt} = 0.$$

3. The absorptivity, α_λ, and emissivity ϵ_λ are equal to unity.

Equation 5 then reduces to:

$$E_{sol} + E_{alb} + E_{pla} = \sigma_s T^4 \tag{6}$$

where:

$$E_{sol} = \sum e_{\lambda\, sol} \cdot l$$

Differentiating Equation 6 and dividing by the original equation, we obtain:

$$\frac{\Delta E_{tot}}{E_{tot}} = 4\frac{\Delta T}{T} \tag{7}$$

where:

$$E_{tot} = E_{sol} + E_{alb} + E_{pla} \tag{8}$$

The maximum temperature variation of a surface section, ΔT, can be used as the basis for a set of radiation simulation tolerances. Rather than select a fixed ΔT value however, let us consider instead the temperature variation and the corresponding tolerances as variables of the simulation system. On this basis let us select, for tolerance studies, temperature variations ranging from 3 to 9 Kelvin degrees and examine the energy tolerances required. Further let us assume that the standard vehicle temperature is 300°K. Under these conditions $\frac{\Delta T}{T}$ ranges from 1% to 3% and the percentage change in the total energy rate varies from 4% to 12%.

To stay within the allowable energy variation for any specific ΔT, the same maximum energy tolerance could be placed on each of the component energy sources. This limitation would be unnecessarily restrictive, however, particularly on the complex energy sources such as albedo. Since the surface temperature is a function of the total energy, the limitation on energy variation should be placed only on total energy and greater freedom should be allowed in the variation of the energy of the individual components. By this philosophy a tightening of the tolerances on the large solar radiation component would allow relaxation of the tolerances on the smaller albedo and planet radiation components.

1. Angular Distribution

The angular distribution of several radiation components should be closely approximated because of:

1. Variations in satellite shape.
2. Variations in the satellite conductivity.
3. Variations in the satellite surface absorptivity and emissivity.

If the material of a satellite has infinite conductivity, unit absorptivity, and unit emissivity and if the satellite is spherical in shape, the direction from which the radiant energy is supplied is not significant. All the radiant energy could be supplied from a single direction without altering the resulting energy and temperature condition. However, under unidirection illumination a variation in any one of these parameters would lead to an error in the energy temperature distribution. For example, the temperature discrepancy due to a variation in the satellite shape can be determined as follows. Assume that all of the radiation is beamed from a single direction with an intensity I. At equilibrium the energy balance is:

$$I A_p = A_t \sigma_s T^4 \tag{9}$$

where:

A_p = area of illuminated surface

A_t = area of emitting surface

For a few simple cases the values of A_t, A_p and the ratio A_t/A_p are:

	A_t	A_P	A_t/A_P
Sphere	$4\pi R^2$	πR^2	4
Cylinder (axis parallel to radiation)	$2\pi RL + 2\pi R^2$	πR^2	$2(L/R+1)$
Cone (axis parallel to radiation)	$\pi R\sqrt{R^2+L^2} + \pi R^2$	πR^2	$\sqrt{(L/R)^2+1} + 1$

The incident energy-temperature relation for these several bodies become:

Sphere	Cylinder	Cone
$I = 4\sigma_s T^4$	$I = 2(L/R + 1)\sigma_s T^4$	$I = (\sqrt{(L/R)^2 + 1} + 1)\sigma_s T^4$

For an intensity of 0.1396 watts/cm^2 corresponding to the solar constant at the earth, and an L/R ratio of 3, the surface temperatures for highly conductive bodies of the several shapes would be:

Shape	Surface Temperature
Sphere	280°K
Cylinder	255°K
Cone	276°K

Thus the surface temperature accompanying a collimated-beam is dependent upon the shape and orientation of the receiving body. If the thermal conductivity of the material were lower, the heat energy would not be distributed as readily throughout the body, and the temperature of a section of the surface would be more dependent upon the radiation energy incident upon that section.

Figure 24 shows surface temperatures, under two conditions, for three satellite shapes using low-conductivity materials. The surface temperatures for illumination by solar radiation are indicated in Figure 24a. Surface temperatures over the β parameter ($\gamma = 0$, $\sigma = 30°$, h = 100 s.m.) for albedo and planet radiation added to the solar are plotted in Figure 24b. In both situations the cylinder and cone are considered as sun-oriented.

The temperatures over the satellite surface would vary even more if the absorptivity and emissivity were to change with surface location. For these reasons it is desirable that the angular energy distribution be approximated as closely as possible. Numerical tolerance values placed on this parameter must be based, of course, on economical considerations as well as technical. It is inappropriate therefore to fix definite tolerances on the angular distribution prior to an anlysis of the possible simulation systems.

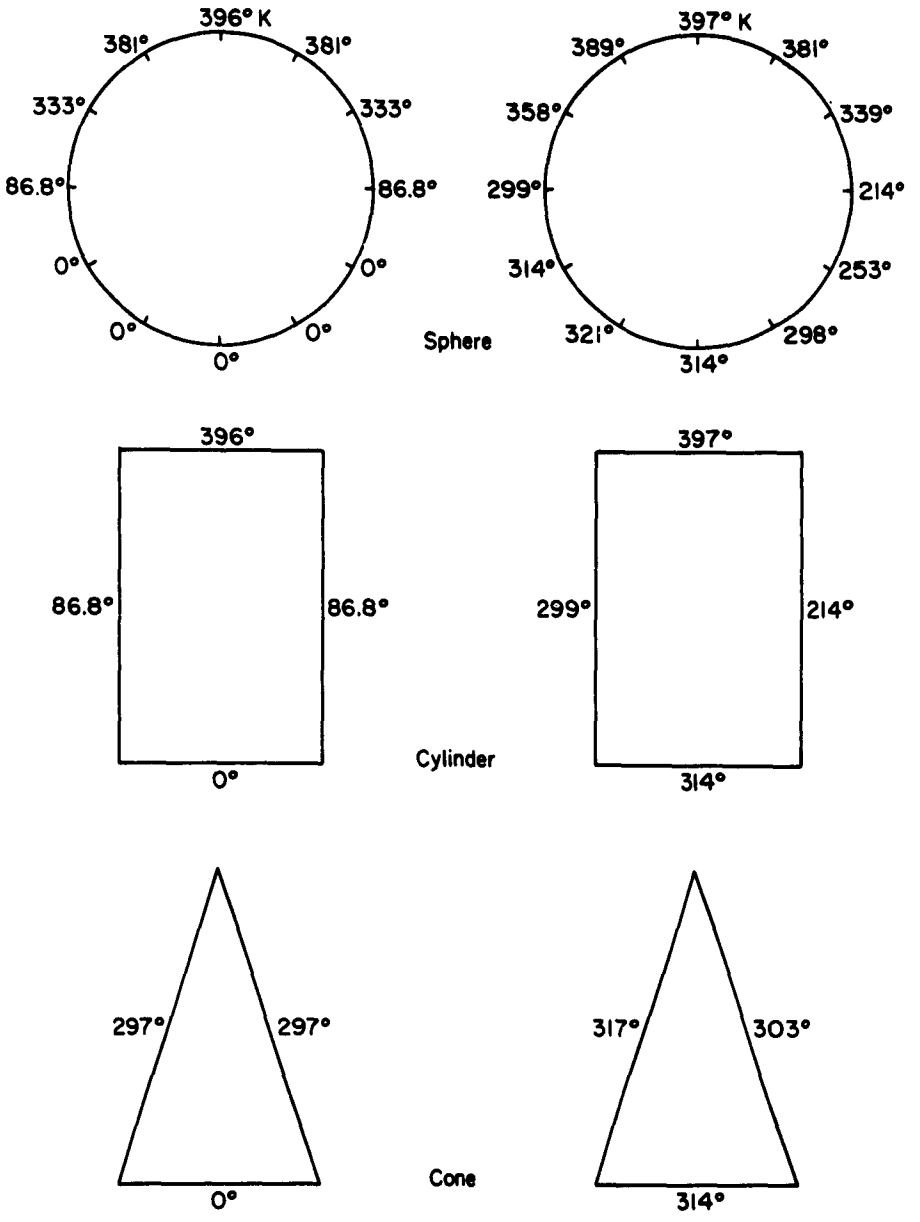

a. Solar Radiation

b. Solar Albedo and Planet Radiation
σ = 30, h = 100 S.M.

Fig. 24 Surface Temperature on Three Sun-Oriented Bodies Having Low Thermal Conductivity

2. Spectral Distribution

A match of the spectral distribution of the radiant energy is necessary to properly simulate conditions creating the material effects and to duplicate the correct total absorbed energy. This spectral match should be close in the ultraviolet region for materials effects testing and in the region of maximum spectral irradiance for thermal performance measurements. Beyond these wavelengths, tolerances on spectral match can be relaxed as long as total energy specifications are met.

Table VII lists the spectral distribution recommended for solar simulation by General Electric [26]. Note that General Electric recommends larger tolerances in the ultraviolet and infrared than in the region of peak spectral irradiance.

Tolerances placed by Arnold Engineering Development Center on the solar radiation spectral quality for their Mark I facility are presented in Table VIII. Energy increments for sample bandwidths and the allowed energy tolerance for these bandwidths are also listed. By choosing bands of various widths across the spectrum it is possible to keep the energy increment in each band at about the same size and therefore hold the bandwidth energy tolerance at approximately the same value. On the basis of a constant energy interval, it would be appropriate to subdivide the bands in the region of maximum spectral irradiance to 1000 A intervals and to combine the last several bands in the infrared.

Albedo, as previously indicated, has a spectral distribution similar to solar radiation and a maximum intensity approximately a third that of solar. Therefore the energy increments of albedo in comparable spectral bandwidths are under maximum condition only a third as great as the solar. Thus, in setting up spectral match specifications based on the same bandwidth energy tolerance (ΔE_λ) as solar, the albedo bandwidth can either be expanded by a factor of three or the percentage error increased in each band by the same factor.

TABLE VII

TOLERANCES RECOMMENDED BY GENERAL ELECTRIC FOR SOLAR SPECTRAL MATCH

Spectral Band A	Portion of Total Energy %	General Electric Energy Match %
2000 - 2500	.2	±15
2500 - 3300	2.8	10
3300 - 4000	6	10
4000 - 5000	14	10
5000 - 7000	26	10
7000 - 8000	9	10
8000 - 9000	8	10
9000 - 11,000	11	10
11,000 - 15,000	12	10
15,000 - 20,000	6	15
20,000 - 30,000	4	15

TABLE VIII

SPECIFICATIONS FOR SPECTRAL DISTRIBUTION OF THE SOLAR RADIATION COMPONENT IN THE AEDC AEROSPACE SIMULATOR

MARK I

Spectral Range (A)	Bandwidth (A)	Tolerance (%)
2000 - 4000	500	± 10
4000 - 12,000	1000	5
12,000 - 35,000	2000	10

Spectral Range (A)	$E\lambda$ (watt/cm^2)	$\Delta E\lambda$ (watt/cm^2)
2000 - 2500	0.2×10^{-3}	0.02×10^{-3} (10%)
3000 - 3500	4.0	0.4 (10%)
4000 - 5000	0.9	0.95
6000 - 7000	15.5	0.77 (5%)
8000 - 9000	10.0	0.55
10,000 - 11,000	6.5	0.0325
12,000 - 14,000	8.0	0.8
20,000 - 22,000	2.4	0.24 (10%)
30,000 - 32,000	1.2	0.12

The spectral distribution of simulated planet radiation need not match the actual distribution too closely for the following reasons:

1) Material effects caused by radiations in the infrared range are practically negligible.

2) Absorptivity and emissivity do not vary to an appreciable extent over the infrared range.

3) Actual spectral radiance at any wavelength varies by a factor of two depending upon the cloud cover conditions.

Therefore, tolerances in the order of ± 40% over 2μ bandwidths should be sufficient.

3. Cost Effects

While close tolerances are desirable from a technical point of view, it is unfortunately true that close tolerances and high accuracy are accompanied by high costs. The relation between tolerances and cost is probably a hyperbolic function such as the curve plotted in Figure 25. As illustrated in this curve a small decrease in the tolerances at comparatively large tolerance settings would not appreciably increase the facility cost. However, a further decrease of tolerances when the tolerances are already small would result in a considerable cost increase.

For this reason the recommendation of radiation tolerances has been deferred until a cost estimate is made of various simulation systems. Following the determination of a cost-tolerance curve, a design tolerance or range of tolerances can be established based on both technical and economical grounds.

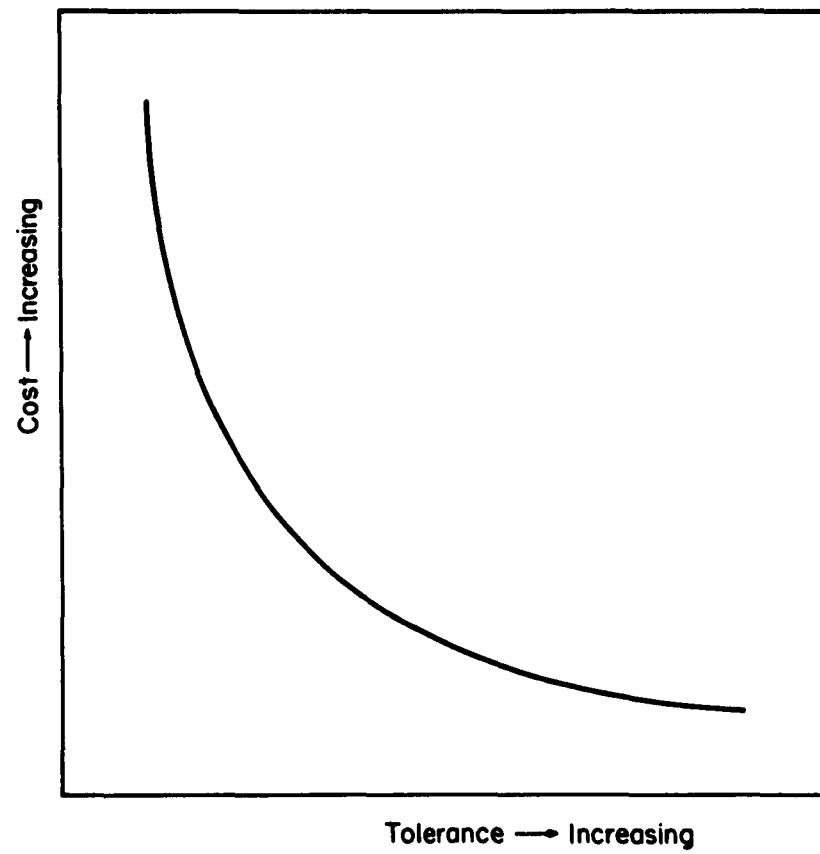

Fig. 25 Effect of Tolerance on Cost

VI. REFERENCES

1. Tousey, R., "The Solar Spectrum in Space," Astronautics, 6, No. 7, pp. 32-33, 52-54 (June 1961).

2. Versluys, W., et al., "Ultraviolet Effects on Space Vehicle Operation in Ultrahigh Vacuum Environment," AEDC-TDR-62-17 (January 1962)

3. Johnson, F. S., "The Solar Constant," Journal of Meteorology, 11, No. 6, pp. 431-439 (December 1954).

4. S. Chandrasekhar, Radiative Transfer, New York: Dover, 1960

5. Danjon, A., "Albedo, Color, and Polarization of the Earth," The Earth As a Planet, Ed: G. P. Kuiper, U. of Chicago Press (1954).

6. Simpson, G. C., "Further Studies in Terrestrial Radiation," Memoirs of the Royal Meteor. Soc., 3, pp. 1-26 (1928).

7. Baur, F., and Phillips, H., Gerlands Beitr. Geophys. 42, pp. 160-207 (1934).

8. Baur, F., and Phillips, H., Gerlands Beitr. Geophys. 45, pp. 82-132 (1935).

9. Fritz, S., "Solar Radiant Energy and Its Modification by the Earth and its Atmosphere," Compendium of Meteorology, Am. Meteor. Soc. (1951)

10. Houghton, H. G., "On the Annual Heat Balance of the Northern Hemisphere," Journal of Meteorology, 2, pp. 1-9 (1954).

11. Dubois, J. E., "Etude Photometrique et Colormetrique de la Lumiere Cendree de la Lune," Ciel et Terre, 59, pp. 375-91 (1943).

12. Camack, W. G., "Albedo and Earth Radiation," IES, 1962 Proc., pp. 391-396 (1962).

13. Byers, H. R., "The Atmosphere Up to 30 Kilometers," The Earth as A Planet, Ed: G. P. Kuiper, University of Chicago Press (1954).

14. Goldberg, L., "The Atmospheric Spectrum of the Atmosphere," The Earth as a Planet, Ed: G. P. Kuiper, University of Chicago Press (1954).

15. Minzner, R. A., Ripley, W. S. , Condron, T. P., "U. S. Extension to the ICAO Standard Atmosphere," U. S. Government Printing Office (1958).

16. Kellog, W. W., and Sagan, C., "The Atmospheres of Mars and Venus," Publication 944, National Academy of Sciences, National Research Council (1961).

17. Dennison, A. J. "Illumination of a Space Vehicle Surface Due to Sunlight Reflected from Earth," American Rocket Society; Journal, 32, pp. 635-637 (April 1962).

18. Dennison, A. J., "Illumination of a Cell Surface in Space Due to the Sunlight Reflected From the Earth", TIS 61SD101 , General Electric, Missile and Vehicle Department, (June 20, 1961).

19. Feigelson, E. M., Malkevich, M. S., Kogen, S. Ya., Koronatova, I. D., Glazova, K. S., and Kuznetsova, M. A., " Calculation of the Brightness of Light in the Case of Anisotropic Scattering," translated from the Russian, Consultant's Bureau, Inc., (1960).

20. Waldram, J. M., "Measurements of the Photometric Properties of the Upper Atmosphere," Royal Meteorology Soc.; Quarterly Journal, 71, pp. 309-310 (1945).

21. Goetz, D., and Grosch C. B., "Earth Emitted Infrared Radiation Incident Upon a Satellite," J. of Aerospace Sc., pp. 521-524 (May, 1962).

22. Jaffe, L. D., and Rittenhouse, J. B.,"Behavior of Materials in Space Environments," TR 32-150, Jet Propulsion Laboratory, 1 November 1961.

23. Kress, Eileen B., "Spacecraft Temperature Control: Breakthrough on Transit," Vol. 36, No. 1, Space/Aeronautics (July, 1961), pp 60-1.

24. Clauss, F. J., Mauri, R. E., Smith, E. C., Drake, S., IES: 1961 Proc., pp 475-488.

25. Simpson, Maurice H., "Effects of Space Environment on Propellent Actuated Devices," IES: 1962 Proc., pp 401-418.

26. Gelhard, J. C. and S. W. Meyer, "Design Solution for a Space Environment Simulator," IES: 1961 Proc., pp 335-347.

27. Swalley, F. E., "Thermal Radiation Incident on an Earth Satellite," NASA Technical Note D-1524, December 1962.

SUPPLEMENT 1

by WARREN J. KERZON
Captain, USAF

TITLE Comparison of TIROS II Radiation Data with Vitro Values

SUMMARY AND PURPOSE

The purpose of this memo will be to compare the albedo and thermal radiation data from the TIROS II Meterorological Satellite with the albedo and thermal radiation values defined by Vitro Laboratories in their Technical Note No. 3 under Contract AF 40(600)-951.

The TIROS II radiation experiment is inadequate for the purpose of thoroughly checking the secondary radiation characteristics as described in the Vitro report. Albedo data from TIROS II is unreliable. However, the samplings of thermal data do check well with the limits established in the Vitro report. It is not recommended that TIROS II data be investigated further.

DISCUSSION

The Vitro report (Reference 1) reviewed the characteristics of albedo and thermal radiation. In addition, tolerances for simulating these secondary radiation effects were derived for incorporation into an aerospace environmental facility. By comparing the Vitro values with samples of TIROS II radiation data, a check will be made of the correctness of the maximum, minimum, and expected or average values of albedo and thermal radiation.

The TIROS II was placed in orbit 23 November 1960. Instrumentation included two television cameras and two radiometers. One radiometer was a wide field, low resolution, non-scanning instrument. The second radiometer was a five-channel, medium resolution, scanning instrument. An operation schematic of the latter radiometer is illustrated in Figure 1. By means of the rotary chopper disc, the space-viewed (zero radiation level) beam is compared to the earth-viewed beam. The net result is a chopped output which produces a D.C. signal proportional to the $\Delta\bar{W}$ in energy flux from the reference and scan beams. A detailed description and calibration explanation of this instrument can be found in Reference. 2.

Channels 3 and 4 are of interest for the purposes of comparing secondary radiation data. Channel 3 detected, recorded, and transmitted data over a spectral range of from 0.25 to 6.0 microns (albedo). Channel 4 was sensitive to radiation flux over a range of 8.0 to 30.0 microns (thermal).

Altitude Correlation

In order to compare the TIROS II data directly with the values of secondary radiation summarized in Reference 1, the decrease of radiation intensity with altitude must be taken into account. Using the relationship $I(h) = I_o\left[\frac{(R_o)}{(R_o + h)}\right]^2$, the plots of albedo and planet or thermal radiation flux will be reduced by 19 and 17 percent, corresponding to the apogee and perigee of the satellite. Figures 2 and 3 are plots of secondary radiation maximums and minimums with this altitude correlation taken into account.

Albedo Radiation

Values of earth albedo flux (watts/meter^2) were detected by Channel 3 over a spectral range of 0.25 to 6.0 microns. As a result, an average or integrated value was recorded and later transmitted for each scan point.

After a preliminary review of the available albedo data, it was determined that a detailed tabulation would be of little value. All data points fall short of the expected average albedo. This is due apparently to the poor signal-to-noise ratio of Channel 3. The estimated accuracy of Channel 3 came to ± 60 watts/meter^2 for albedos of about .10 solar constant. Under conditions of less than .10 solar constant, albedo data is totally unreliable (Reference 3).

An integration of the maximum and minimum albedos depicted in Figure 2 will yield approximately 1400 x .55 x .83 or 638 watts/meter^2, maximum, and 1400 x .15 x .81 or 170 watts/meter^2, minimum.

The average albedo values have been derived from the six available grid maps in Reference 4. Each value represents the total average over the entire grip map. These values are tabulated in Table 1. Note that all values are far below the expected value of 1400 x .36 x .80 or 403 watts/meter^2. In orbits 31, 61, and 93, the average values fall short of the anticipated minimum of 170 watts/meter^2.

TABLE 1

Orbit No.	4	31	61	89	91	93
Grid Map	B	D	B	B	E	H
$\bar{W}_a$	178	103	90	186	187	168
a	.16	.09	.08	.17	.17	.15

Thermal Radiation

Values of earth thermal flux were detected by TIROS II over a spectral range of 8 to 30 microns. The estimated accuracy of the data from this channel is ± 5.0 watts/meter^2. As with the albedo, the grid point data represent integrated values of radiation flux. Although a spectral intensity plot of thermal data cannot be made, a calibration curve (Figure 4) is provided for Channel 4, giving effective radiant emittance versus equivalent blackbody temperature. This plot provides a means for direct comparison with the established values of maximum and minimum thermal radiation values set forth in the Vitro report.

From seven orbits chosen at random, average values of thermal radiation have been derived along parallels of latitude covered by each selected grid map. Geographic locations of individual thermal averages are depicted in Figures 5-11. Note that all grid maps do not contain the same number of plots. This is because grid values did not occur for all grid points.

The Grip Map Average represents the integrated thermal radiation value for all grid points with data.

(NOTE: This grid point average appears at all grid points without data. Therefore, the most reliable Grid Map Average appears for those maps which contain a maximum number of plots).

A survey of the seven selected grip maps will show that the thermal radiation for these particular geographic locations and times varies from 28.3 to 59.4 watts/meter^2. These values correspond to equivalent blackbody temperatures of 230 and 272°K (Figure 4).

REFERENCES

1. "Albedo and Planet Radiation Intercepted by an Earth Satellite," Technical Note No. 3, Contract AF 40(600)-951, 13 July 1962.

2. "TIROS II Radiation Data Users' Manual," NASA, Goddard Space Flight Center, 15 August 1961.

3. "TIROS II Radiation Data Users' Manual, Supplement," NASA, Goddard Space Flight Center, 15 May 1962.

4. "TIROS II Radiation Data Catalog," NASA, Goddard Space Flight Center, 15 August 1961.

DEFINITIONS

a - Albedo radiation value, expressed as a fraction of the mean solar constant, 1400 watts/meter^2

h - Satellite altitude, KM

I(h) - Spectral intensity, watts/meter$^2\mu$, as a function of h

I_o - Spectral intensity at the effective earth radiating radius

R_o - Effective earth radiating radius, 6377 KM

T_{BB} - Equibalent blackbody temperature

W - Effective radiant emittance, watts/meter^2, defined by Equation 3, Reference 2.

BLOCK DIAGRAM OF ONE CHANNEL OF THE
MEDIUM RESOLUTION SCANNING RADIOMETER

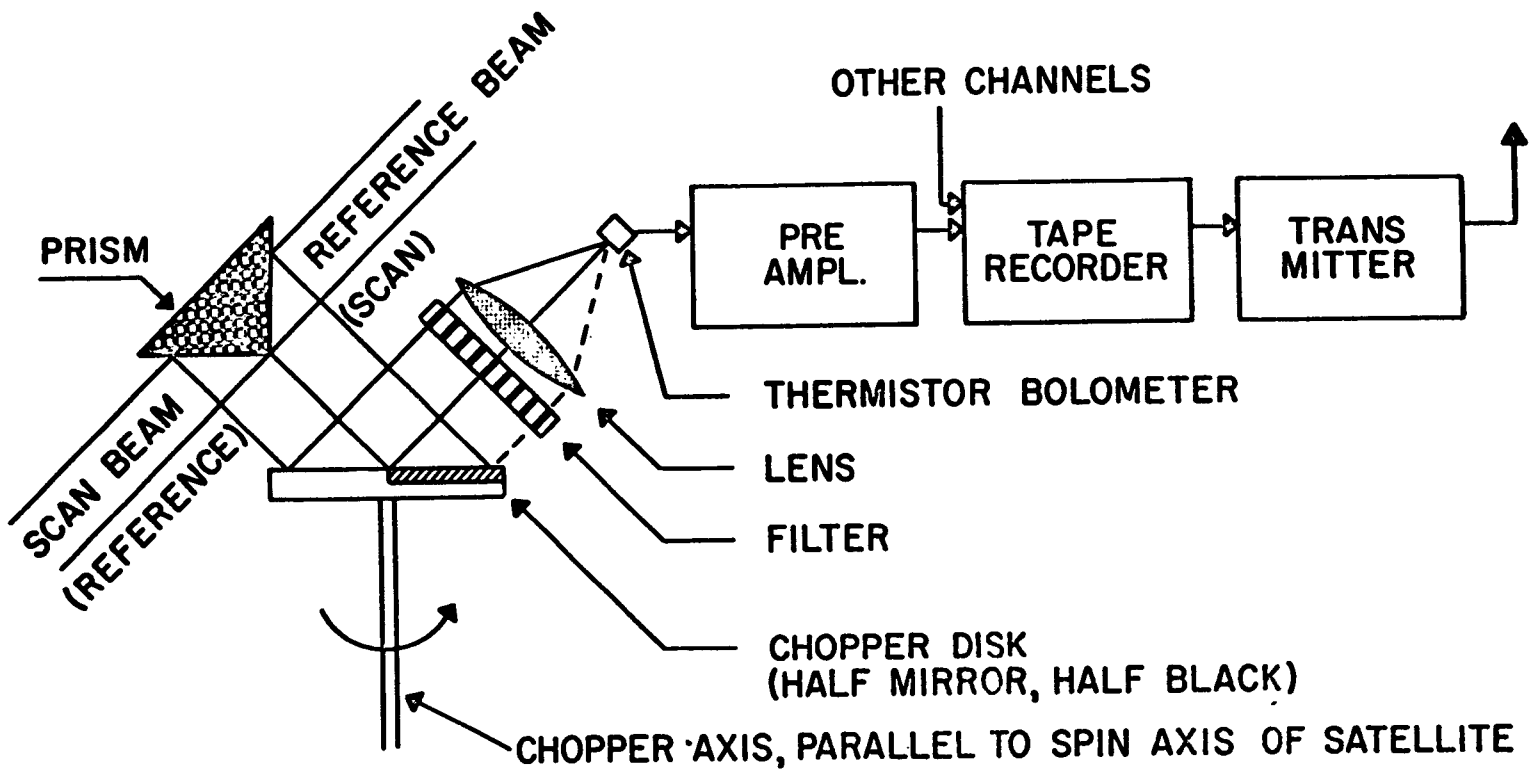

Reference 2

Figure 1

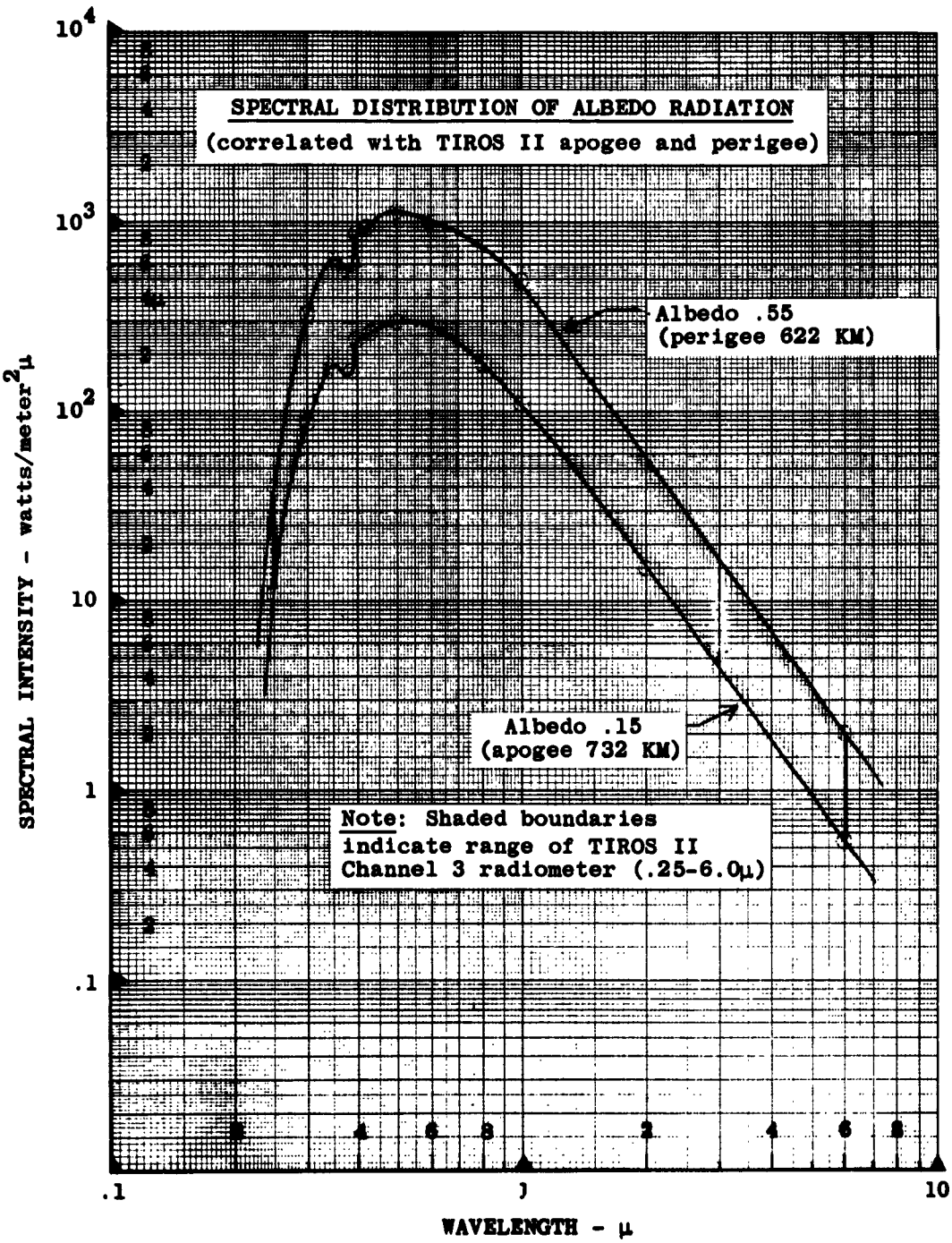
SPECTRAL DISTRIBUTION OF ALBEDO RADIATION
(correlated with TIROS II apogee and perigee)
Albedo .55
(perigee 622 KM)
Albedo .15
(apogee 732 KM)
Note: Shaded boundaries
indicate range of TIROS II
Channel 3 radiometer (.25-6.0μ)
SPECTRAL INTENSITY - watts/meter²μ
WAVELENGTH - μ
10⁴
10³
10²
10
1
.1
.1
1
10

Figure 2

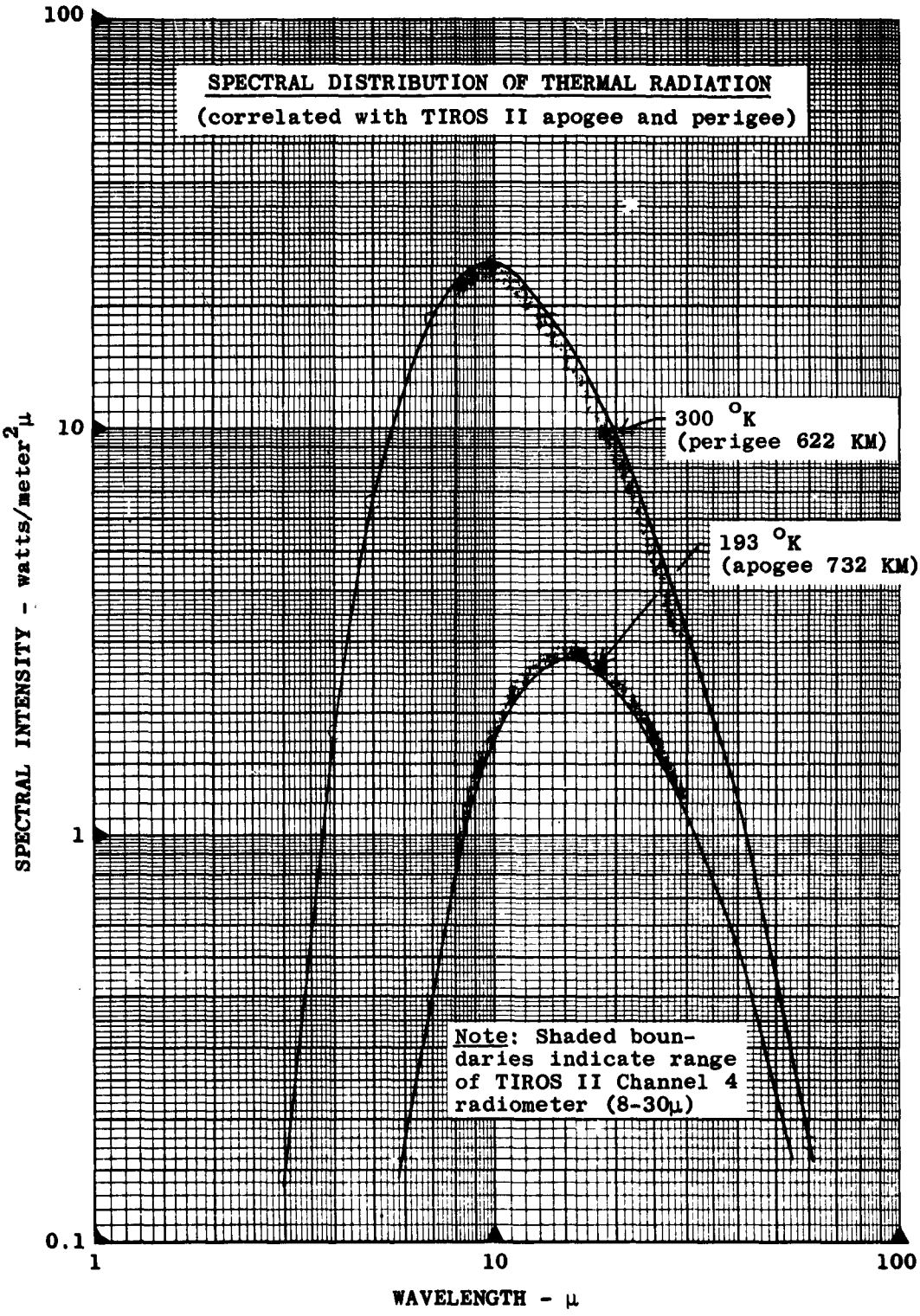
SPECTRAL DISTRIBUTION OF THERMAL RADIATION
(correlated with TIROS II apogee and perigee)
300 °K
(perigee 622 KM)
193 °K
(apogee 732 KM)
Note: Shaded boundaries indicate range of TIROS II Channel 4 radiometer (8-30μ)
SPECTRAL INTENSITY - watts/meter²μ
WAVELENGTH - μ
100
10
1
0.1
1
10
100

Figure 3

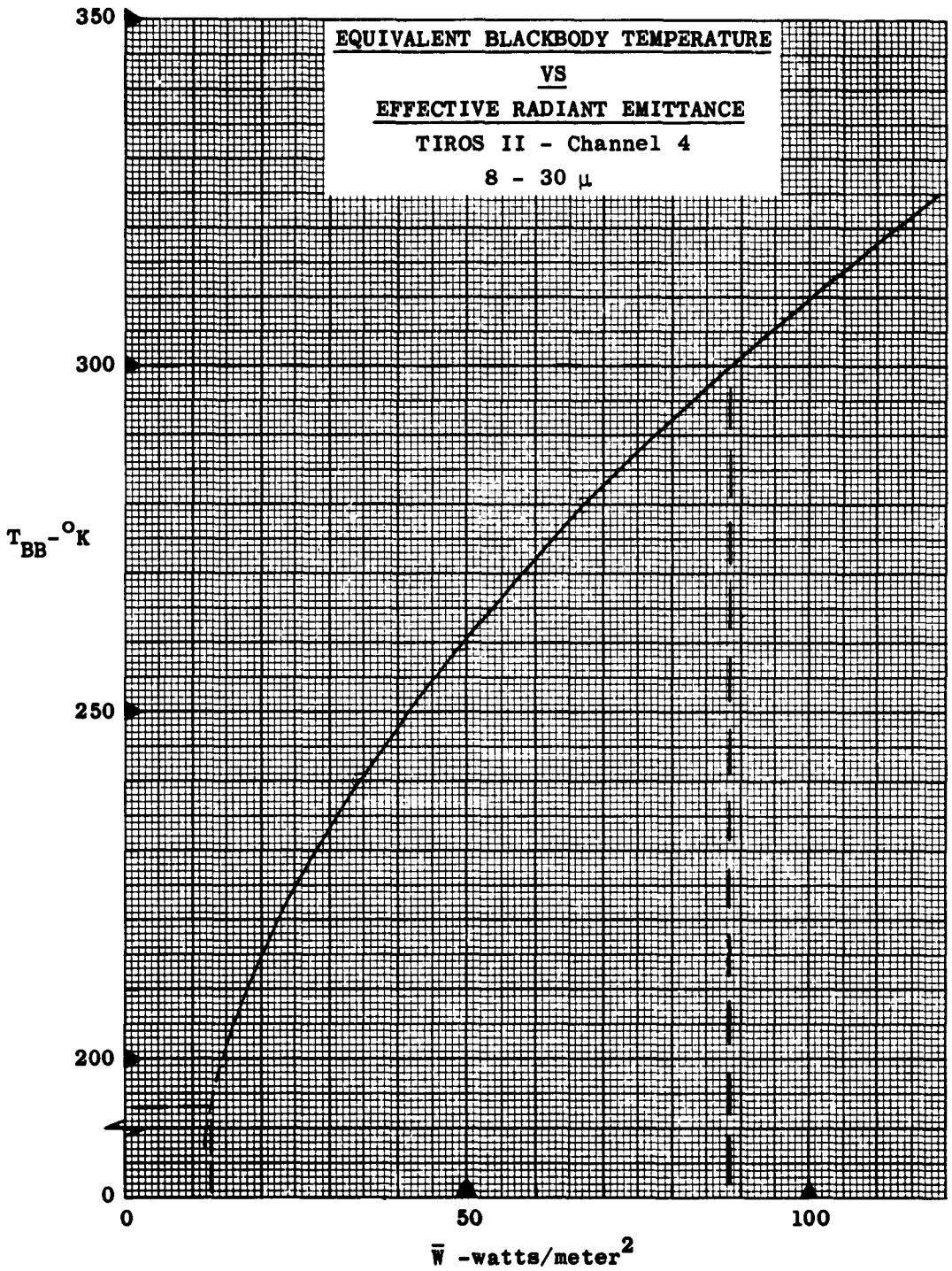
EQUIVALENT BLACKBODY TEMPERATURE
VS
EFFECTIVE RADIANT EMITTANCE
TIROS II - Channel 4
8 - 30 μ
350
300
250
200
0
T_{BB}-°K
0
50
100
$\bar{W}$ -watts/meter^2

Figure 4

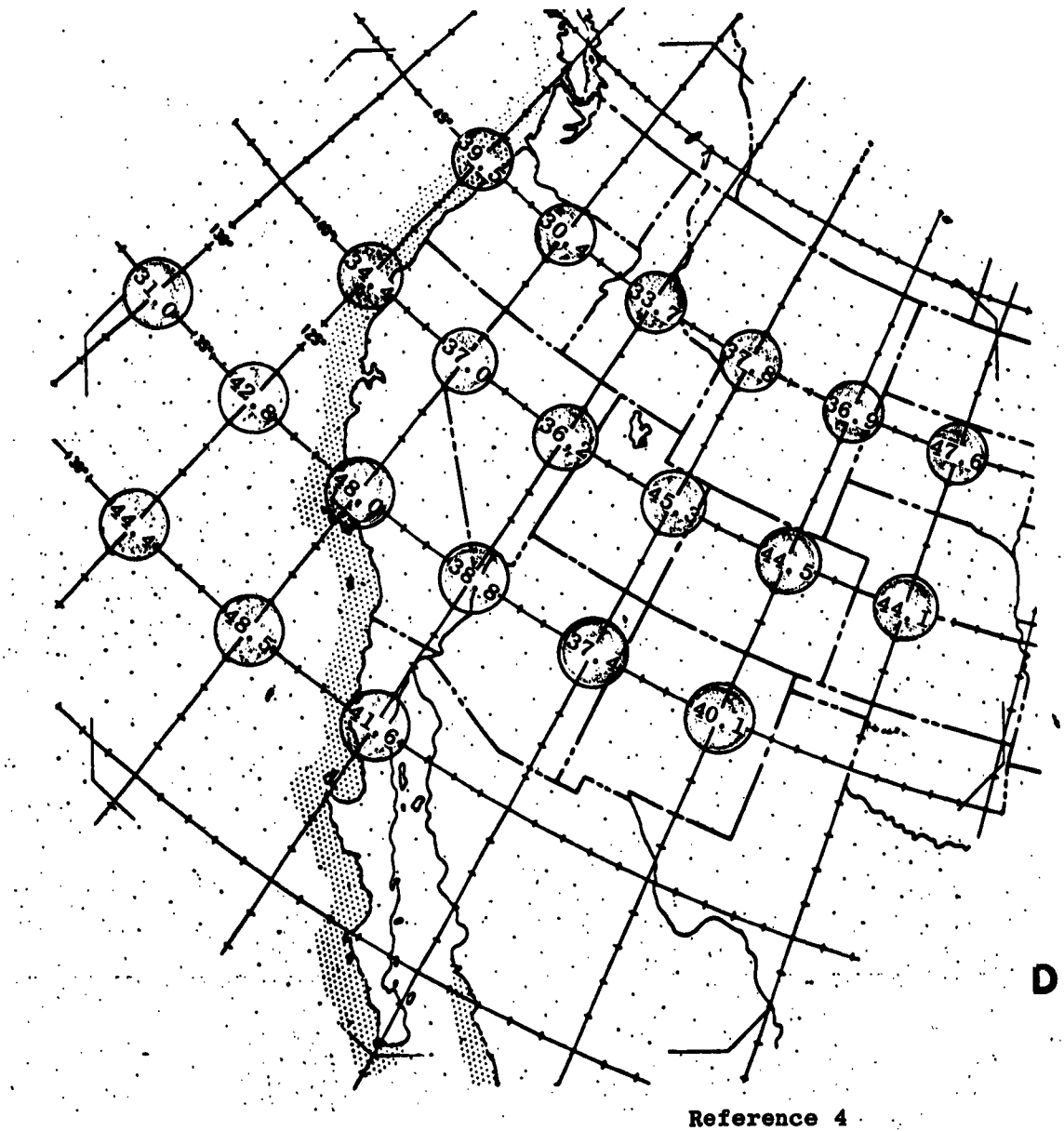

Reference 4

Orbit 31

25 Nov 60

1405 Z (approx. 0635 local mid-Meridian)

Channel 4 (8-30 microns)

Grip Map Average: 39.8 w/m^2

Figure 5

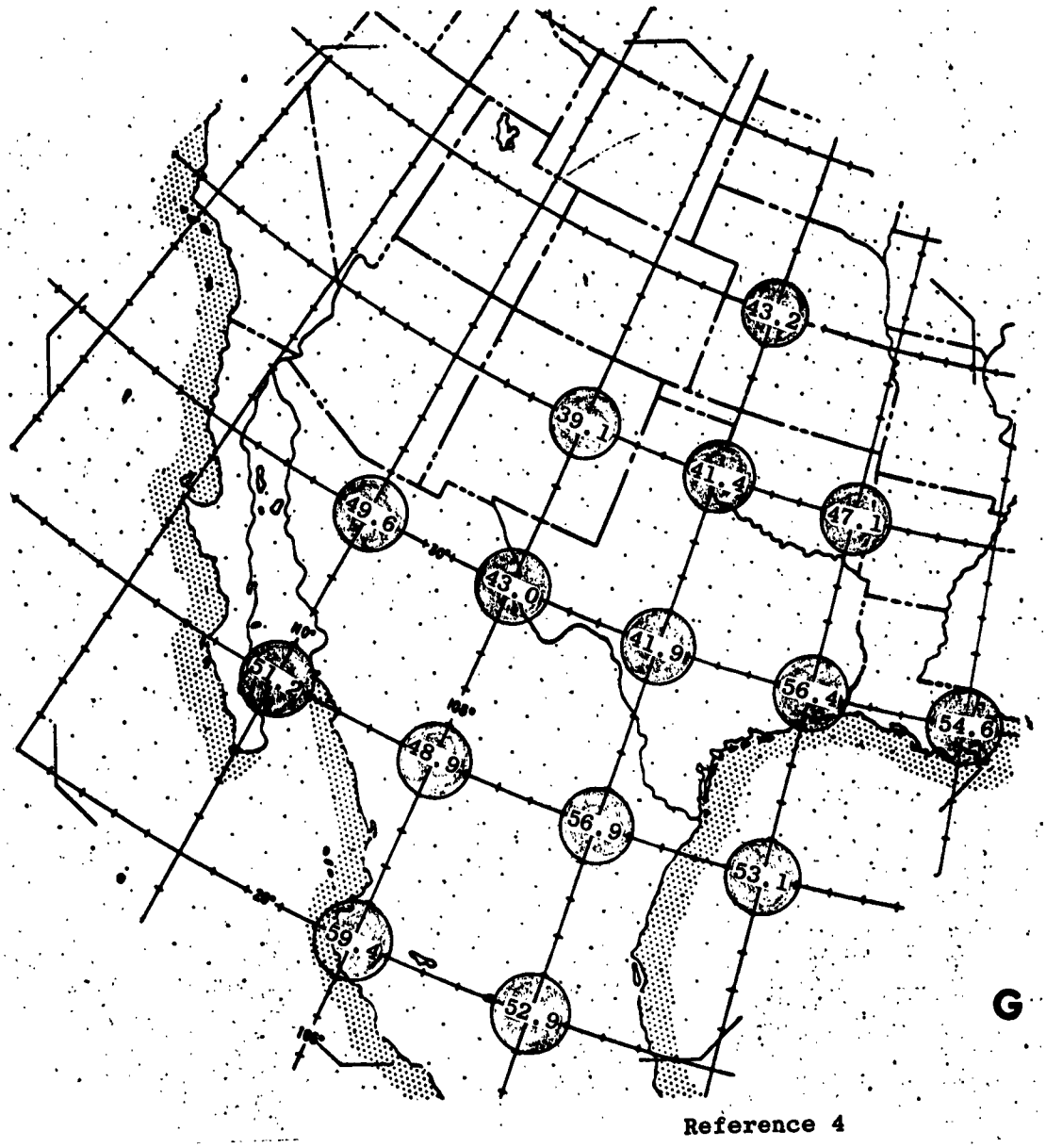

Reference 4

Orbit 44

26 Nov 60

1115 Z (approx. 0415 local mid-Meridian)

Channel 4 (8-30 microns)

Grid Map Average: 50.8 w/m^2

Figure 6

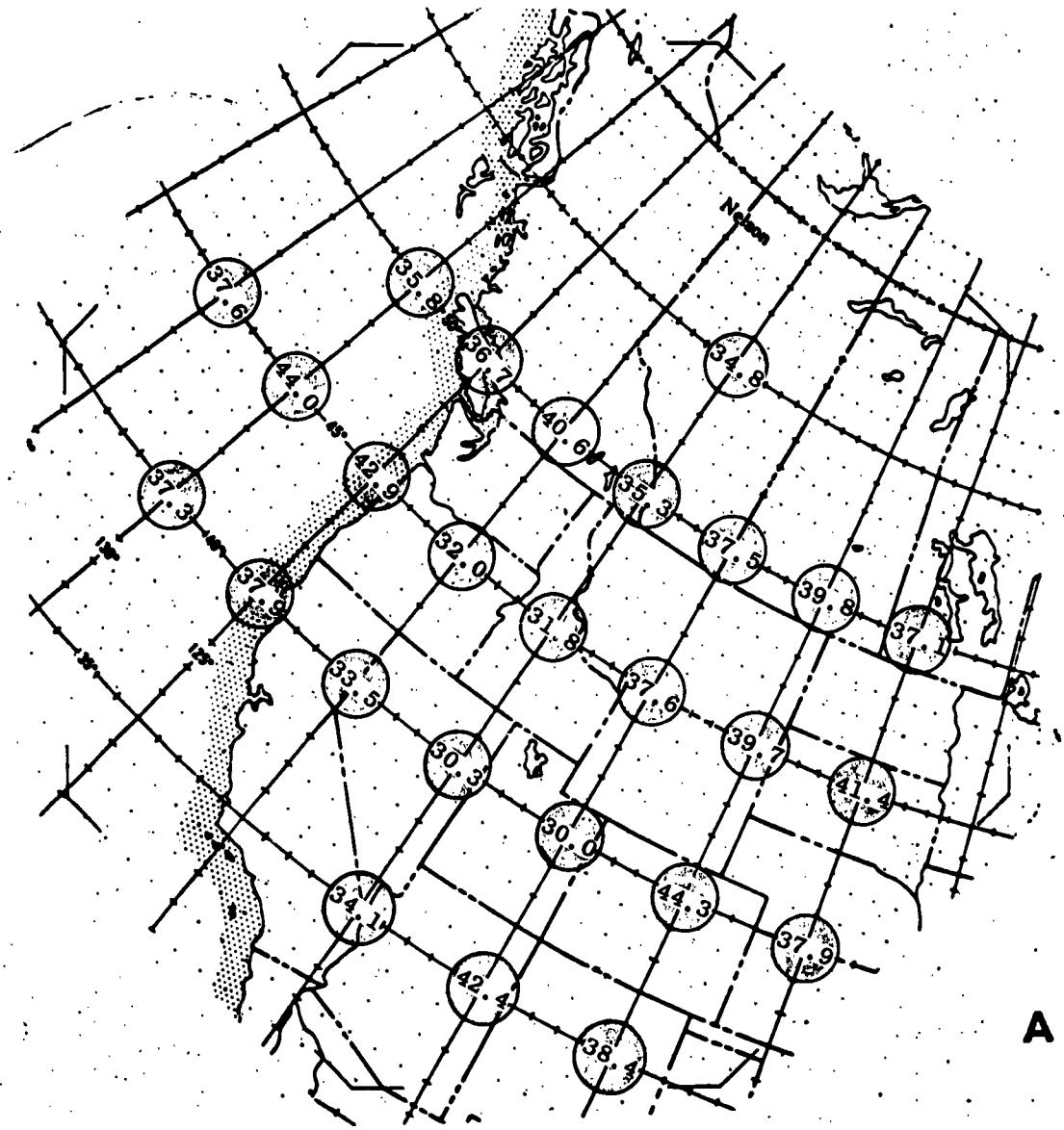

Reference 4

Orbit 46

26 Nov 60

1440 Z (approx. 0700 local mid-Meridian)

Channel 4 (8-30 microns)

Grip Map Average: 37.1 w/m^2

Figure 7

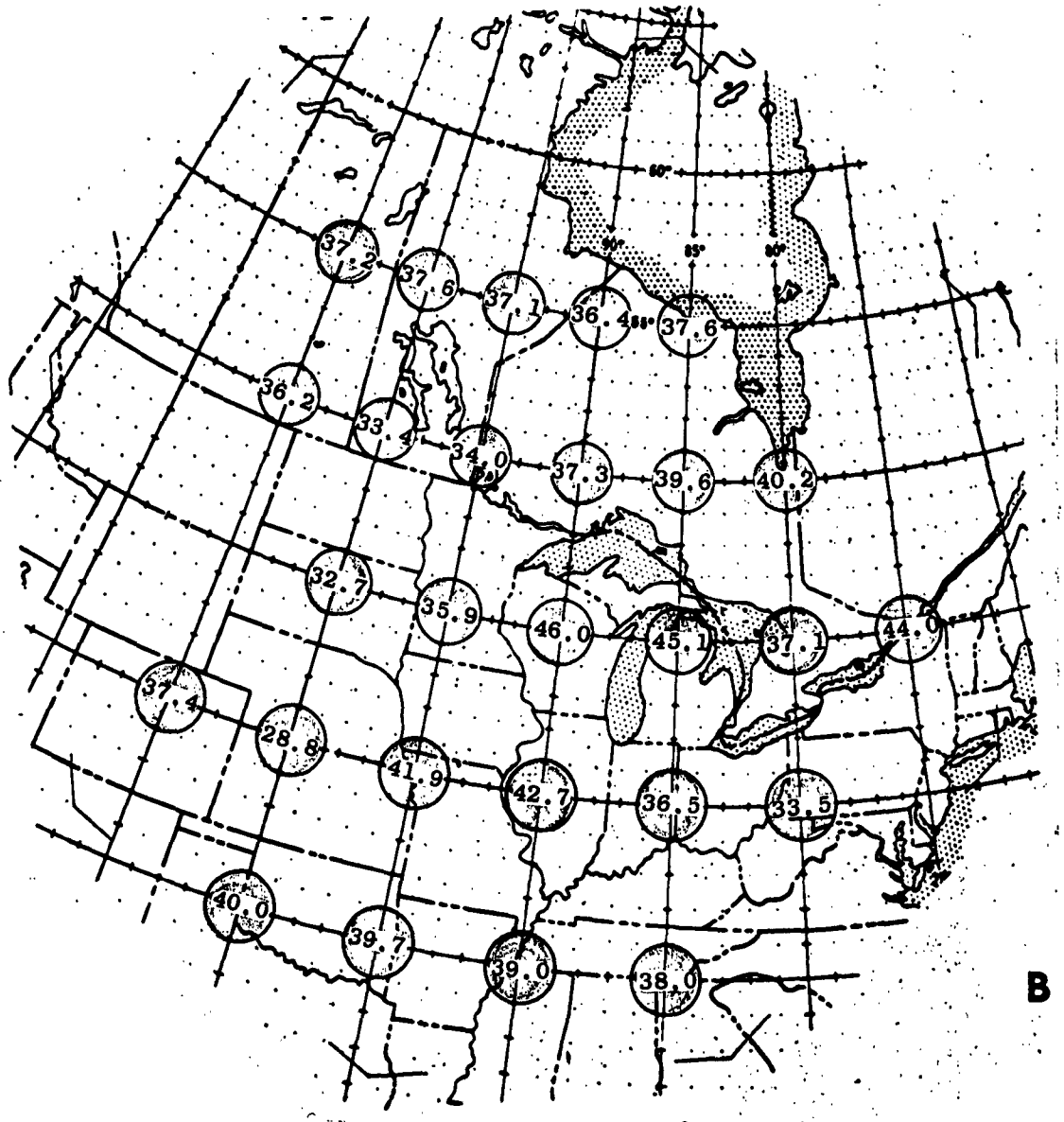

Reference 4

Orbit 61

27 Nov 60

1522 Z (approx. 0910 local mid-Meridian)

Channel 4 (8-30 microns)

Grip Map Average: 38.5 w/m^2

Figure 8

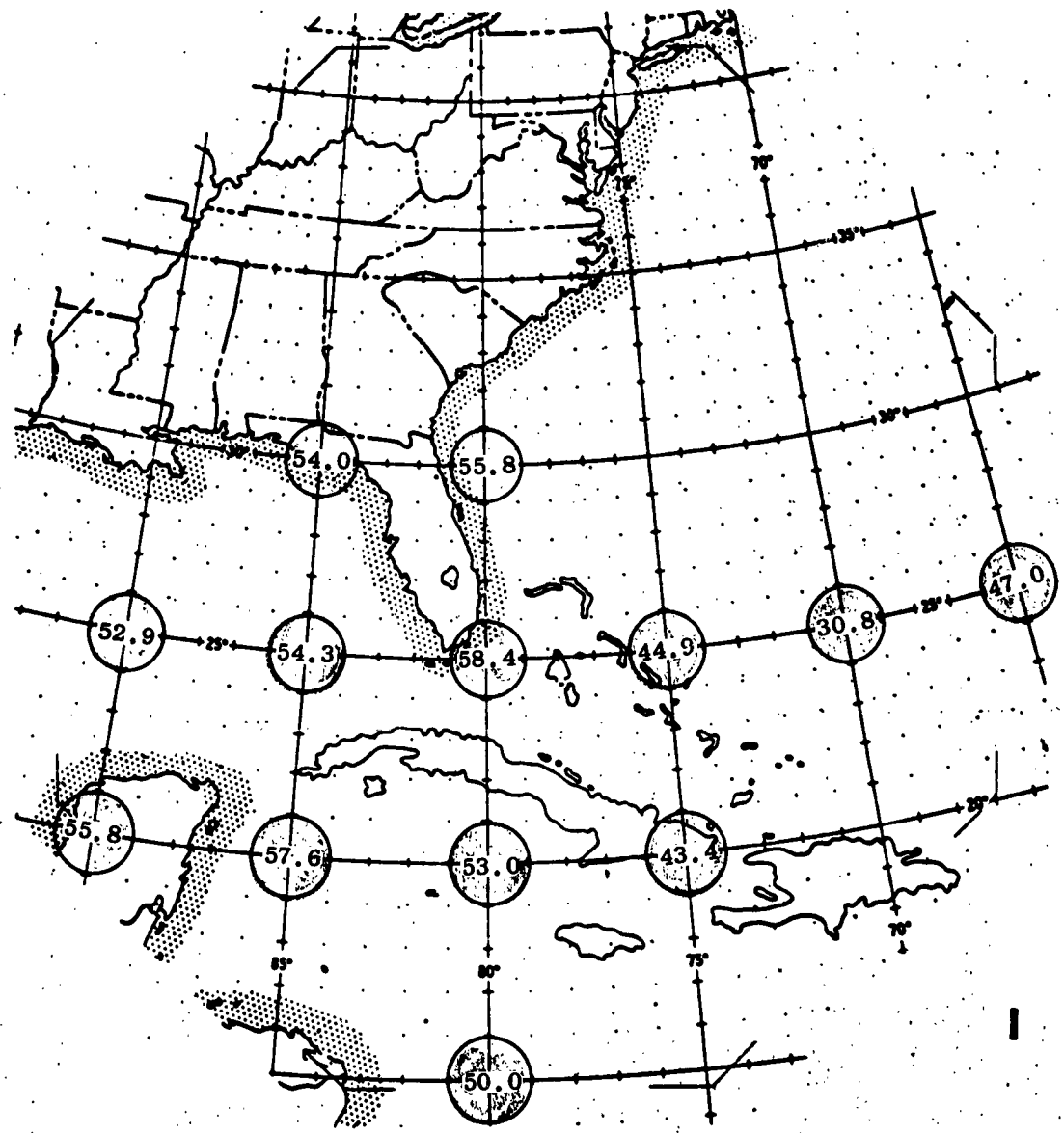

Reference 4

Orbit 72

28 Nov 60

0903 Z (approx. 0345 local mid-Meridian)

Channel 4 (8-30 microns)

Grid Map Average: 51.2 w/m^2

Figure 9

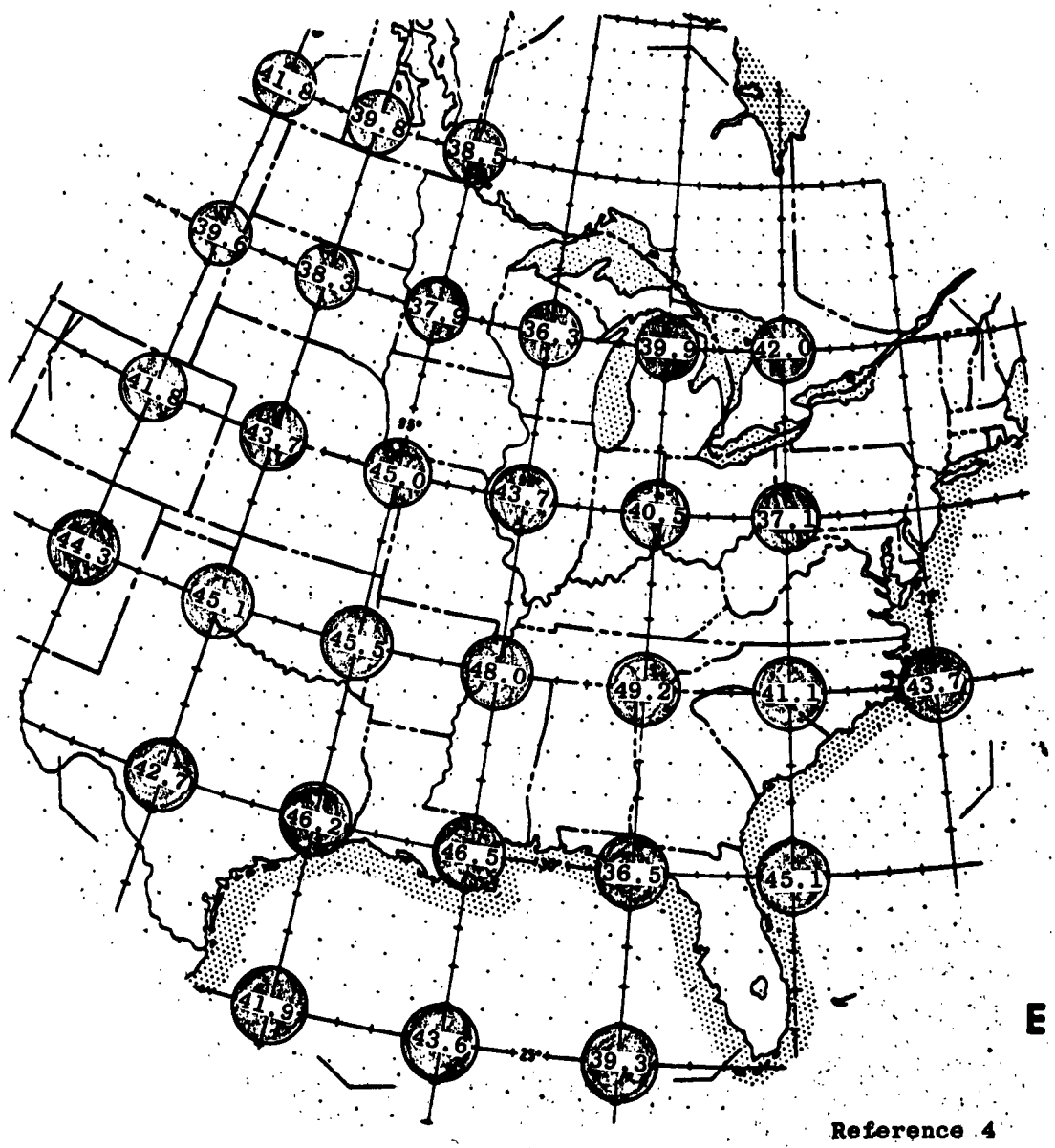

Orbit 91

29 Nov 60

1634 Z (approx. 1030 local mid-meridian)

Channel 4 (8-30 microns)

Grid Map Average: 42.0 w/m^2

Figure 10

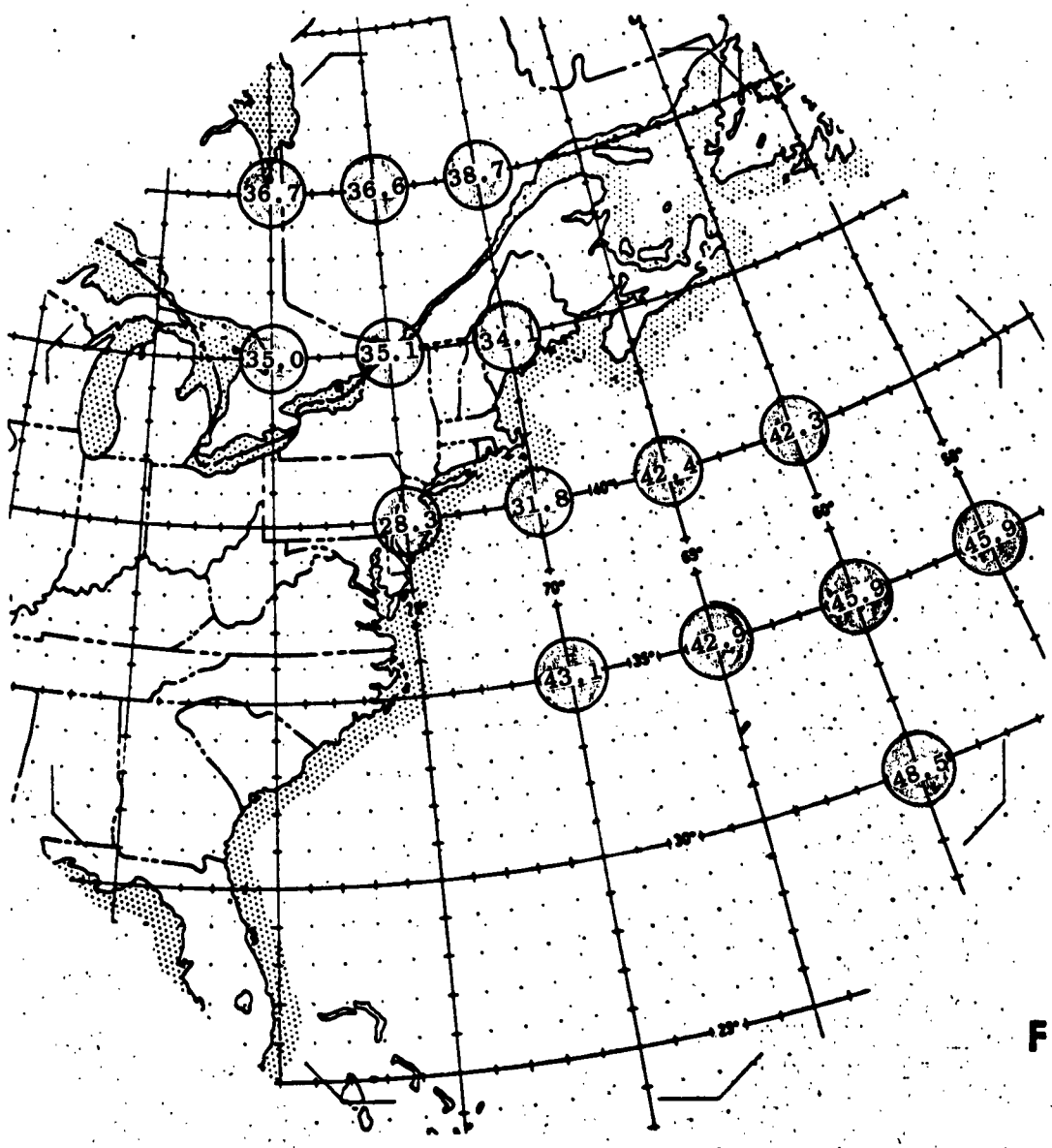

Reference 4

Orbit 409

21 Dec 60

0742 Z (approx. 0300 local mid-Meridian)

Channel 4 (8-30 microns)

Grip Map Average: 42.7 w/m^2

Figure 11

SUPPLEMENT 2

by G. MacFARLANE
Flight Lieutenant, RCAF

Summary of TIROS III Radiation Data:

The TIROS III carried similar radiation measuring equipment to that on the TIROS II; namely, a non-scanning radiometer and a five-channel scanning radiometer. The later instrument covered the IR and visible ranges as follows:

a. 0.5 to 0.75μ - This wavelength range covers the region of maximum solar energy distribution.

b. 0.2 to 7.0μ - This is the wavelength range of the reflected solar energy (albedo).

c. 5.9 to 6.7μ - This is the maximum absorptive band for H_2O vapor.

d. 7.5 to 13.5μ - This is the atmospheric "window" band which, due to the maximum optical depth range into the atmosphere, gives readings indicative of the actual surface temperature of the earth in the absence of cloud cover.

e. 7.0 to 32.0μ - This channel collects approximately 80 per cent of the total earth black body radiation.

Radiation data, obtained at roughly local noon, were analyzed for three areas: namely, the tropical Atlantic ocean in the vicinity of the Guiana coast; the north eastern region of the United States; and over the north eastern corner of Africa. Table 1 summarizes the measured black body temperature of the earth, as measured by the various channels. Table 2 lists the albedo fraction over the various surfaces under cloudy and clear conditions. Table 3 gives the total outward energy flux at local noon.

The black body temperature of the earth, as measured by the instrumentation on the satellite, is strongly influenced by the presence of water vapor. This is most obvious when the temperatures of the 5.9 - 6.7μ channel are compared with those of the 7.5 - 13.5- channel. The temperatures measured by the former are consistently lower. Even in the "window" observation range, the temperatures measured over areas where the air has a high water vapor content (as over the tropical Atlantic) are much lower than the actual surface temperature. This is indicative of a considerable energy loss by absorption.

In general, the values of albedo and the black body temperature of the earth fall within the range of values predicted by Vitro.

For further discussion refer to NASA Technical Note D-1338, May 1962, by W. Nordberg, W. R. Bandeen, B. J. Conrath, V. Kunde, and I. Persano, of Goddard Space Flight Center, Greenbelt, Maryland.

TABLE 1

BLACK BODY TEMPERATURES OF EARTH

LOCATION	SKY CONDITIONS	TEMPERATURE °K			
		5.9 – 6.7μ	7.5–13.5μ	7.0–32.0μ	NON SCANNING RADIOMETER
Tropical Atlantic	Clear	244	277	262	259
Eastern U.S.	Clear	236	283	266	N/A
Eastern U.S.	Cloudy	233	252	260	247
Libyan Desert	Clear	260	310	287	305
Tropical Sudan	Partly Cloudy	230	285	255	260

TABLE 2

ALBEDO FRACTION

LOCATION	SURFACE CONDITIONS	SKY CONDITIONS	ALBEDO FRACTION		
			.5–.75μ	.2–7.0μ	NON SCANNING RADIOMETER
Tropical Atlantic	Water	Clear	.07	.04	.09
Mediterranean	Water	Clear	.18	.15	.14
Indian Ocean	Water	Clear	N/A	N/A	.15
Libyan Desert	Arid	Clear	.27	.21	.29
Central Sudan	Vegeta-tion	Partly Cloudy	.40	.30	.28
Blue Nile Valley	Vegeta-tion	Clear	.20	.15	N/A
Libya	Uplands	Partly Cloudy	.18	.16	.16
Eastern U.S.	Vegeta-tion	Cloudy	.50 - .55	.35 - .40	.29
Eastern U.S.	Vegeta-tion	Clear	.15 - .20	.08 - .12	.22

TABLE 3

OUTWARD ENERGY FLUX

SURFACE	CLIMATIC ZONE	SKY CONDITIONS	NOON-TIME ENERGY FLUX (W/M^2)
Land	Temperate	Clear	265
Land	Temperate	Cloudy	192
Water	Tropical	Clear	250
Land	Desert-Subtropical	Clear	340

Arnold Engineering Development Center
Arnold Air Force Station, Tennessee
Rpt. No. AEDC-TDR-63-92. ALBEDO AND PLANET RADIATION INTERCEPTED BY AN EARTH SATELLITE. May 1963, 104 p. incl 27 refs., illus., tables.

Unclassified Report

The characteristics of the secondary radiation environment of an earth satellite were analyzed and compared with the characteristics of solar radiation. Of the total incident radiation, 27% is reflected from earth and clouds and 9% is scattered, bringing the total albedo contribution to 36%. The remaining 64% of the incident energy is absorbed by the earth and reradiated as planet radiation. Of this energy, 17% is radiated as thermal radiation from the earth, and 47% as thermal radiation from the stratosphere. The spectral distribution of the reflected solar radiation corresponds to that of a blackbody at 6000°K while the energy, which is reradiated, corresponds to a blackbody at approximately 250°K. In the wavelength region below 4 microns, albedo radiation has the higher spectral intensity, peaking at about 10^{-1} watts/cm^2 μ; above 4μ peak spectral intensity is approximately 10^{-3} watts/cm$^2\mu$. An analysis was made of the angular distribution of the solar, albedo, and planet radiation received by an earth satellite. Solar radiation has only a 32-minute spread or collimation angle from the sun-earth direction. The intensity of the albedo on area differentials on the satellite surface were calculated as a function of altitude, orbital position with respect to the earth-sun axis, and orientation of the differential area on the satellite surface, using the model suggested by Dennison. The albedo has a maximum intensity on the lower side of the satellite at an orbital position directly between the sun and the earth. This intensity decreases with altitude and with the angle between the actual position and the sun-earth axis falling to zero on the shadowed side of the earth. This analysis of albedo angular distribution was compared with the analysis by Feigelson et al (a group of Russian investigators) which is based on experimental data but is not as complete in the number of parameters considered. The results of the two analyses compare closely, however. The third type of radiation planet radiation was found to be independent of the orbital angular position. Intensity and angular distribution of this radiation are dependent only on the altitude and the amount of cloud cover. Tolerances on simulating the radiation characteristics were analyzed based on possible thermal and material effects upon a space vehicle. It was concluded that the spectral distribution should be matched with a reasonable tolerance in the ultraviolet for material effects, and in the region of maximum spectral irradiance for thermal effects. The angular energy distribution should be matched within 8% to insure a temperature deviation no greater than 2%. The degree of accuracy or tolerance on simulation techniques should be based on economical as well as technical considerations.

1. Albedo
2. Solar radiation
3. Space environmental conditions
4. Satellites (artificial)
I. AFSC Program Area 850E, Project 7778, Task 777801
II. Contract AF 40(600)-951
III. Vitro Labs, Div. of Vitro Corp. of America, West Orange, N. J.
IV. C. D. Fitz, S. J. Lukasik, E. A. Mayer, and D. R. Simon
V. Secondary Report No. VL-2244-11-O
VI. Available from OTS
VII. In ASTIA Collection

Arnold Engineering Development Center
Arnold Air Force Station, Tennessee
Rpt. No. AEDC-TDR-63-92. ALBEDO AND PLANET RADIATION INTERCEPTED BY AN EARTH SATELLITE. May 1963, 104 p. incl 27 refs., illus., tables.

Unclassified Report

The characteristics of the secondary radiation environment of an earth satellite were analyzed and compared with the characteristics of solar radiation. Of the total incident radiation, 27% is reflected from earth and clouds and 9% is scattered, bringing the total albedo contribution to 36%. The remaining 64% of the incident energy is absorbed by the earth and reradiated as planet radiation. Of this energy, 17% is radiated as thermal radiation from the earth, and 47% as thermal radiation from the stratosphere. The spectral distribution of the reflected solar radiation corresponds to that of a blackbody at 6000°K while the energy, which is reradiated, corresponds to a blackbody at approximately 250°K. In the wavelength region below 4 microns, albedo radiation has the higher spectral intensity, peaking at about 10^{-1} watts/cm^2 μ; above 4μ peak spectral intensity is approximately 10^{-3} watts/cm$^2\mu$. An analysis was made of the angular distribution of the solar, albedo, and planet radiation received by an earth satellite. Solar radiation has only a 32-minute spread or collimation angle from the sun-earth direction. The intensity of the albedo on area differentials on the satellite surface were calculated as a function of altitude, orbital position with respect to the earth-sun axis, and orientation of the differential area on the satellite surface, using the model suggested by Dennison. The albedo has a maximum intensity on the lower side of the satellite at an orbital position directly between the sun and the earth. This intensity decreases with altitude and with the angle between the actual position and the sun-earth axis falling to zero on the shadowed side of the earth. This analysis of albedo angular distribution was compared with the analysis by Feigelson et al (a group of Russian investigators) which is based on experimental data but is not as complete in the number of parameters considered. The results of the two analyses compare closely, however. The third type of radiation planet radiation was found to be independent of the orbital angular position. Intensity and angular distribution of this radiation are dependent only on the altitude and the amount of cloud cover. Tolerances on simulating the radiation characteristics were analyzed based on possible thermal and material effects upon a space vehicle. It was concluded that the spectral distribution should be matched with a reasonable tolerance in the ultraviolet for material effects, and in the region of maximum spectral irradiance for thermal effects. The angular energy distribution should be matched within 8% to insure a temperature deviation no greater than 2%. The degree of accuracy or tolerance on simulation techniques should be based on economical as well as technical considerations.

1. Albedo
2. Solar radiation
3. Space environmental conditions
4. Satellites (artificial)
I. AFSC Program Area 850E, Project 7778, Task 777801
II. Contract AF 40(600)-951
III. Vitro Labs, Div. of Vitro Corp. of America, West Orange, N. J.
IV. C. D. Fitz, S. J. Lukasik, E. A. Mayer, and D. R. Simon
V. Secondary Report No. VL-2244-11-O
VI. Available from OTS
VII. In ASTIA Collection